LYAPUNOV-BASED CONTROL OF DISTRIBUTED MULTI-AGENT SYSTEMS WITH INTERMITTENT COMMUNICATION

By

FEDERICO MAXIMILIANO ZEGERS URRUTIA

A DISSERTATION PRESENTED TO THE GRADUATE SCHOOL
OF THE UNIVERSITY OF FLORIDA IN PARTIAL FULFILLMENT
OF THE REQUIREMENTS FOR THE DEGREE OF
DOCTOR OF PHILOSOPHY

UNIVERSITY OF FLORIDA

2021

To *Carmen Gloria Urrutia Santos*, *Catalina Anastasia Zegers Urrutia*, and *Álvaro Sebastián Torres Urrutia*

ACKNOWLEDGMENTS

I kindly thank my advisor, Dr. Warren Dixon, for his encouragement, patience, and guidance throughout my time as a Ph.D. student. Dr. Dixon is a constant source of inspiration, and I am grateful to him for honing my skills as a control theory researcher. I thank my committee members Dr. John Shea, Dr. Matthew Hale, and Dr. Amor Menezes for their support and oversight. I thank Dr. Dan Guralnik for his mentorship and meticulous care when teaching mathematics. Thank you, Dr. Sean Phillips, for advising me as a virtual intern in the Space Scholars Program, Air Force Research Laboratory during the Summer of 2020. Thank you to the Nonlinear Controls and Robotics group for all the laughs and exciting discussions on controls research. I would also like to thank the Air Force Office of Scientific Research, the Air Force Research Laboratory, Munitions Directorate at Eglin AFB, the Air Force Research Laboratory, Space Vehicles Directorate at Kirtland AFB, the National Science Foundation, the Office of Naval Research, and the Naval Engineering Education Consortium. This dissertation is supported in part by A Task Order contract with the Air Force Research Laboratory, Munitions Directorate at Eglin AFB, NSF award 1509516, Office of Naval Research Grant N00014-13-1-0151, NEEC award number N00174-18-1-0003, AFOSR award number FA9550-18-1-0109, and AFOSR award number FA9550-19-1-0169. Lastly, I thank Haley Weber for all her strength, support, and words of wisdom.

TABLE OF CONTENTS

LIST OF TABLES

LIST OF FIGURES

LIST OF ABBREVIATIONS

a.e.	Almost Everywhere
ARE	Algebraic Riccati Equation
BMI	Bilinear Matrix Inequality
CMAS	Cooperative Multi-Agent System
C-MAS	Clustered Multi-Agent System
DoS	Denial-of-Service
ETC	Event-Triggered Control
FCLT	Formation Control and Leader Tracking
FDI	False Data Injection
GES	Globally Exponentially Stable
IoT	Internet of Things
LTI	Linear Time-Invariant
MAS	Multi-Agent System
STC	Self-Triggered Control
TSD	Time-Delay Switch
UUB	Uniformly Ultimately Bounded
W-MSR	Weighted-Mean-Subsequence-Reduced

Abstract of Dissertation Presented to the Graduate School
of the University of Florida in Partial Fulfillment of the
Requirements for the Degree of Doctor of Philosophy

LYAPUNOV-BASED CONTROL OF DISTRIBUTED MULTI-AGENT SYSTEMS WITH INTERMITTENT COMMUNICATION

By

Federico Maximiliano Zegers Urrutia

August 2021

Chair: Warren E. Dixon
Major: Mechanical Engineering

The Internet of Things (IoT) has revolutionized the world by connecting previously isolated technologies to enable advanced capabilities, anticipate demands, and promote efficiency. Cost-effective gadgets endowed with the power to sense, actuate, communicate, and make local decisions have dominated consumer products, industry, and defense. A collection of such devices working together to achieve a desired behavior forms a multi-agent system (MAS) and is a particular instance of the IoT. The research literature on MASs shows their far-reaching applications, such as in social networks, economics, biology, and robotics. The common link between these disciplines is Network Science, which precisely describes how local interactions between agents affects the global behavior of a MAS. Generally, MASs can be engineered as either centralized or distributed. A centralized MAS relies on a master agent to make all decisions and provide a command to all agents. Conversely, a distributed MAS has each agent make its own decision and govern itself. While the behavior of a centralized MAS is directly controlled by the master agent, distributed MASs exhibit the aggregate behavior of all agents. Distributed MASs offer several advantages over their centralized counterparts by way of improved task flexibility, robustness to multiple points of failure, and increased productivity through scaling. Oftentimes, MASs, such as satellite constellations or platoons of autonomous vehicles, operate using a limited portable power supply and coordinate over a wireless communication network that has a finite network bandwidth.

Continuous communication, especially over large networks, may be wasteful and lead to degraded system performance via bandwidth saturation. Therefore, it is desirable to design control algorithms that require each agent in a MAS to communicate only when necessary to preserve a desired performance level. Intermittent and asynchronous communication between agents can achieve this goal, where intermittent communication refers to an agent having broadcast times that are discontinuous, and asynchronous communication refers to when the broadcast times of any pair of agents are desynchronized. Furthermore, in contested settings, reduced communication can promote concealment, which also motivates intermittent communication.

A distributed MAS can be modeled as a graph, which consists of nodes and edges. The nodes of a graph represent the agents in a MAS, and the edges depict the ability of certain pairs of agents to exchange information through communication. In practice, radios, cameras, and other sensors capable of providing information about an agent are effective within a fixed physical distance. Hence, the ability of two agents to communicate over a wireless communication network depends on the physical distance between them and explains why an edge may not exist between any pair of agents in a distance-based graph. An important graph property is connectivity, where a graph is said to be connected whenever information can be ferried between any pair of agents. In the context of static graphs, i.e., graphs with time-invariant nodes and edges, the desired behavior of a distributed MAS depends on several factors, where graph connectivity is a critical element. Another important component is the exchange accurate and reliable information. Like all control systems, the quality of feedback impacts the system's performance, where poor feedback can lead to unacceptable enactments.

While distributed MASs have the potential to offer several unrivaled and appealing qualities, the engineering of such systems is challenged by the need to develop control strategies capable of (a) preserving an initially connected graph under intermittent

and asynchronous state feedback, (b) testing the quality of received information in a distributed way, and (c) making decisions and acting upon information deemed reliable. This dissertation focuses on these challenges, where Chapter 1 provides an in-depth review of the literature and introduces necessary notation, graph theoretic concepts, and elements from hybrid systems literature to discuss Chapters 2–5.

One technique that facilitates the control of continuous-time dynamical systems using intermittent state feedback is event-triggered control (ETC), which promotes the efficient use of resources, like communication energy and bandwidth, through trigger-based sensing, actuation, and/or communication. Moreover, the trigger mechanism can be designed to ensure desired performance and stability properties. Self-triggered control (STC) improves upon ETC by leveraging model knowledge to design trigger mechanisms that enable an agent to determine their future event-times, as opposed to continuously monitoring a trigger mechanism like in ETC. However, ETC and STC are vulnerable to cyber-attacks due to their reduced employment of state feedback, which can produce undesirable and unsafe behaviors. Hence, this dissertation provides two strategies that create resilience to a particular class of cyber-attacks, i.e., the Byzantine attack.

Within the computer science literature, there exist multiple tactics an individual or process can launch to negatively influence a computer network. Examples of cyber-attacks include False-Data Injection (FDI), Denial-of-Service (DoS), Time-Delay-Switch (TDS), and Byzantine attacks. An FDI attack occurs when artificial information is introduced into the sensors of a system in an attempt to disrupt ordinary behavior. DoS attacks attempt to isolate and paralyze a system by saturating its communication bandwidth. TDS attacks employ a middleman that takes in information from one agent and transmits it to another with a time delay. A Byzantine attack occurs when an agent communicates false, delayed, or no information, and, therefore, can be thought

of as a combination of FDI, DoS, and TDS attacks. Because of their overarching characterization, this dissertation focuses on Byzantine attacks.

In Chapter 2, distributed event- and self-triggered controllers are developed for approximate leader-follower consensus with robustness to adversarial Byzantine agents for a class of homogeneous MASs. A strategy is developed for each agent to detect Byzantine agent behaviors within their neighbor set and then selectively disregard their transmission. Selectively removing Byzantine agents results in time-varying discontinuous changes to the network topology. Nonsmooth dynamics also result from the use of event/self-triggered strategies and triggering condition estimators that enable intermittent communication. Nonsmooth Lyapunov methods are used to prove approximate consensus of the MAS consisting of the remaining cooperative agents. Simulations are included to validate the result and to outline the trade-off between communication and performance.

Chapter 3 improves upon Chapter 2 by developing a model-free reputation strategy that can identify and isolate Byzantine agents from the remaining cooperative MAS. In particular, a distributed event-triggered controller for formation control and leader tracking (FCLT) with robustness to adversarial Byzantine agents and a class of heterogeneous MASs is created. Assuming each agent can accurately measure the state of a neighbor whenever the neighbor broadcasts its state, the reputation strategy allows each agent to detect Byzantine agent behaviors within their neighbor set and then selectively disregard Byzantine state information. Selectively ignoring Byzantine agents results in a time-varying network topology. Nonsmooth dynamics also result from intermittent communication due to the event-triggered strategy, which facilitates the efficient use of resources. Nonsmooth Lyapunov methods are used to prove stability and FCLT of the MAS consisting of the remaining cooperative agents.

As previously mentioned, one attractive property of MASs is their flexibility. One way to design flexibility into MASs is to divide a MAS into groups and have the groups

coordinate to achieve a desired task. In Chapter 4, the consensus problem for a clustered multi-agent system (C-MAS) is investigated. Given a MAS, the agents are organized into disjoint clusters, where each cluster forms a connected network. The agents that are within the same cluster can communicate continuously with their neighbors. Between some cluster pairs, there exists an inter-cluster that enables the relay of information between the two clusters. Agents that have neighbors in clusters different from their own can communicate intermittently and asynchronously with their different-cluster neighbors. The goal of each agent in the C-MAS is to have their state converge to an agreement value by sharing local information of a continuous-time homogeneous process. Note that the intermittent communication events of the continuous-time process are inherently hybrid. Therefore, a unique coupling between a static consensus protocol and a hybrid consensus protocol is designed. A closed-loop network model is presented using a hybrid systems framework. The consensus problem is then recast into a set stability problem and sufficient conditions of the consensus set are presented by leveraging a Lyapunov-based stability analysis. A C-MAS composed of 16 agents that is partitioned into 3 clusters and 2 inter-clusters is used to illustrate the results through numerical simulations and shown to achieve consensus using the proposed control strategy.

Chapter 5 explores the rendezvous problem for a MAS with distance-limited, intermittent communication and sensing. Unlike previous works that provide specific event-triggered controllers, a framework that characterizes a family of distributed event-triggered controllers leveraging non-singular edge-potentials to achieve approximate rendezvous while maintaining the initial distance-limited graph is provided. The proposed framework excludes the possibility of Zeno behavior and accommodates the development of self-triggered controllers. The combination of continuous and impulsive dynamics results in a hybrid system, where a closed-loop dynamics of the MAS are presented and analyzed using hybrid differential inclusions. The approximate rendezvous

problem is recast into a set stabilization problem and sufficient conditions of the rendezvous set are obtained through a Lyapunov-based analysis. Simulation results are provided to validate the development.

Chapter 6 concludes the dissertation by highlighting the contributions of the developed controllers and discussing future extensions.

CHAPTER 1
INTRODUCTION

1.1 Background

A group of agents that collaborate to achieve a desired behavior is referred to as a multi-agent system (MAS). While there is no size or intelligence restriction on an agent, agents are capable of controlling their actions and internal states to some degree, interacting with other agents through a communication protocol, perceiving and reacting to their environment, and actuating in a manner that generates objective-oriented behavior. MASs can produce numerous utilities such as radionavigation (e.g., GPS) from a satellite network, the surveillance of a region of interest, such as a battlefield or a habitat by autonomous aerial, ground, surface, and/or underwater vehicles, and the internet, which is a product of distributed computing. By cooperating and sharing resources, MASs may outperform a single agent, and, in certain cases, overcome challenges that may be too difficult for a monolithic system. MASs can be categorized as either centralized or distributed. A *centralized* MAS is defined as a MAS that is controlled by a single master agent based on information provided by all other agents, i.e., one robot makes decisions for itself and all other members of the system. Conversely, a *distributed* MAS is a MAS where each agent makes its own decisions and governs its own conduct while only using local information, i.e., information from neighbors, where the number of neighbors of any agent is strictly smaller than the total number of agents.

The reliance on a master agent to control a large centralized MAS leads to control algorithms that are computationally intensive, difficult to scale, and vulnerable due to having a single point of failure (the master agent). Furthermore, centralized MASs may be ill-suited for applications conducted over an expanse since the master agent's need for global information may be challenged by unmanageable communication delays. Distributed MASs bypass these complications by allowing each agent to function

independently while yielding coordinated outcomes. Such division of labor, however, is achieved at the expense of additional complexity and cost.

The consensus problem is a fundamental and widely explored area of research within the controls and network science communities [1–5]. Consensus can be found in numerous applications, such as in the rendezvous of mobile robots [6, 7], attitude synchronization between multiple satellites [8, 9], and verification of distributed ledgers to promote blockchain security [10]. One popular variant of consensus is approximate leader-follower consensus. With respect to a mobile MAS, approximate leader-follower consensus is achieved whenever the follower agents of a MAS are driven within a small distance of the leader's position and remain within such a distance for all future time (forward-invariance of a neighborhood of the leader's position). Most consensus results consider continuous-time dynamical MASs and assume continuous communication and sensing. However, physical constraints on a network, like communication bandwidth, data packet losses, and delays, may inhibit continuous communication.

Motivated by intermittent communication challenges, event-triggered control (ETC) enables the manipulation of continuous-time dynamical systems under intermittent state feedback (cf. [11–16]). ETC opportunistically selects when to update the system to efficiently perform a task [17]. In a MAS, inter-agent communication occurs at times dictated by an event-trigger mechanism, which is derived from the need to preserve system stability and, if desired, a performance criterion [18]. For example, [11] investigates event-triggered pinning control for the synchronization of complex networks of nonlinear dynamical systems. A multi-agent formation control problem is investigated in [19] with ETC updates and additive disturbances, where agents only communicate by exchanging information via a cloud repository. In [13], a decentralized controller is developed that uses ETC scheduling to enable leader-follower consensus under fixed and switching communication topologies.

The event-trigger design can have significant ramifications on the overall system performance. Typically, agents are required to continuously monitor their trigger condition while each neighbor continuously monitors a neighbor's communication. Self-triggered control (STC) provides a more efficient triggering method that leverages the system model to predict when to monitor/communicate (cf. [20, 21]). Moreover, a STC strategy can also be developed that eliminates the need for an agent's neighbors to continuously monitor for information requests.[1] While ETC and STC strategies provide numerous benefits, critical communication timing conditions introduce potential vulnerabilities. Specifically, since the trigger conditions are based on feedback from multiple agents, erroneous feedback can lead to undesired outcomes.

Assuming knowledge of the number of adversarial agents, the authors in [23] study event-triggered secure cooperative control of linear MASs under Denial-of-Service (DoS) attacks. Static networks with cooperative and malicious nodes have been extensively studied within the computer science literature [24, 25], resulting in iterative consensus algorithms for distributed computing applications that are robust to components subject to faults. Different research communities are beginning to extend these architectures to MAS applications consisting of mobile agents, which requires the nontrivial study of motion planning to preserve algebraic graph properties, such as connectivity. For example, [26] addresses the problem of resilient in-network consensus in the presence of Byzantine nodes [24], where resilience is designed for worst-case security breaches and omnipotent malicious nodes. The Weighted-Mean-Subsequence-Reduced (W-MSR) algorithm enables each node to receive state information from its neighbors, sort the states, and neglect at most F extreme states relative to the node's state. While asymptotic consensus is obtained using the W-MSR algorithm, the

[1] Eliminating the need for continuous monitoring allows the potential for power savings [22].

result requires an upper bound of the maximum number of Byzantine agents. Such an approach requires at least $2F + 1$ reliable neighbors, which is difficult to scale with increasing node number. Moreover, information is shared with all agents regardless of their cooperative/Byzantine status, which can impact secure MAS consensus. The result in [27] also enables resilient consensus assuming the maximum number of malicious agents is known. The result in [28] achieves resilient approximate consensus by removing extreme values similar to the W-MSR algorithm while enabling asynchronous communication through a self-triggered strategy given a known upper bound for the maximum number of Byzantine agents. The result in [29] achieves consensus tracking of an arbitrary piecewise continuous step function for a network of agents using the W-MSR algorithm provided the network is strongly $(2F + 1)-$robust. While malicious agent identification is not required, MAS consensus is limited to at most F malicious agents. Nonetheless, ETC and STC strategies that enable secure MAS consensus while detecting and mitigating against Byzantine adversaries require further investigation.

In graph theoretic terms, antagonistic interactions can be modeled by replacing the standard communication graph, characterized by nonnegative weights, with a signed graph displaying both positive and negative weights (cf. [30, 31]). Positive directed/undirected paths correspond to cooperative interactions with agents, while negative directed/undirected paths describe interactions with antagonistic agents. The work in [32] develops the concept of bipartite consensus among agents with antagonistic interaction, where bipartite consensus or agreed dissensus is defined as when all agents in the MAS converge to a state that is the same in magnitude but not in sign, effectively enabling each team to reach their own consensus state. By addressing the classical example of homogeneous agents modeled as simple scalar integrators, [32] proves that if the signed, weighted and connected communication graph describing the agents' interactions is structurally balanced, then the agents reach bipartite consensus. If the interactions are antagonistic, but not structurally balanced,

the only agreement that can be achieved among the agents is the trivial one, where all the agents' states converge to zero.

The authors in [33] extend the results in [32] to a MAS consisting of N agents with linear time-invariant (LTI) dynamics and establish conditions to ensure consensus and bipartite consensus under the assumption that the agent interactions can be described by a weighted, signed, connected, and structurally balanced graph. Moreover, bipartite consensus can always be reached under the assumption that the agent dynamics are stabilizable. However, consensus to a common state for the two antagonistic groups can be achieved only under more restrictive requirements on the Laplacian associated with the communication graph and on the agents' description. In particular, consensus may be achieved only if there is some equilibrium between the two groups, both in terms of cardinality and in terms of the weights of the conflicting interactions among agents. The result in [34] considers the bipartite consensus problem for a MAS composed of agents with LTI dynamics and input saturation over directed and unbalanced networks.

The works in [32–34] share the common goal of enabling both teams in the antagonistic network to reach their own respective consensus, which assumes both consensus states can coexist. However, signed graphs can also be extended to applications, where the goal of one team is to reach consensus while the goal of the opposition is to prevent the other team from reaching consensus. Such a scenario works under the assumption that each team has a goal and must cooperatively work together to reach their goal. However, it is not possible for both teams to reach their goal simultaneously. Hence, if one team is to conspire against the other in a cooperative manner, then signed graphs can be leveraged to model these interactions. However, if one group is organized while the other is not, a traditional graph is sufficient to model the cooperative interactions of the organized team.

Common threats in contested environments include: Denial-of-Service (DoS) attacks, Time-Delay Switch (TDS) attacks, and Byzantine attacks. A DoS attack occurs

when an adversary interrupts communication within a network [23], a TDS attack occurs when an adversary imparts time delays on communication within a network [35], and a Byzantine attack is a more general threat where communication can be delayed, corrupted, and/or interrupted arbitrarily [24]. As a result, we focus on Byzantine threats since they are a generalization of DoS and TDS attacks. As in [36], we consider two types of Byzantine behavior. A *Type I Byzantine agent* remains in the mobile network, where it can halt, delay, or corrupt information communicated to its neighbors temporarily or indefinitely. A *Type II Byzantine agent* abandons the mobile network while communicating true or no state information about itself temporarily or indefinitely. These designations are not fixed for all time, and any adversary can be categorized as either type at any time.

Results such as [26, 27, 29] attain consensus in the presence of Type I Byzantine adversaries. However, they are not able to identify Byzantine threats nor can they alter the communication network to stop data sharing between the cooperative and Byzantine agents as in [36]. In [36], Byzantine adversaries are identified through a Lyapunov-based detector that compares communicated state information to worst-case state estimates that are based on accurate past neighbor state information and model knowledge. While such a strategy enables Byzantine agent detection, it is limited in the sense that the detector requires an upper bound on the control of each neighboring agent, which may be unknown *a priori*. Moreover, once an agent is categorized as a Byzantine adversary, it cannot be reincorporated back into the cooperative agent set even if it becomes cooperative. Such a scenario can occur when the communication links between a group of cooperative agents is temporarily jammed by an adversary. These limitations can potentially be circumvented through the use of a reputation algorithm [37], which does not require exact model knowledge of each neighbor's dynamics, does not require bounds on neighbor quantities, such as control, and enables

the re-integration of rehabilitated agents, i.e., agents that convert from Byzantine to cooperative.

While early results on consensus were built on undirected connected communication graphs [38], works like [39] enable consensus through the use of weight-balanced directed communication graphs that are infinitely often jointly strongly connected. Because continuous communication between neighbors in a network places a constraint on the physical distance between agent pairs, control algorithms constructed on infinitely often jointly connected graphs, which allow for the intermittent relaxation of physical distance constraints, have grown in interest [40–42].

Akin to the idea of intermittently connected graphs, clustered MASs have also been an active area of research since they impart high-level task division among subgroups of the whole MAS. For example, the work in [43] presents a distributed cluster consensus control algorithm, where if the communication between clusters is directed and acyclic, then each cluster can achieve local consensus for both fixed and switching graphs. The authors in [44] study the clustered formation control problem for MASs with intermittent and delayed communication. Given a MAS that is divided into M clusters, the result presents a distributed controller that enables each cluster to assemble a unique formation.

While cluster control strategies grant each component of a MAS autonomy, these same techniques can be leveraged to obtain system-wide consensus while reducing the communication between clusters. Recently, [45] proposed a distributed controller that enables system-wide consensus for a clustered MAS (C-MAS), i.e., a MAS that is partitioned into clusters, consisting of agents with LTI dynamics. The result designates each cluster a single leader, where only the leaders of each cluster are allowed to intermittently communicate through a fixed directed graph. Furthermore, the communication topology within each cluster is modeled as a fixed and directed graph, where agents in the same cluster can continuously communicate with their neighbors. While [45]

relaxes the communication load when compared to systems that require continuous communication in the entire MAS, the result is limited in the sense that each cluster can only have a single leader, where all cluster leaders communicate intermittently at the same time. This implies that all cluster leaders must be physically close to enable communication.

Network communication is often expressed in terms of distance-based constraints: two agents may communicate if they are sufficiently close. Even though network connectivity is a necessary component for achieving MAS objectives, it is often the case that assumptions are introduced about the network remaining connected or that continuous communication along edges is always possible [17, 37, 46–48]. Ensuring connectivity in real-time poses non-trivial challenges, even in the presence of continuous communication [49]. Centralized and distributed variants of the connectivity maintenance problem under continuous inter-agent communication have been extensively studied [49–54], as well as in discrete-time [55], where connectivity maintenance can be addressed inductively. Conversely, few results on distributed event-triggered control with connectivity maintenance are available [56–58], all based on some version of consensus dynamics (i.e., the right-hand side of the closed-loop dynamics of the ensemble is the product between the weighted graph Laplacian and the state of the ensemble). In general, there is no straightforward reduction of the event-triggered version of this problem to either the smooth or discrete-time settings.

The result in [56] presents an event-triggered control approach to approximate rendezvous for a MAS. Piecewise continuous state-dependent gains on the standard (unweighted) consensus dynamics are used to preserve the edges of a distance-based communication graph. However, the proposed event trigger requires continuous access to inter-agent displacements, which implies continuous demand for sensing and/or communication, where only the controller updates are intermittent. The result in [57] investigates formation control with event-triggered connectivity preservation. The

objective is achieved with intermittent sensing and broadcasting. Maintenance of the initial graph is achieved using unbounded edge-tension functions, originally presented in [7], where the Laplacian is weighted by the tension functions. In practice, unbounded tension functions impose unnecessary restrictions on the space of initial configurations, due to actuation limitations. Recently, the authors in [58] developed an event-triggered controller and observer that achieve leader-follower consensus while maintaining the edges of an initially connected graph. Edge preservation is achieved through the use of bounded edge-potentials and intermittent communication determined by event triggers. The results in [57] and [58] provide inroads to MAS coordination with graph maintenance. These results share an approach of matching specific pre-selected time-based triggers to the MAS dynamics as a means to guarantee the desired properties (graph-maintenance, continuous-time completeness, and stability).

1.2 Contributions of the Dissertation

Control systems operating under intermittent state feedback are vulnerable to cyber-attacks, where the injection of inaccurate or nefarious information can lead to undesirable and unsafe system behavior. Distributed network control systems can also be subjected to cyber-attacks, where damaging key nodes in a network with low vertex connectivity may cause the network to become disconnected, and, as a result, lead to instability. Given the multitude of attacks, this dissertation focuses on the Byzantine attack model, which captures the communication of inaccurate, delayed, or no information. Therefore, distributed MASs coordinating with intermittent state feedback are especially sensitive to Byzantine attacks, which motivates the development of Byzantine-resilient control algorithms.

In Chapter 2 and the result in [59], the approximate leader-follower consensus problem for cooperative agents in the presence of Byzantine adversaries is investigated, where approximate leader-follower consensus is achieved when the state of the followers is driven into a forward invariant neighborhood of the state of the leader. Since only

the cooperative followers must collaborate to reach leader-follower consensus and the Byzantine adversaries are assumed to operate independently (i.e., do not work together against the cooperative followers), a traditional unsigned graph is used to model the network topology of the followers. Moreover, this chapter presents event- and self-triggered strategies for the approximate leader-follower consensus problem while providing robustness to Byzantine adversaries. Unlike methods such as W-MSR, that need to know an upper bound on the number of Byzantine agents *a priori* and then reject some amount of outlier information, the work in this chapter uses a Lyapunov-based detection strategy to identify Byzantine actors online. Motivated by the potential for different ways in which an agent can be compromised (e.g., different combinations of sensing, actuation, or computation can be degraded) and different potential responses to such behavior, Chapter 2 segregates Byzantine agents into different categories. Based on the agent category, the resulting graph can become directed, time-varying, and unbalanced. Despite these complications, the result achieves approximate leader-follower consensus, between the leader and cooperative followers, in a distributed manner, where each agent's control input is computed from local neighbor interactions. Moreover, in the absence of Byzantine adversaries, this work can recover the result in [13] for static graphs, which did not consider Byzantine agents. The stability of the event- and self-triggered control strategies are examined through a nonsmooth Lyapunov analysis. This result is a generalization of the precursory result in [36]. Specifically, this chapter provides broader context, additional mathematical development for the stability analysis, a more detailed fault detection method, and simulation results investigating the trade-off between the event- and self-triggered strategies with respect to power savings, communication bandwidth, and performance.

The Byzantine agent detector used in Chapter 2 relies on model knowledge, which is not readily applicable to MASs with uncertain dynamics. As a result, Chapter 3 and the result in [60] improve upon Chapter 2 by developing a trust model and a

reputation algorithm that can identify Byzantine agents without the need of a dynamic model. The trust model and reputation algorithm are then used in a distributed event-triggered controller to achieve Byzantine-resilient formation control and leader tracking (FCLT) for a MAS consisting of agents with uncertain heterogeneous control-affine dynamics. Specifically, FCLT refers to a set of follower agents tracking the trajectory of a leader agent while the follower agents maintain a predefined formation. The reputation strategy enables coordination between cooperative agents only, while enabling the capability of reintegrating rehabilitated agents. Additionally, this strategy also enables malfunctioning agents to be isolated from the cooperative MAS to ensure safety and enable the remaining agents to achieve the objective. A malfunctioning agent can be reintegrated into the network once functional operational control can be established. By coordinating only with cooperative neighbor information, the influence from each Byzantine adversary is cut out from the network consisting of only the cooperative followers. The Byzantine detection strategy is based on two-point authentication, e.g., comparing communicated and sensed state information, where the redundancy in state information enables Byzantine agent detection. Selectively ignoring Byzantine agents results in a time-varying graph topology. Nonsmooth dynamics also result from intermittent communication due to an event-triggered strategy, which facilitates the efficient use of resources. Nonsmooth Lyapunov methods are used to prove stability and FCLT of the MAS consisting of the remaining cooperative agents.

The preliminary result in [46] established the concept of using a zero-order hold to enable formation control and leader tracking with intermittent communication between the followers only and the use of trust and reputation models to impart resilience to Byzantine adversaries. In this chapter and the result in [60], a more complete development of the ideas in [46] is provided by: (a) a revised, more detailed, and more rigorous narrative and presentation, (b) a generalization of the mathematics to relax the previous requirement of continuous communication with the leader to allow only

intermittent feedback, (c) a proof of the existence of a positive uniform lower bound for the difference between consecutive broadcast events for each agent, including the leader, and (d) simulation results that demonstrate the performance of the developed methods.

Flexibility is an attractive property of MASs. One way to design flexibility into MASs is to partition the node set and assign each subset of the node set (*cluster*) a desired task. Note that the graph structure connecting two clusters is referred to as an *inter-cluster*. Motivated by [45] and [61], Chapter 4 and the result in [62] develop a distributed controller that enables a C-MAS composed of agents with LTI dynamics to obtain system-wide consensus, where the number of agents that can communicate between clusters is not restricted and the communication between clusters can be both intermittent and asynchronous. Since this dissertation focuses on intermittent communication as a means to conserve resources, the communication rate within inter-clusters is limited to alleviate the communication demands of the global network. Such a strategy also accommodates scenarios where clusters are often physically separated from each other but can exchange information by occasionally meeting. Given a MAS coordinating over a communication topology that is modeled with an undirected graph, the agents are organized into disjoint clusters, where each cluster forms a connected network. Within each cluster, each agent is allowed to continuously communicate with their neighbors that are within the same cluster. Conversely, agents within an inter-cluster are allowed to intermittently communicate with their neighbors that are within the same inter-cluster. The result is a mixture of continuous communication and both intermittent and asynchronous communication within the global network. The goal of each agent in the C-MAS is to have their state converge to an agreement value by sharing local information of a continuous-time homogeneous process. Note that the intermittent communication events of the continuous-time process are inherently hybrid. Therefore, a unique coupling between a static consensus protocol and a hybrid

consensus protocol is designed. The closed-loop network model is presented using the hybrid systems framework of [63]. The consensus problem is then recast into a set stability problem and sufficient conditions of the consensus set are presented through a Lyapunov-based stability analysis. A C-MAS composed of 16 agents that is partitioned into 3 clusters and 2 inter-clusters is used to illustrate the results through numerical simulations and shown to achieve consensus using the proposed control strategy.

The last key issue addressed in this dissertation is the design of event-triggered controllers capable to preserving the connectivity of an initially connected graph. Chapter 5 and the result in [64] study the event-triggered rendezvous problem while also seeking to preserve the edges of an initially connected graph for a MAS consisting of single-integrator agents. The result differs from [56–58] in that it characterizes a family of distributed event/self-triggered controllers that (a) utilize continuously differentiable (i.e., class C^1) edge-potentials for graph maintenance; (b) ensure completeness of maximal solutions while excluding Zeno behavior; and (c) given a user-defined parameter $\nu > 0$, exponentially drive the MAS to ν-approximate rendezvous. Note that ν-approximate rendezvous occurs when a MAS is in a configuration where all agent states are within a distance of at most ν from each other. Furthermore, this framework identifies specific properties that the trigger mechanisms must satisfy and provides users the relative freedom to design an event trigger mechanism that satisfies their needs. The novelty of this result is that it provides a general formal treatment of event/self-triggered control for MAS rendezvous with graph maintenance within the hybrid differential inclusions framework of [63]. Using hybrid time enables a particularly concise analysis of the interactions between the clocks of the individual agents, event triggers, and dynamical properties of the overall system in this setting. The theoretical guarantees are independent of the particular form of the trigger, allowing for a variety of trigger designs. Finally, this chapter and the result in [64] expand the result of [54] in two significant ways. First, the new proposed edge-tension function removes the restriction

from [54] on the length of the initial edges (which are required to be significantly shorter than the communication radius), and illuminate the trade-off between how close an edge is to breaking and the control effort required to preserve the edge. Hence, unnecessary restrictions on the admissible set of initial configurations are removed. Second, the need for continuous communication/sensing is relaxed by employing an event/self-triggered control strategy. A simulation example for a 9-agent MAS with single integrator dynamics is presented and confirms the results.

Chapter 6 concludes the dissertation by providing a summary of the contributions for Chapters 2–5 and discussing future work.

1.3 Preliminaries

1.3.1 Notation

Let $\mathbb{R}$ and $\mathbb{Z}$ denote the set of real numbers and integers, respectively. Additionally, let $\mathbb{R}_{\geq x} \triangleq [x, \infty)$, $\mathbb{R}_{>x} \triangleq (x, \infty)$, $\mathbb{R}_{<x} \triangleq (-\infty, x)$, $\mathbb{Z}_{\geq x} \triangleq \mathbb{R}_{\geq x} \cap \mathbb{Z}$, and $\mathbb{Z}_{>x} \triangleq \mathbb{R}_{>x} \cap \mathbb{Z}$ for $x \in \mathbb{R}$. For $p, q, n \in \mathbb{Z}_{>0}$, the $p \times q$ zero matrix and the $p \times 1$ zero column vector are denoted by $0_{p\times q}$ and 0_p, respectively. The $p\times p$ identity matrix and the $p\times 1$ column vector of ones are denoted by I_p and 1_p, respectively. The Euclidean norm of a vector $r \in \mathbb{R}^p$ is denoted by $\|r\| \triangleq \sqrt{r^\top r}$. For $x, y \in \mathbb{R}^n$, the inner product between x and y is denoted by $\langle x, y\rangle$, where $\langle x, y\rangle = x^\top y$. Given a positive integer M, define $[M]$ as the set $\{1, 2, ..., M\}$. The Kronecker product of $A \in \mathbb{R}^{p\times q}$ and $B \in \mathbb{R}^{u\times v}$ is denoted by $(A \otimes B) \in \mathbb{R}^{pu\times qv}$. The block diagonal matrix whose diagonal blocks consist of $G_1, G_2, ..., G_n$ is denoted by diag$(G_1, G_2, ..., G_n)$. The i^{th} eigenvalue of a symmetric matrix $G \in \mathbb{R}^{p\times p}$ is denoted by $\lambda_i(G) \in \mathbb{R}$. The maximum and minimum eigenvalues of G are denoted by $\lambda_{\max}(G) \in \mathbb{R}$ and $\lambda_{\min}(G) \in \mathbb{R}$, respectively. The maximum singular value of $A \in \mathbb{R}^{p\times q}$ is denoted by $S_{\max}(A) \in \mathbb{R}_{\geq 0}$. The symbols $\wedge$, $\vee$, and $\neg$ denote logical AND, OR, and NOT, respectively. The complement and power set of the set $\mathcal{S}$ are denoted by $\mathcal{S}^{\complement}$ and $2^{\mathcal{S}}$, respectively. The Frobenius norm of $A \in \mathbb{R}^{p\times q}$ is denoted by $\|A\|_F \triangleq \sqrt{1_p^\top (A \odot A) 1_q}$, where $\odot$ denotes the Hadamard product. The class C^1 refers to the set of continuously

differentiable functions. Let f be an essentially bounded measurable function. Then, $f \in \mathcal{L}_\infty$ if and only if $\inf\{C \geq 0 : |f(x)| \leq C \text{ for almost every } x\} \in \mathbb{R}_{\geq 0}$. For any sets A, B, a function f of A with values in B is denoted by $f\colon A \to B$, whereas $f\colon A \rightrightarrows B$ refers to a *set-valued* function $f\colon A \to 2^B$. The exponential function with base e and argument x is denoted by either $\exp(x)$ or e^x. Given a closed set $A \subset \mathbb{R}^n$ and a point $x \in \mathbb{R}^n$, the distance of x to A is denoted by $|x|_A \triangleq \inf\{\|x - y\| : y \in A\} \geq 0$.

1.3.2 Graphs

Let $\mathcal{G}(t) \triangleq (\mathcal{V}, \mathcal{E}(t), \mathcal{A}(t))$ be a time-varying, weighted, and undirected graph with node set $\mathcal{V} \triangleq [N]$ for some $N \in \mathbb{Z}_{>0}$, undirected edge mapping $\mathcal{E} : [0,\infty) \to 2^{\mathcal{V}\times\mathcal{V}}$, and weighted adjacency matrix $\mathcal{A}(t) \triangleq [a_{ij}(t)]$, where $a_{ij} : [0,\infty) \to [0,1]$. Within the context of this work, no self-loops are considered, and therefore, $a_{ii}(t) \triangleq 0$ for all $i \in \mathcal{V}$ and $t \geq 0$. In general, $a_{ij}(t) \neq a_{ji}(t)$, but equality is possible. An undirected edge is defined as an ordered pair (j,i), where $(j,i) \in \mathcal{E}(t)$ if and only if $(i,j) \in \mathcal{E}(t)$. Note that $(j,i) \in \mathcal{E}(t)$ implies node j can send information to node i. Moreover, $a_{ij}(t) \geq 0$ if $(j,i) \in \mathcal{E}(t)$, and $a_{ij}(t) = 0$ if $(j,i) \notin \mathcal{E}(t)$. An undirected graph is called connected if and only if there exists a sequence of edges in $\mathcal{E}(t)$ between any two distinct nodes. The time-varying neighbor set of node i is defined by $\mathcal{N}_i : [0,\infty) \to 2^{\mathcal{V}}$, where $\mathcal{N}_i(t) \triangleq \{j \in \mathcal{V} \setminus \{i\} : (j,i) \in \mathcal{E}(t)\}$.

The diagonal degree matrix of the undirected graph $\mathcal{G}(t)$ is denoted by $\Delta(t) \triangleq [\Delta_{ij}(t)]$, where, for all $i \neq j$ and $t \geq 0$, $\Delta_{ij}(t) \triangleq 0$ and $\Delta_{ii}(t) \triangleq \sum_{j\in\mathcal{V}} a_{ij}(t)$. The graph Laplacian $L : [0,\infty) \to \mathbb{R}^{N\times N}$ of the undirected graph $\mathcal{G}(t)$ is given by $L(t) \triangleq \Delta(t) - \mathcal{A}(t)$. Consider a single node, indexed by 0, along with the mapping $D : [0,\infty) \to \mathbb{R}^{N\times N}_{\geq 0}$ such that $D \triangleq [d_{ij}]$ and $d_{ij} : [0,\infty) \to [0,a]$ for some $a \in \mathbb{R}_{>0}$. For all $i \neq j$ and $t \geq 0$, $d_{ij}(t) \triangleq 0$. Let $d_i(t) \triangleq d_{ii}(t)$, where, if there exists an edge between nodes 0 and i, then $d_i(t)$ denotes the weight assigned to this edge. Therefore, $D(t)$ is a diagonal pinning matrix. The flow of information between the agents of a MAS consisting of N followers is encoded through the graph Laplacian $L(t)$. If a MAS

consists of a leader and N follower agents, then the flow of information between the agents is represented by $H : [0, \infty) \to \mathbb{R}^{N \times N}$ such that $H(t) \triangleq L(t) + D(t)$. The Laplacian of the complete graph on N nodes is denoted by $L_C \in \mathbb{R}^{N \times N}$.

1.3.3 Hybrid Systems

A hybrid system $\mathcal{H}$ with state $z \in \mathbb{R}^n$ and data (C, f, D, G) is defined as

$$\mathcal{H}: \begin{cases} \dot{z} = f(z), & z \in C, \\ z^+ \in G(z), & z \in D, \end{cases} \tag{1–1}$$

where $f : \mathbb{R}^n \to \mathbb{R}^n$ denotes the flow map that models continuous behavior, $C \subset \mathbb{R}^n$ denotes the flow set over which the system continuously evolves, $G : \mathbb{R}^n \rightrightarrows \mathbb{R}^n$ denotes the set-valued jump map that models discrete behavior, and $D \subset \mathbb{R}^n$ denotes the jump set over which the system discretely evolves. A solution ϕ to the hybrid system $\mathcal{H}$ is parameterized with respect to hybrid-time as denoted by $(t, j) \in \mathbb{R}_{\geq 0} \times \mathbb{Z}_{\geq 0}$. Observe that t denotes continuous time, and j denotes discrete time. The domain dom $\phi \subset \mathbb{R}_{\geq 0} \times \mathbb{Z}_{\geq 0}$ is called a hybrid time domain if for all $(T, J) \in$ dom ϕ, dom $\phi \cap ([0, T] \times \{0, 1, ..., J\})$ can be expressed as $\cup_{j=0}^{J}(I_j \times \{j\})$, where $I_j \triangleq [t_j, t_{j+1}]$ for a time sequence $0 = t_0 \leq t_1 \leq ... \leq t_{J+1}$.[2] Note that t_j indicates the j^{th} instance the state z jumps. A solution ϕ to $\mathcal{H}$ is called maximal if ϕ cannot be extended, that is, ϕ is not a truncated version of another solution. A solution is called complete if its domain is unbounded. A solution is said to be precompact if it is complete and bounded. The set $\mathcal{S}_{\mathcal{H}}$ contains all maximal solutions to $\mathcal{H}$, where the set $\mathcal{S}_{\mathcal{H}}(\xi)$ contains all maximal solutions to $\mathcal{H}$ from ξ. A hybrid system $\mathcal{H} = (C, f, D, G)$ with data in (1–1) is said to satisfy the *hybrid basic conditions* if it satisfies the conditions in [63, Assumption 6.5].

[2] Given a set-valued mapping $H : \mathbb{R}^m \rightrightarrows \mathbb{R}^n$, the domain of H is the set dom $H \triangleq \{x \in \mathbb{R}^m : H(x) \neq \varnothing\}$ [63, Definition 2.1].

1.3.4 Relevant Stability Notions

Definition 1.1. [65, Definition 4.6] *(uniformly ultimately bounded)* The solutions to $\dot{x} = f(x,t)$ are *uniformly ultimately bounded* if there exist positive constants b and c, independent of $t_0 \geq 0$, and for every $a \in (0,c)$, there is a $T = T(a,b) \geq 0$, independent of t_0, such that

$$\|x(t_0)\| \leq a \Longrightarrow \|x(t)\| \leq b, \ \forall t \geq t_0 + T.$$

Definition 1.2. [66] *(global exponential stability)* Let a hybrid system $\mathcal{H}$ be defined on $\mathbb{R}^n$. Let $\mathcal{A} \subset \mathbb{R}^n$ be closed. The set $\mathcal{A}$ is said to be *globally exponentially stable* (GES) for $\mathcal{H}$ if there exist $\kappa, \alpha > 0$ such that every maximal solution ϕ to $\mathcal{H}$ is complete and satisfies

$$|\phi(t,j)|_{\mathcal{A}} \leq \kappa \exp(-\alpha(t+j))|\phi(0,0)|_{\mathcal{A}}$$

for each $(t,j) \in$ dom ϕ.

CHAPTER 2
EVENT/SELF-TRIGGERED APPROXIMATE LEADER-FOLLOWER CONSENSUS WITH RESILIENCE TO BYZANTINE ADVERSARIES

Distributed event- and self-triggered controllers are developed for approximate leader-follower consensus with robustness to adversarial Byzantine agents for a class of homogeneous MASs. A strategy is developed for each agent to detect Byzantine agent behaviors within their neighbor set and then selectively disregard their transmission using accurate past information and model knowledge. Selectively removing Byzantine agents results in time-varying discontinuous changes to the network topology. Nonsmooth dynamics also result from the use of event/self-triggered strategies and triggering condition estimators that enable intermittent communication. Nonsmooth Lyapunov methods are used to prove approximate consensus of the MAS consisting of the remaining cooperative agents.

2.1 Agent Dynamics and Network Topology

Consider a homogeneous MAS consisting of a single leader indexed by 0 and a set of $N \in \mathbb{Z}_{>0}$ follower agents indexed by $\mathcal{V}$. The linear time-invariant model of agent $i \in \mathcal{V} \cup \{0\}$ is

$$\dot{x}_i(t) = Ax_i(t) + Bu_i(t), \tag{2–1}$$

where $x_i : [0, \infty) \to \mathbb{R}^m$ denotes the position, $\dot{x}_i : [0, \infty) \to \mathbb{R}^m$ denotes the velocity, $A \in \mathbb{R}^{m \times m}$ denotes the known constant state matrix, $B \in \mathbb{R}^{m \times n}$ denotes the known full-row rank control effectiveness matrix, and $u_i : [0, \infty) \to \mathbb{R}^n$ denotes the control input for agent i. Within this work, the followers can be categorized as either Byzantine or cooperative. Let the mapping $\mathcal{B} : [0, \infty) \to 2^{\mathcal{V}}$ define the time-varying set of Byzantine agents and the mapping $\mathcal{C} : [0, \infty) \to 2^{\mathcal{V}}$ define the time-varying set of cooperative agents, where $\mathcal{B}(t) \cap \mathcal{C}(t) = \varnothing$ and $\mathcal{B}(t) \cup \mathcal{C}(t) = \mathcal{V}$ for all $t \geq 0$. The following assumptions are made to facilitate the subsequent analysis.

Assumption 2.1. Each agent is capable of measuring its own position for all $t \geq 0$.

Assumption 2.2. The pair (A, B) is stabilizable.

Assumption 2.3. The control and state of the leader are continuous and bounded, i.e., there exists $M_0,\ \overline{M}_0 \in \mathbb{R}_{>0}$ such that $\|u_0(t)\| \leq M_0$ and $\|x_0(t)\| \leq \overline{M}_0$ for all $t \geq 0$.

The flow of information between the followers of the MAS is modeled by a time-varying, weighted, and undirected graph $\mathcal{G}(t) = (\mathcal{V}, \mathcal{E}(t), \mathcal{A}(t))$. Within this work, $(j, i) \in \mathcal{E}(t)$ if and only if $\|x_i(t) - x_j(t)\| \leq R_{\text{com}}$, where $R_{\text{com}} \in \mathbb{R}_{>0}$ denotes the communication radius of each agent $i \in \mathcal{V} \cup \{0\}$. It then follows that $\mathcal{N}_i(t) = \{j \in \mathcal{V} \setminus \{i\} : \|x_i(t) - x_j(t)\| \leq R_{\text{com}}\}$. Let $\mathcal{E}_C(t)$ denote the undirected edge set and $\mathcal{A}_C(t)$ denote the weighted adjacency matrix associated with all cooperative followers in $\mathcal{C}(t)$. The sub-MAS consisting of only the cooperative followers is modeled by the time-varying, weighted, and undirected graph $\mathcal{G}_C(t) \triangleq (\mathcal{C}(t), \mathcal{E}_C(t), \mathcal{A}_C(t))$ and is referred to as the cooperative MAS (CMAS).

Assumption 2.4. The leader is a cooperative agent for all $t \geq 0$.

Assumption 2.5. The graph $\mathcal{G}_C(t)$ is connected for all $t \geq 0$, and $d_i(t) = 1$ for some $i \in \mathcal{C}(t)$ for all $t \geq 0$.[1]

2.2 Objectives

The objective is to design distributed event- and self-triggered controllers for each cooperative agent governed by (2–1) to achieve approximate leader-follower consensus while identifying Byzantine adversaries and disregarding their disruptive inputs. Resilience to Byzantine adversaries is achieved by providing each follower the ability to detect Byzantine agents in their neighbor set and delete existing edges between themselves and all Byzantine neighbors. The result ensures each cooperative agent coordinates its motion based only on information from cooperative neighbors

[1] Future works will develop network connectivity maintenance methods for the CMAS. Potential inroads to such results include [51].

yielding $\mathcal{G}_C(t)$. To quantify the consensus objective, let $e_{1,i} : [0, \infty) \to \mathbb{R}^m$ be defined as

$$e_{1,i}(t) \triangleq x_i(t) - x_0(t). \tag{2–2}$$

Approximate leader-follower consensus is achieved when $e_{1,i}(t)$ is uniformly ultimately bounded (UUB) for all cooperative followers $i \in \mathcal{V}$. Since the behavior of Byzantine agents cannot be guaranteed, the objective can only be satisfied by the cooperative agents. The use of ETC/STC methods also motivates the development of an observer to provide state estimates. The state estimation error of follower i is defined by $e_{2,i} : [0, \infty) \to \mathbb{R}^m$, where

$$e_{2,i}(t) \triangleq \hat{x}_i(t) - x_i(t) \tag{2–3}$$

such that $\hat{x}_i : [0, \infty) \to \mathbb{R}^m$ denotes the state estimate of x_i for each $i \in \mathcal{V}$.

2.3 Agent Models, Detection, and Mitigation

A detection method is presented in this section that provides distributed detection, where each agent formulates an inequality-based test to determine if an agent is Byzantine. Since (sufficiently disturbing) Byzantine actions violate the inequality, the detection method is considered instantaneous (or finite-time over the duration between communication events) in the sense that the inequality condition is interrogated at each communication event. Example strategies that enable finite-time Byzantine agent detection include [67–70]. Note that the methods in [68–70] are not directly applicable to the results in this paper since these techniques utilize observers that require continuous communication. Furthermore, while [67] provides an alternative detection strategy, like our detector, it also does not guarantee detection of Byzantine adversaries that have complete knowledge of the detection strategy.

2.3.1 Agent Definitions

Within this work, a Byzantine agent is defined as a non-compliant follower (cf. [24, 71]). Since non-compliance covers a broad scope of behaviors, this chapter

narrows its focus to two types of Byzantine agents, namely, Type I and Type II. A Type I Byzantine agent is defined as a follower that executes the intended controller but communicates false state information about itself to its neighbors. A Type II Byzantine agent is defined as a follower that executes a controller that is different from the intended controller or executes the intended controller under the influence of faulty hardware, while communicating true or no state information about itself to its neighbors. Consequently, a Type I Byzantine agent remains within the communication range of the CMAS since a Type I Byzantine agent executes the intended controller. In contrast, a Type II Byzantine agent may potentially leave the communication range of the CMAS. Note that non-responsive communication is a characteristic of Type II Byzantine behavior and can occur due to a follower leaving the CMAS, radio failure, or malicious intent. A cooperative agent is defined as a follower that successfully executes the intended controller and provides true state information about itself to all its neighbors.

2.3.2 Agent Models and Detection

The Byzantine agent detection problem is similar to fault detection since a Byzantine agent can elicit undesirable behavior in a MAS. Several methods can enable Byzantine agent detection, e.g., performance-based fault detection and model-based fault detection [72, 73]. Such detection strategies are threshold-based methods, which compare an error metric to some user-defined threshold. There are multiple ways to determine a threshold, e.g., through a statistical analysis of data generated by a simulation/experimental study or an analysis-based derivation. Yet, no threshold strategy is perfect, and Byzantine agent detection is not guaranteed for all instances and all types of Byzantine behavior. Hence, Byzantine agent detection is an open problem that requires further investigation.

Let $\{t_k^i\}_{k=0}^{\infty} \subset \mathbb{R}_{\geq 0}$ be an increasing sequence of event-times determined by a subsequently defined event-trigger (see Theorem 2.1). Note that t_k^i denotes the k^{th} instance follower i broadcasts its state to its neighbors. Suppose follower i broadcasts

its state information to all followers $j \in \mathcal{N}_i(t)$ at time t_k^i, where $x_i(t_k^i)$ denotes the true state of follower i at time t_k^i, and $x_{i,j}(t_k^i) \in \mathbb{R}^m$ denotes the state information that is broadcast from follower i to follower j at time t_k^i. Given the ETC strategy, the state estimate of follower i is reset to the broadcast state of follower i as defined in (2–11), where $\hat{x}_i(t_k^i) = x_{i,j}(t_k^i)$ for each $j \in \mathcal{N}_i(t)$. Moreover, let $\hat{x}_i^-(t_k^i)$ denote the state estimate of follower i the moment before being reset to $x_{i,j}(t_k^i)$, where the mismatch between the state estimate of follower i before and after the reset at time t_k^i with respect to follower j is defined as

$$\bar{e}_{i,j}\left(t_k^i\right) \triangleq \hat{x}_i^-\left(t_k^i\right) - x_{i,j}\left(t_k^i\right). \tag{2–4}$$

Similarly, let

$$e_{2,i}^-\left(t_k^i\right) \triangleq \hat{x}_i^-\left(t_k^i\right) - x_i^-\left(t_k^i\right) \tag{2–5}$$

denote the state estimation error of follower i the moment before being reset at time t_k^i. In a cooperative setting, follower i broadcasts its true state to all of its neighbors at time t_k^i, i.e., $x_i(t_k^i) = x_{i,j}(t_k^i)$ for all $j \in \mathcal{N}_i(t)$, where it can be shown that $e_{2,i}^-(t_k^i) = \bar{e}_{i,j}(t_k^i)$. Let $\Psi_{i,k}$ denote an upper bound[2] for $\left\|e_{2,i}^-(t_k^i)\right\|$, where

$$\left\|e_{2,i}^-\left(t_k^i\right)\right\| \leq \Psi_{i,k}. \tag{2–6}$$

Since $\left\|e_{2,i}^-(t_k^i)\right\| = \|\bar{e}_{i,j}(t_k^i)\|$ and $\left\|e_{2,i}^-(t_k^i)\right\| \leq \Psi_{i,k}$, $\|\bar{e}_{i,j}(t_k^i)\| \leq \Psi_{i,k}$. However, within a contested environment, it is possible for $x_i(t_k^i)$ to differ from $x_{i,j}(t_k^i)$, i.e., follower i can provide misinformation about its state. Therefore, the Byzantine agent detector that

[2] See Remark 2.4 (for ETC) or Remark 2.7 (for STC) for specific examples of $\Psi_{i,k}$.

follower j uses to determine the status of follower $i \in \mathcal{N}_j(t)$ at time t_k^i is[3]

$$\Xi_{i,k} \triangleq \left\| \bar{e}_{i,j}\left(t_k^i\right) \right\| - \Psi_{i,k}, \tag{2–7}$$

where follower i is a cooperative neighbor of follower j at time t_k^i if $\Xi_{i,k} \leq 0$, and follower i is a Byzantine neighbor of follower j at time t_k^i if $\Xi_{i,k} > 0$. The estimated state of follower i before the reset is compared to the potential state estimate update of follower i after the reset in (2–4). Therefore, this strategy enables instantaneous detection of Byzantine adversaries that provide sufficiently disturbing state information.

The following atomic propositions are presented to precisely model the behavior of Type I Byzantine agents, Type II Byzantine agents, and cooperative agents within this work. Let $\mathcal{D}_{k,i}$ define the statement $\Xi_{i,k} \leq 0$, $\mathcal{X}_{i,j}$ define the statement $x_i(t) = x_{i,j}(t)$, and $\mathcal{T}_{k,i}$ define the statement $t_k^i \leq t_{k-1}^i + \Delta_i$, where $\Delta_i \in \mathbb{R}_{>0}$ is a constant parameter that is defined in Remark 2.5. Hence, $\mathcal{D}_{k,i}$, $\mathcal{X}_{i,j}$, and $\mathcal{T}_{k,i}$ are each either true or false.

Observe that $\mathcal{D}_{k,i}$, $\mathcal{X}_{i,j}$, and $\mathcal{T}_{k,i}$ encode acceptable agent motion, honest state reporting, and punctual state reporting, respectively, for follower i at time t_k^i. With respect to follower j and for each broadcast time t_k^i, follower $i \in \mathcal{N}_j(t)$ is

$$\begin{cases} \text{cooperative,} & \mathcal{D}_{k,i} \wedge \mathcal{X}_{i,j} \wedge \mathcal{T}_{k,i}, \\ \text{Type I,} & \neg\left(\mathcal{D}_{k,i} \vee \mathcal{X}_{i,j}\right) \wedge \mathcal{T}_{k,i}, \\ \text{Type II,} & \neg\left(\mathcal{D}_{k,i} \wedge \mathcal{T}_{k,i}\right) \wedge \mathcal{X}_{i,j}. \end{cases} \tag{2–8}$$

[3] $\Psi_{i,k}$ in (2–6) represents a threshold that is used for Byzantine agent detection. As with any threshold detection method, if the adversary knows this threshold, then it can inject small perturbations below the threshold to yield some effect. These small perturbations can be modeled as a bounded disturbance, which leads to a larger UUB bound given the proposed controller. An open problem for all such detection strategies is to determine the most sensitive threshold that balances detection with false positives, especially in the presence of noise.

Hence, given the agent models in (2–8), the set of cooperative neighbors of follower j is given by

$$\mathcal{C}_j(t) \triangleq \left\{ i \in \mathcal{N}_j(t) : \forall t_k^i \leq t \; \mathcal{D}_{k,i} \wedge \mathcal{T}_{k,i} \right\},$$

and the set of Byzantine neighbors of follower j is given by

$$\mathcal{B}_j(t) \triangleq \left\{ i \in \mathcal{N}_j(t) : \exists t_k^i \leq t \; \neg \left(\mathcal{D}_{k,i} \wedge \mathcal{T}_{k,i} \right) \right\}.$$

By convention, if follower i does not provide follower j with state information within a predetermined time period, i.e., $t_k^i > t_{k-1}^i + \Delta_i$, then follower j categorizes follower i as Byzantine, i.e., $i \in \mathcal{B}_j(t)$. Efforts in this paper focus only on detectable Type I and Type II behaviors, and additional efforts are required to generalize the development to broader classes of adversarial behaviors.

2.3.3 Mitigation

Since the objective is to achieve approximate leader-follower consensus by the cooperative followers, and both the detector in (2–7) and the communication timing condition, i.e., $t_k^i \leq t_{k-1}^i + \Delta_i$, allows each follower to identify their cooperative and Byzantine neighbors, the edge weights can be intermittently updated according to the status of each neighbor. Hence, for all $t \in [t_k^j, t_{k+1}^j)$, the piecewise constant edge weight $a_{ij}(t)$ is defined by

$$a_{ij}(t) \triangleq \begin{cases} 1, & j \in \mathcal{C}_i(t) \\ 0, & j \in \mathcal{B}_i(t). \end{cases} \tag{2–9}$$

From (2–9), the edge weight $a_{ij}(t) = 1$ for all $t \in [t_k^j, t_{k+1}^j)$ if follower j is a cooperative neighbor of follower i at time t_k^j, and $a_{ij}(t) = 0$ for all $t \in [t_k^j, t_{k+1}^j)$ if follower j is a Byzantine neighbor of follower i at time t_k^j.

Although the proposed detection and mitigation strategy enables each cooperative agent to insulate itself from Byzantine neighbors, the choice remains to allow each

cooperative agent to communicate state information about itself to Byzantine neighbors or not. Communication could enable a Type I Byzantine adversary to be regulated to a desired location for remediation. However, communicating with a compromised agent could endanger security. Without loss of generality, the subsequent work enables communication from cooperative agents to their Byzantine neighbors.

Assumption 2.6. For all $j \in \mathcal{B}_i(t)$ and each $i \in \mathcal{V}$, follower i communicates state information about itself to follower j.[4]

Remark 2.1. While a threshold-based detection strategy is used to categorize the neighbors of follower i as either cooperative or Byzantine for each $i \in \mathcal{V}$, any other detection method that enables the construction of (2–9) can be implemented along with the observer in (2–10)–(2–11), controller in (2–12)–(2–13), and event-trigger in (2–24) to achieve the objective.

2.4 State Estimation and Event-Triggered Control

2.4.1 Control and Observer Development

Given the use of an event-triggered strategy, the state estimate of follower $j \in \mathcal{V}$ is generated by the following observer

$$\dot{\hat{x}}_j(t) \triangleq A\hat{x}_j(t),\ t \in \left[t_k^j, t_{k+1}^j\right) \tag{2–10}$$

$$\hat{x}_j\left(t_k^j\right) \triangleq x_{j,i}\left(t_k^j\right), \tag{2–11}$$

which is synchronized among all followers $i \in \mathcal{N}_j(t) \cup \{j\}$. Note that for each $j \in \mathcal{V}$, self-communication does not occur and $\hat{x}_j(t_k^j) \triangleq x_j(t_k^j)$. Moreover, recall that $x_{j,i}(t_k^j) = x_j(t_k^j)$ provided follower j is cooperative. The solution to (2–10) over $[t_k^j, t_{k+1}^j)$ is $\hat{x}_j(t) = e^{A\left(t-t_k^j\right)}\hat{x}_j(t_k^j)$. Hence, accurate estimation of the state of follower j requires an accurate initial condition, i.e., correct state estimation is ensured provided $\hat{x}_j(t_k^j) = x_j(t_k^j)$.

[4] The leader will also communicate state information about itself to all neighbors.

Therefore, in this work, if $j \in \mathcal{B}_i(t_k^j)$, then $j \in \mathcal{B}_i(t)$ for all $t \geq t_k^j$. The Byzantine designation is permanent since follower i does not have an accurate state of the follower in question with which to propagate the estimate forward and compare to the corresponding sampled state. There are various methods to allow the inclusion of a rehabilitated follower into the cooperative follower set, e.g., trusted third party information can be used to reset the observer or a reputation algorithm such as in [37] can potentially be used as an alternative to adjust the graph edge weights. These potential extensions merit further investigation and are beyond the scope of this work.

Assumption 2.7. All followers are cooperative agents at time $t = 0$.

Assumption 3.7 enables the detection of Byzantine followers after the initial time $t = 0$. Like most fault or change detection methods, a baseline condition (i.e., at $t = 0$) is first required for comparison (cf. [72, 73]). However, Byzantine follower detection can be accomplished using the threshold-based detector in (2–7) at the initial time provided all followers know the initial position of their neighbors. Motivated by [13], the controller for follower $i \in \mathcal{V}$ is

$$u_i(t) \triangleq K z_i(t) + K e_{2,i}(t) \tag{2–12}$$

$$z_i(t) \triangleq \sum_{j \in \mathcal{N}_i(t)} a_{ij}(t)\left(\hat{x}_j(t) - \hat{x}_i(t)\right) + d_i(t)\left(x_0(t) - \hat{x}_i(t)\right), \tag{2–13}$$

where $z_i : [0, \infty) \to \mathbb{R}^m$ is the estimate-based consensus control effort. The gain matrix $K \in \mathbb{R}^{n \times m}$ in (2–12) is designed as $K \triangleq B^\top P$, where $P \in \mathbb{R}^{m \times m}$ is the symmetric and positive definite solution to the Algebraic Riccati Equation (ARE) given by

$$A^\top P + PA - \lambda_{\min}(H_{\min}) 2PBB^\top P + kI_m = 0_{m \times m}. \tag{2–14}$$

Note that $\lambda_{\min}(H_{\min}) \triangleq \min\{\lambda_{\min}(H_{\text{sym}}(t))\} \in \mathbb{R}_{>0}$ such that $H_{\text{sym}}(t) \triangleq \frac{1}{2}\left(H(t) + H(t)^\top\right) \in \mathbb{R}^{N \times N}$ and $k \geq k_1 + \frac{\rho^2}{\delta}$, where $\rho > 2\sqrt{N} M_0 S_{\max}(PB) \in \mathbb{R}_{>0}$, $k_1 \triangleq k_2 + k_3$, and $k_2,\ k_3,\ \delta \in \mathbb{R}_{>0}$ are user-defined parameters. Rather than use a traditional sample-and-hold event-triggered consensus control law such as in [21],

the combined use of (2–10)–(2–13) enable each follower i to continuously compute a control input that evolves according to the leader's drift dynamics [74].

By using (2–1)–(2–3), (2–12), and (2–13), the time-derivative of (2–2) can be expressed as

$$\dot{e}_{1,i}(t) = Ae_{1,i}(t) - BKd_i(t)\, e_{1,i}(t) - BKd_i(t)\, e_{2,i}(t) + BK \sum_{j \in \mathcal{N}_i(t)} a_{ij}(t) \left(e_{1,j}(t) - e_{1,i}(t)\right)$$
$$+ BK \sum_{j \in \mathcal{N}_i(t)} a_{ij}(t) \left(e_{2,j}(t) - e_{2,i}(t)\right) + BKe_{2,i}(t) - Bu_0(t). \tag{2–15}$$

Similarly, using (2–1)–(2–3), (2–10), (2–12) and (2–13), the weak time-derivative[5] of (2–3) can be expressed as

$$\dot{e}_{2,i}(t) = Ae_{2,i}(t) + BKd_i(t)\, e_{2,i}(t) + BKd_i(t)\, e_{1,i}(t) - BK \sum_{j \in \mathcal{N}_i(t)} a_{ij}(t) \left(e_{2,j}(t) - e_{2,i}(t)\right)$$
$$- BK \sum_{j \in \mathcal{N}_i(t)} a_{ij}(t) \left(e_{1,j}(t) - e_{1,i}(t)\right) - BKe_{2,i}(t). \tag{2–16}$$

The stacked forms of (2–2) and (2–3) are defined as

$$e_1(t) \triangleq \left[e_{1,1}^\top(t), e_{1,2}^\top(t), ..., e_{1,N}^\top(t)\right]^\top \in \mathbb{R}^{mN}, \tag{2–17}$$
$$e_2(t) \triangleq \left[e_{2,1}^\top(t), e_{2,2}^\top(t), ..., e_{2,N}^\top(t)\right]^\top \in \mathbb{R}^{mN}, \tag{2–18}$$

respectively. Substituting (2–15) and (2–16) into the time-derivative of (2–17) and (2–18), respectively, and compactly expressing the results with the Kronecker product yields

$$\dot{e}_1(t) = (I_N \otimes A)\, e_1(t) + ((I_N - H(t)) \otimes BK)\, e_2(t) - (H(t) \otimes BK)\, e_1(t) - (1_N \otimes Bu_0(t)), \tag{2–19}$$

$$\dot{e}_2(t) = (I_N \otimes (A - BK))\, e_2(t) + (H(t) \otimes BK)\, e_2(t) + (H(t) \otimes BK)\, e_1(t), \tag{2–20}$$

[5] Weak time-derivative refers to the existence of the time-derivative for almost all time.

respectively. The stacked form of (2–13) is defined by $z(t) \triangleq \left[z_1^\top(t), z_2^\top(t), ..., z_N^\top(t)\right]^\top \in \mathbb{R}^{mN}$. Substituting $\hat{x}(t) \triangleq \left[\hat{x}_1^\top(t), \hat{x}_2^\top(t), ..., \hat{x}_N^\top(t)\right]^\top \in \mathbb{R}^{mN}$ and (2–13) for all $i \in \mathcal{V}$ into $z(t)$ yields

$$z(t) = -(H(t) \otimes I_m)\hat{x}(t) + (D(t) \otimes I_m)(1_N \otimes x_0(t)). \tag{2–21}$$

Moreover, substituting (2–2), (2–3) and (2–13) for all $i \in \mathcal{V}$ into $z(t)$ yields

$$z(t) = -(H(t) \otimes I_m)e_2(t) - (H(t) \otimes I_m)e_1(t). \tag{2–22}$$

Since the objective is achieved when $e_{1,i}(t)$ is UUB for all cooperative followers $i \in \mathcal{V}$, it is sufficient to show that $e_1(t)$ is UUB. However, since $e_1(t)$ may contain error signals belonging to Byzantine followers, where the behavior of Byzantine followers cannot be controlled, the objective can only be guaranteed for the cooperative followers. Hence, if follower j is categorized as a Byzantine agent at t_k^j for some $k \in \mathbb{Z}_{\geq 0}$, then $e_{1,j}(t) \triangleq 0_m$ and $e_{2,j}(t) \triangleq 0_m$ for all $t \geq t_k^j$.

2.4.2 Stability Analysis

To facilitate the subsequent stability analysis, let

$$\begin{aligned}
\gamma &\triangleq \max\left\{\left\|(I_N - H(t)) \otimes 2PBB^\top P\right\|\right\} \in \mathbb{R}_{>0},\\
\phi_1 &\triangleq k_2 - \frac{\kappa(2k_3 + \gamma)}{2} \in \mathbb{R}_{>0},\\
\phi_2 &\triangleq k_3 + \frac{2k_3 + \gamma}{2\kappa} \in \mathbb{R}_{>0},\\
\phi_3 &\triangleq \frac{k_3}{\max\left\{\|H(t) \otimes I_m\|^2\right\}} \in \mathbb{R}_{>0},
\end{aligned}$$

where $\kappa \in \mathbb{R}_{>0}$ is a user-defined parameter used in Young's inequality. Moreover, let $\bar{\delta} \triangleq \delta + \theta \in \mathbb{R}_{>0}$, where $\delta \in \mathbb{R}_{>0}$ is a user-defined parameter used to compensate for the effect of the leader's control input, and $\theta \in \mathbb{R}_{>0}$ is a user-defined parameter used to exclude Zeno behavior. Based on the definition of $\bar{\delta}$, additional constants are defined to

facilitate the analysis

$$\beta_1 \triangleq \sqrt{\frac{\lambda_{\max}\left(I_N \otimes P\right)\bar{\delta}}{\lambda_{\min}\left(I_N \otimes P\right)\phi_1}} \in \mathbb{R}_{>0},$$
$$\beta_2 \triangleq \sqrt{\frac{V_1\left(e_1\left(0\right)\right)}{\lambda_{\min}\left(I_N \otimes P\right)}} \in \mathbb{R}_{\geq 0},$$
$$\beta_3 \triangleq \frac{\phi_1}{2\lambda_{\max}\left(I_N \otimes P\right)} \in \mathbb{R}_{>0}.$$

Given Assumption 2.2, the ARE in (2–14) has a positive definite solution P provided $\lambda_{\min}\left(H_{\min}\right) > 0$ [13, 74]. The following lemma shows $\lambda_{\min}\left(H_{\min}\right) > 0$.

Lemma 2.1. *Suppose Assumptions 2.4–2.6 are satisfied. If all cooperative followers detect their Byzantine neighbors and employ* (2–9)*, then* $\lambda_{\min}\left(H_{\min}\right) > 0$.

Proof. See Appendix A.1. ■

Theorem 2.1. *The edge weight policy in* (2–9)*, state observer in* (2–10) *and* (2–11)*, and controller in* (2–12) *and* (2–13) *ensure the leader-follower error* $e_1\left(t\right)$ *is globally uniformly ultimately bounded as*

$$\left\|e_1\left(t\right)\right\| \leq \beta_1 + \beta_2 e^{-\beta_3 t} \tag{2–23}$$

provided state feedback is available as dictated by the event-trigger in

$$t_{k+1}^i \triangleq \inf\left\{t > t_k^i : \phi_2 \left\|e_{2,i}\left(t\right)\right\|^2 \geq \phi_3 \left\|z_i\left(t\right)\right\|^2 + \frac{\theta}{N}\right\} \tag{2–24}$$

for all $i \in \mathcal{V}$*, Assumptions 2.1–3.7 are satisfied, and the following sufficient user-defined parameter conditions are selected as follows: use Algorithm 2.1 to determine* P*, and select* $\kappa > 0$, $\delta > 0$, $\theta > 0$, $\rho > 2\sqrt{N}M_0 S_{\max}\left(PB\right)$, $k_3 > 0$, $k_2 > \frac{\kappa(2k_3+\gamma)}{2}$*, and* $k \geq k_1 + \frac{\rho^2}{\delta}$.

Proof. Consider the following candidate Lyapunov function $V_1 : \mathbb{R}^{mN} \to \mathbb{R}_{\geq 0}$ defined as

$$V_1\left(e_1\left(t\right)\right) \triangleq e_1^\top\left(t\right)\left(I_N \otimes P\right)e_1\left(t\right). \tag{2–25}$$

By the Rayleigh quotient

$$\lambda_{\min}\left(I_N \otimes P\right)\left\|e_1\left(t\right)\right\|^2 \leq V_1\left(e_1\left(t\right)\right) \leq \lambda_{\max}\left(I_N \otimes P\right)\left\|e_1\left(t\right)\right\|^2. \tag{2–26}$$

Suppose $g : [0,\infty) \to \mathbb{R}^{mN}$ is a Filippov solution to the differential inclusion $\dot{g}\left(t\right) \in \overline{K}\left[h\right]\left(g\left(t\right)\right)$, where $g\left(t\right) = e_1\left(t\right)$, $\overline{K}\left[\cdot\right]$ is defined as in [75], and $h : \mathbb{R}^{mN} \to \mathbb{R}^{mN}$ is defined as $h\left(g\left(t\right)\right) = \dot{e}_1\left(t\right)$. The time-derivative of V_1 exists almost everywhere (a.e.), i.e., for almost all $t \in [0,\infty)$, and

$$\dot{V}_1\left(g\left(t\right)\right) \overset{a.e.}{\in} \dot{\tilde{V}}_1\left(g\left(t\right)\right), \tag{2–27}$$

where $\dot{\tilde{V}}_1\left(g\left(t\right)\right)$ is the generalized time-derivative of V_1 along the Filippov trajectories of $\dot{g}\left(t\right) = h\left(g\left(t\right)\right)$. By [76, Equation 13],

$$\dot{\tilde{V}}_1\left(g\left(t\right)\right) \triangleq \bigcap_{\xi \in \partial V_1\left(g\left(t\right)\right)} \xi^{\top}\left[\overline{K}\left[h\right]^{\top}\left(g\left(t\right)\right),\ 1\right]^{\top},$$

where $\partial V_1\left(g\left(t\right)\right)$ denotes the Clarke generalized gradient of $V_1\left(g\left(t\right)\right)$. Since $V_1\left(g\left(t\right)\right)$ is continuously differentiable in $g\left(t\right)$, $\partial V_1\left(g\left(t\right)\right) = \left\{\nabla V_1\left(g\left(t\right)\right)\right\}$, where ∇ denotes the gradient operator. The generalized time-derivative of (2–25) is

$$\dot{\tilde{V}}_1\left(g\left(t\right)\right) \subseteq 2e_1^{\top}\left(t\right)\left(I_N \otimes P\right)\overline{K}\left[h\right]\left(g\left(t\right)\right). \tag{2–28}$$

Using the calculus of $\overline{K}\left[\cdot\right]$ from [75] along with (2–28) and simplifying the substitution of (2–19) and $K = B^{\top}P$ into the generalized time-derivative of (2–25) yields

$$\begin{aligned}\dot{\tilde{V}}_1\left(g\left(t\right)\right) \subseteq{}& \left\{e_1^{\top}\left(t\right)\left(I_N \otimes \left(A^{\top}P + PA\right)\right)e_1\left(t\right)\right\} - e_1^{\top}\left(t\right)\overline{K}\left[H\left(t\right) \otimes 2PBB^{\top}P\right]e_1\left(t\right) \\ &+ e_1^{\top}\left(t\right)\overline{K}\left[\left(\left(I_N - H\left(t\right)\right) \otimes 2PBB^{\top}P\right)e_2\left(t\right)\right] - \left\{e_1^{\top}\left(t\right)\left(1_N \otimes 2PBu_0\left(t\right)\right)\right\}.\end{aligned} \tag{2–29}$$

Let $M \triangleq H\left(t\right) \otimes 2PBB^{\top}P \in \mathbb{R}^{mN \times mN}$, $M_{\text{sym}} \triangleq \frac{1}{2}\left(M + M^{\top}\right) \in \mathbb{R}^{mN \times mN}$, and $M_{\text{skew}} \triangleq \frac{1}{2}\left(M - M^{\top}\right) \in \mathbb{R}^{mN \times mN}$, where $M = M_{\text{sym}} + M_{\text{skew}}$. Since M_{skew} is a skew symmetric

matrix, it follows that $e_1^\top(t)\left(H(t)\otimes 2PBB^\top P\right)e_1(t) = e_1^\top(t)M_{\text{sym}}e_1(t)$. It follows from the definition of M_{sym} that $e_1^\top(t)M_{\text{sym}}e_1(t) = e_1^\top(t)\left(H_{\text{sym}}(t)\otimes 2PBB^\top P\right)e_1(t)$. Hence, $e_1^\top(t)\left(H(t)\otimes 2PBB^\top P\right)e_1(t) = e_1^\top(t)\left(H_{\text{sym}}(t)\otimes 2PBB^\top P\right)e_1(t)$. Since $H_{\text{sym}}(t)$ is a real, symmetric matrix, $H_{\text{sym}}(t)$ is diagonalizable, where there exists an orthogonal eigenvector matrix $T(t) \in \mathbb{R}^{N\times N}$ and eigenvalue matrix $\Lambda(t) \in \mathbb{R}^{N\times N}$ such that $H_{\text{sym}}(t) = T(t)\Lambda(t)T^\top(t) \in \mathbb{R}^{N\times N}$. Hence, the eigendecomposition of $H_{\text{sym}}(t)$, the ARE, and (2–27) enable (2–29) to yield

$$\begin{aligned}\dot{V}_1(e_1(t)) \overset{a.e.}{\leq} & -ke_1^\top(t)e_1(t) - e_1^\top(t)(1_N\otimes 2PBu_0(t)) \\ & + e_1^\top(t)\left((I_N - H(t))\otimes 2PBB^\top P\right)e_2(t).\end{aligned} \tag{2–30}$$

Using Assumption 2.3 and selecting $k \geq k_1 + \frac{\rho^2}{\delta}$, (2–30) can be upper bounded by

$$\dot{V}_1(e_1(t)) \overset{a.e.}{\leq} -k_1\|e_1(t)\|^2 + \delta + \gamma\|e_2(t)\|\|e_1(t)\|. \tag{2–31}$$

Using (2–22), (2–31) can be further upper bounded by

$$\dot{V}_1(e_1(t)) \overset{a.e.}{\leq} -\phi_1\|e_1(t)\|^2 + \bar{\delta} + \sum_{i\in\mathcal{V}}\left[\phi_2\|e_{2,i}(t)\|^2 - \phi_3\|z_i(t)\|^2 - \frac{\theta}{N}\right]. \tag{2–32}$$

By selecting $k_3 > 0$ and $k_2 > \frac{\kappa(2k_3+\gamma)}{2}$, $\phi_1 > 0$, $\phi_2 > 0$, and $\phi_3 > 0$. Based on (2–32), the event-trigger for each follower $i \in \mathcal{V}$ is given by (2–24). Hence, provided state feedback is available according to (2–24), it follows that

$$\dot{V}_1(e_1(t)) \overset{a.e.}{\leq} -\phi_1\|e_1(t)\|^2 + \bar{\delta} \tag{2–33}$$

for all $t \geq 0$. Substituting (2–26) into (2–33) yields

$$\dot{V}_1(e_1(t)) \overset{a.e.}{\leq} -\frac{\phi_1}{\lambda_{\max}(I_N\otimes P)}V_1(e_1(t)) + \bar{\delta}. \tag{2–34}$$

Since the set of discontinuities as given by $\bigcup_{k\in\mathbb{Z}_{\geq 0}}\bigcup_{i\in\mathcal{V}}\{t_k^i\}$ is countable, $\dot{V}_1(e_1(t))$ and $V_1(e_1(t))$ are Lebesgue integrable over $\mathbb{R}_{\geq 0}$. The result in (2–23) then follows from (2–34) [77, Theorem 2.5.1. Part V]. Observe that the constant β_1 can be made small,

resulting in a small steady state error for $e_1(t)$. Since $e_1(t) \in \mathcal{L}_\infty$ by (2–23), $e_{1,i}(t) \in \mathcal{L}_\infty$ for all $i \in \mathcal{C}(t)$. From Assumption 2.3, $x_0(t) \in \mathcal{L}_\infty$. By (2–2) and $x_0(t) \in \mathcal{L}_\infty$, $x_i(t) \in \mathcal{L}_\infty$ for each $i \in \mathcal{C}(t)$. Given (2–10) and (2–11), one has that $\hat{x}_i(t) = e^{A\left(t-t_k^i\right)}\hat{x}_i\left(t_k^i\right)$ over $t \in \left[t_k^i, t_{k+1}^i\right)$, where $\hat{x}_i\left(t_k^i\right) = x_i\left(t_k^i\right)$ for all $k \in \mathbb{Z}_{\geq 0}$. Therefore, $\hat{x}_i(t) \in \mathcal{L}_\infty$ for each $i \in \mathcal{C}(t)$, which then implies $e_{2,i}(t) \in \mathcal{L}_\infty$ by (2–3) for each $i \in \mathcal{C}(t)$. Hence, $u_i(t) \in \mathcal{L}_\infty$ for each $i \in \mathcal{C}(t)$. ■

Remark 2.2. There are two reasons why uniformly ultimately bounded (UUB) stability is obtained rather than asymptotic stability. In (2–30), since

$$-e_1^\top(t)\left(1_N \otimes 2PBu_0(t)\right) \leq \|e_1(t)\| \left\|1_N \otimes 2PBu_0(t)\right\|,$$

where $\left\|1_N \otimes 2PBu_0(t)\right\| \leq c$ for some $c \in \mathbb{R}_{>0}$ by Assumption 2.3, $-\left(1_N \otimes 2PBu_0(t)\right)e_1(t) \leq c\|e_1(t)\|$. Since the controller in (2–12)–(2–13) does not employ a sliding mode term or one of its variants, $c\|e_1(t)\|$ can only be compensated with high-gain, which results in a residual $\delta > 0$. Note that it is not clear how to incorporate a sliding mode term into the controller in (2–12)–(2–13) since doing so would require $\text{sgn}\left(e_{1,i}(t)\right)$ and $e_{1,i}(t)$ is not measurable by all followers. Next, the event-trigger strategy requires exclusion from Zeno behavior, which is accomplished by injecting $\theta > 0$ into (2–32), as shown in the proof of Theorem 2.2. Hence, the $\theta > 0$ term is combined with the residual $\delta > 0$ resulting in $\bar{\delta} = \delta + \theta$, and hence, UUB stability.

2.4.3 Exclusion of Zeno Behavior

Theorem 2.2. *For each follower $i \in \mathcal{V}$, the difference between consecutive broadcast times generated by the event-trigger of follower i in* (2–24) *is uniformly lower bounded by*

$$t_{k+1}^i - t_k^i \geq \frac{1}{\|A - BK\|} \ln\left(\frac{\|A - BK\|}{\|BK\|\,\bar{z}_i}\sqrt{\frac{\theta}{N\phi_2}} + 1\right) \tag{2–35}$$

for all $k \in \mathbb{Z}_{\geq 0}$.

Proof. Let $t \in [t_k^i, \infty)$. Substituting (2–1), (2–10), and (2–12) into the time-derivative of (2–3) yields $\dot{e}_{2,i}(t) = (A - BK) e_{2,i}(t) - BKz_i(t)$. Since $\|x_0(t)\| \leq \overline{M}_0$ by Assumption 2.3 and $\hat{x} \in \mathcal{L}_\infty$ by the proof of Theorem 2.1, (2–21) implies the existence of $\bar{z}_i \in \mathbb{R}_{>0}$ such that $\|z_i(t)\| \leq \bar{z}_i$ for all $t \in \mathbb{R}_{\geq 0}$. It then follows that

$$\|\dot{e}_{2,i}(t)\| \leq \|A - BK\| \|e_{2,i}(t)\| + \|BK\| \bar{z}_i. \tag{2–36}$$

Let $\upsilon_i : [t_k^i, \infty) \to \mathbb{R}_{\geq 0}$ satisfy $\dot{\upsilon}_i(t) = \|A - BK\| \upsilon_i(t) + \|BK\| \bar{z}_i$ with initial condition $\upsilon_i(t_k^i) = \|e_{2,i}(t_k^i)\|$. Then, $\upsilon_i(t_k^i) = 0$ and

$$\upsilon_i(t) = \frac{\|BK\| \bar{z}_i}{\|A - BK\|} \left(e^{\|A-BK\|\left(t - t_k^i\right)} - 1 \right). \tag{2–37}$$

Since $\frac{d}{dt}\|e_{2,i}(t)\| \overset{a.e.}{\leq} \|\dot{e}_{2,i}(t)\|$, (2–36) implies $\frac{d}{dt}\|e_{2,i}(t)\| \overset{a.e.}{\leq} \|A - BK\| \|e_{2,i}(t)\| + \|BK\| \bar{z}_i$, where $\|e_{2,i}(t)\| \leq \upsilon_i(t)$ for all $t \in [t_k^i, \infty)$. Since $\|e_{2,i}(t)\| \leq \upsilon_i(t)$ and $\|z_i(t)\| \geq 0$, (2–24) implies (2–35), where $\frac{1}{\|A-BK\|} \ln\left(\frac{\|A-BK\|}{\|BK\|\bar{z}_i} \sqrt{\frac{\theta}{N\phi_2}} + 1 \right) > 0$ since $\frac{\|A-BK\|}{\|BK\|\bar{z}_i} \sqrt{\frac{\theta}{N\phi_2}} > 0$. ■

Remark 2.3. Since the event-trigger in (2–24) is free from Zeno behavior by the proof of Theorem 2.2, no follower continuously broadcasts state information about itself to its neighbors. Moreover, the difference between consecutive event-times can be made large by selecting a large θ. Since $\beta_1 = \sqrt{\frac{\lambda_{\max}(I_N \otimes P)\bar{\delta}}{\lambda_{\min}(I_N \otimes P)\phi_1}}$, where $\bar{\delta} = \delta + \theta$, selecting a large θ forces β_1 to be large as well. Hence, there is a trade-off between the size of the neighborhood containing the cooperative followers and leader once approximate consensus is achieved and the amount of communication.

Remark 2.4. Define (2–37) over $\left[t_{k-1}^i, t_k^i\right)$, and observe that since $\|e_{2,i}(t)\| \leq \upsilon_i(t)$ over $\left[t_{k-1}^i, t_k^i\right)$, $\|e_{2,i}(t_k^i)\| = 0$, and $\upsilon_i(t)$ in (2–37) is strictly increasing, it follows that $\left\|e_{2,i}^-(t)\right\|$ defined in (2–5) satisfies the inequality $\left\|e_{2,i}^-(t)\right\| \leq \upsilon_i(t_k^i)$. Therefore, $\upsilon_i(t_k^i)$ is a candidate for $\Psi_{i,k}$.

Remark 2.5. If the event-trigger condition in (2–24) is satisfied for all $t \geq 0$, then

$$\phi_2 \|e_{2,i}(t)\|^2 \leq \phi_3 \|z_i(t)\|^2 + \frac{\theta}{N}.$$

Since $\|z_i(t)\| \leq \bar{z}_i$ for all $t \in \mathbb{R}_{\geq 0}$, substituting $\|z_i(t)\| \leq \bar{z}_i$ into $\phi_2 \|e_{2,i}(t)\|^2 \leq \phi_3 \|z_i(t)\|^2 + \frac{\theta}{N}$ yields

$$\|e_{2,i}(t)\| \leq \sqrt{\frac{\phi_3 \bar{z}_i^2}{\phi_2} + \frac{\theta}{N\phi_2}} \in \mathbb{R}_{>0}.$$

Since $\|e_{2,i}(t)\| \leq \upsilon_i(t)$ for all $t \in \left[t_{k-1}^i, t_k^i\right)$, $\upsilon_i(t_k^i) > 0$, and $\|e_{2,i}(t_k^i)\| = 0$, $\|e_{2,i}(t)\| \leq \upsilon_i(t)$ for all $t \in \left[t_{k-1}^i, t_k^i\right]$. Since $\upsilon_i(t)$ will reach $\sqrt{\frac{\phi_3 \bar{z}_i^2}{\phi_2} + \frac{\theta}{N\phi_2}}$ before or at the same time as $\|e_{2,i}(t)\|$, one has that $\frac{\|BK\|\bar{z}_i}{\|A-BK\|}\left(e^{\|A-BK\|\left(t_k^i - t_{k-1}^i\right)} - 1\right) \leq \sqrt{\frac{\phi_3 \bar{z}_i^2}{\phi_2} + \frac{\theta}{N\phi_2}}$ implies $t_k^i \leq t_{k-1}^i + \Delta_{i,\min}$, where

$$\Delta_{i,\min} \triangleq \frac{1}{\|A-BK\|} \ln\left(\frac{\|A-BK\|}{\|BK\|\bar{z}_i}\sqrt{\frac{\phi_3 \bar{z}_i^2}{\phi_2} + \frac{\theta}{N\phi_2}} + 1\right) \tag{2–38}$$

and $\Delta_{i,\min} \in \mathbb{R}_{>0}$. Hence, $\|e_{2,i}(t)\| \leq \sqrt{\frac{\phi_3 \bar{z}_i^2}{\phi_2} + \frac{\theta}{N\phi_2}}$ for all $t \geq 0$ provided $t_k^i \leq t_{k-1}^i + \Delta_i$ for each $k \in \mathbb{Z}_{>0}$, where Δ_i is a user-defined parameter to be selected such that $\Delta_i \geq \Delta_{i,\min}$. Note that an analytical upper bound for Δ_i requires the derivation of a non-zero lower bound for $\|e_{2,i}(t)\|$, which is not obvious.

Algorithm 2.1 presents a method for parameter selection.

Algorithm 2.1 Parameter Selection Protocol

1: Select $\delta,\ \kappa,\ \theta,\ k,\ k_3 \in \mathbb{R}_{>0}$.

2: Compute $\bar{\delta} = \delta + \theta$.

3: Compute $\lambda_{\min}\left(H_{\min}\right) = \min\left\{\lambda_{\min}\left(H_{\mathsf{sym}}\left(t\right)\right)\right\}$.

4: **while** true **do**

5: Compute P from (2–14).

6: Select $\rho > 2\sqrt{N}M_0 S_{\max}\left(PB\right)$.

7: Compute $\gamma = \max\left\{\left\|\left(I_N - H\left(t\right)\right) \otimes 2PBB^{\top}P\right\|\right\}$.

8: Select $k_2 > \frac{\kappa(2k_3+\gamma)}{2}$.

9: Compute $k_1 = k_2 + k_3$.

10: **if** $k_1 + \frac{\rho^2}{\delta} \leq k$ **then**

11: break

12: **else**

13: $k = k_1 + \frac{\rho^2}{\delta}$.

14: **end if**

15: **end while**

16: Compute $K = B^{\top}P$.

17: Compute $\phi_1 = k_2 - \frac{\kappa(2k_3+\gamma)}{2}$.

18: Compute $\phi_2 = k_3 + \frac{2k_3+\gamma}{2\kappa}$.

19: Compute $\phi_3 = \frac{k_3}{\max\left\{\|H(t)\otimes I_m\|^2\right\}}$.

2.5 Self-Triggered Control

When the trigger condition in (2–24) is true, follower i will broadcast its state to each follower $j \in \mathcal{N}_i\left(t\right)$ to reset (2–3) and ensure (2–33). Such an ETC strategy requires follower i to continuously monitor (2–24) and for each follower $j \in \mathcal{N}_i\left(t\right)$ to continuously sense for follower i's broadcast. A STC strategy is developed in this section, where follower i determines and reports to its neighbors the future time when its own trigger

condition will become true, eliminating the need for followers to continuously monitor for a neighbor's broadcast.

Based on (2–32), stability is preserved when $\phi_2 \left\| e_{2,i}(t) \right\|^2 - \phi_3 \left\| z_i(t) \right\|^2 - \frac{\theta}{N} \leq 0$ for each $i \in \mathcal{V}$. Since $\phi_3 > 0$ and $\left\| z_i(t) \right\| \geq 0$, $\phi_3 \left\| z_i(t) \right\|^2 \geq 0$, where stability is preserved provided $\phi_2 \left\| e_{2,i}(t) \right\|^2 - \frac{\theta}{N} \leq 0$ for each $i \in \mathcal{V}$. While triggering based on $\phi_2 \left\| e_{2,i}(t) \right\|^2 - \frac{\theta}{N} \geq 0$ results in more conservative event-times for follower i than when triggering based on $\phi_2 \left\| e_{2,i}(t) \right\|^2 - \phi_3 \left\| z_i(t) \right\|^2 - \frac{\theta}{N} \geq 0$, the former results in a simpler condition from which to develop a self-trigger. Let t_k^i mark the k^{th} instance when $\phi_2 \left\| e_{2,i}(t) \right\|^2 - \frac{\theta}{N} \geq 0$. Hence, an event for follower i occurs at t_k^i provided $\phi_2 \left\| e_{2,i}(t_k^i) \right\|^2 - \frac{\theta}{N} \geq 0$. Note that for $t \in \left[t_k^i, t_{k+1}^i\right)$, $\phi_2 \left\| e_{2,i}(t) \right\|^2 - \frac{\theta}{N} \leq 0$ since $\left\| e_{2,i}(t_k^i) \right\| = 0$ and $\left\| e_{2,i}(t) \right\|$ may increase otherwise.

Substituting (2–1) and (2–10) into the time-derivative of (2–3) yields

$$\dot{e}_{2,i}(t) = A e_{2,i}(t) - B u_i(t). \tag{2–39}$$

The evolution of (2–3) is governed by (2–39), where the solution to (2–39) is not available since $u_i(t)$ is unknown *a priori.* Therefore, follower i cannot determine its own event-times. Let $\breve{e}_{2,i} : [0, \infty) \to \mathbb{R}_{\geq 0}$ denote an estimate of $\left\| e_{2,i}(t) \right\|$, and let $\left\{\hat{t}_k^i\right\}_{k=1}^{\infty} \subset \mathbb{R}_{\geq 0}$ be an increasing sequence of estimated event-times determined by a subsequently developed self-trigger for follower i. The estimate $\breve{e}_{2,i}(t)$ is designed such that

$$\phi_2 \left\| e_{2,i}(t) \right\|^2 - \frac{\theta}{N} \leq \phi_2 \breve{e}_{2,i}^2(t) - \frac{\theta}{N} \tag{2–40}$$

holds for all $t \in \left[t_k^i, t_{k+1}^i\right)$. Hence, executing the consensus protocol based on the estimated event-times originating from a self-trigger using $\breve{e}_{2,i}$ for all $i \in \mathcal{V}$ ensures the stability of the MAS. Based on the subsequent stability analysis, for each $\left[t_k^i, t_{k+1}^i\right)$, the estimate $\breve{e}_{2,i}(t)$ is designed as

$$\breve{e}_{2,i}(t) \triangleq \xi_i \left(e^{S_{\max}(A)\left(t - t_k^i\right)} - 1 \right), \tag{2–41}$$

$$\xi_i \triangleq \frac{S_{\max}(B) M_i}{S_{\max}(A)} \in \mathbb{R}_{>0}. \tag{2–42}$$

In (2–42), $M_i \in \mathbb{R}_{>0}$ is a known upper bound for $\|u_i(t)\|$, which exists given the proof of Theorem 2.1. Furthermore, Lemma 2.2 provides an upper bound for $\|u_i(t)\|$.

Lemma 2.2. *If the conditions in Theorem 2.1 are satisfied, then for each* $i \in \mathcal{C}(t)$ *and all* $t \geq 0$

$$\begin{aligned}\|u_i(t)\| \leq{}& S_{\max}\left(B^\top P\right) \max\{\|H(t) \otimes I_m\|\} \sqrt{\frac{\theta}{\phi_2}} \\ &+ S_{\max}\left(B^\top P\right) \max\{\|H(t) \otimes I_m\|\} (\beta_1 + \beta_2) \\ &+ S_{\max}\left(B^\top P\right) \sqrt{\frac{\theta}{N\phi_2}}.\end{aligned} \tag{2–43}$$

Proof. See Appendix A.2. ■

Theorem 2.3. *The estimate given by* (2–41) *and* (2–42) *satisfies* (2–40) *for all* $t \in \left[t_k^i, t_{k+1}^i\right)$, *where* $\hat{t}_{k+1}^i \leq t_{k+1}^i$ *such that* $\hat{t}_{k+1}^i$ *originates from the self-trigger given by*

$$\hat{t}_{k+1}^i \triangleq \inf\left\{t > \hat{t}_k^i : \phi_2 \breve{e}_{2,i}(t)^2 \geq \frac{\theta}{N}\right\}. \tag{2–44}$$

Proof. To satisfy (2–40), it is equivalent to show that $\breve{e}_{2,i}(t) \geq \|e_{2,i}(t)\|$ for all $t \in \left[t_k^i, t_{k+1}^i\right)$. Let $t \in \left[t_k^i, t_{k+1}^i\right)$. A Lyapunov-like function $V_{2,i} : \mathbb{R}^m \to \mathbb{R}_{\geq 0}$ is defined as

$$V_{2,i}(e_{2,i}(t)) \triangleq \frac{1}{2} e_{2,i}^\top(t) e_{2,i}(t), \tag{2–45}$$

which is continuously differentiable over $t \in \left[t_k^i, t_{k+1}^i\right)$. Substituting (2–39) into the time-derivative of (2–45) results in

$$\dot{V}_{2,i}(e_{2,i}(t)) \leq S_{\max}(A) \|e_{2,i}(t)\|^2 + S_{\max}(B) \|e_{2,i}(t)\| \|u_i(t)\|. \tag{2–46}$$

Based on the proof of Theorem 2.1, $u_i(t) \in \mathcal{L}_\infty$, where $\|u_i(t)\| \leq M_i$ such that M_i is a known bounding constant. Hence, (2–46) can be upper bounded by

$$\dot{V}_{2,i}(e_{2,i}(t)) \leq 2S_{\max}(A) V_{2,i}(e_{2,i}(t)) + S_{\max}(B) M_i \sqrt{2V_{2,i}(e_{2,i}(t))}. \tag{2–47}$$

Since follower i broadcasts its state at t_k^i, $V_{2,i}\left(e_{2,i}\left(t_k^i\right)\right) = 0$. Invoking the Comparison Lemma in [65, Lemma 3.4] on (2–47) yields

$$V_{2,i}\left(e_{2,i}\left(t\right)\right) \leq \left(\frac{\sqrt{2}\xi_i\left(e^{S_{\max}(A)\left(t-t_k^i\right)}-1\right)}{2}\right)^2. \tag{2–48}$$

Substituting (2–45) into (2–48) yields

$$\left\|e_{2,i}\left(t\right)\right\| \leq \xi_i\left(e^{S_{\max}(A)\left(t-t_k^i\right)}-1\right) = \breve{e}_{2,i}\left(t\right).$$

Hence, (2–40) holds for all $t \in \left[t_k^i, t_{k+1}^i\right)$, where the conditions in (2–24) and (2–44) imply $\hat{t}_{k+1}^i \leq t_{k+1}^i$.[6] ■

Remark 2.6. The self-trigger condition in (2–44) is free from Zeno behavior by a similar argument provided in the proof of Theorem 2.2.

Remark 2.7. Define (2–41) over $\left[t_{k-1}^i, t_k^i\right)$, and observe that since $\left\|e_{2,i}\left(t\right)\right\| \leq \breve{e}_{2,i}\left(t\right)$ over $\left[t_{k-1}^i, t_k^i\right)$, $\left\|e_{2,i}\left(t_k^i\right)\right\| = 0$, and $\breve{e}_{2,i}\left(t\right)$ in (2–41) is strictly increasing, it follows that $\left\|e_{2,i}^{-}\left(t\right)\right\|$ defined in (2–5) satisfies the inequality $\left\|e_{2,i}^{-}\left(t\right)\right\| \leq \breve{e}_{2,i}\left(t_k^i\right)$. Therefore, $\breve{e}_{2,i}\left(t_k^i\right)$ is a candidate for $\Psi_{i,k}$.

2.6 Simulation Example

A simulation study is included to demonstrate and compare the performances of the developed approaches. The simulated MAS consists of five follower agents and a single leader agent. The initial positions of each agent, which are equivalent for all simulations, are $x_0\left(0\right) = \left[6,\ 2\right]^\top$ m, $x_1\left(0\right) = \left[12,\ 2.5\right]^\top$ m, $x_2\left(0\right) = \left[12,\ 2\right]^\top$ m, $x_3\left(0\right) = \left[12,\ 1.5\right]^\top$ m, $x_4\left(0\right) = \left[13,\ 2.25\right]^\top$ m, and $x_5\left(0\right) = \left[13,\ 1.75\right]^\top$ m. The known state and control effectiveness matrices used in all simulations are given by

[6] While (2–41) is initialized at t_k^i in the development, implementation of the STC strategy requires communication at $\hat{t}_k^i$.

$$A \triangleq \begin{bmatrix} 0.05 & 0 \\ 0 & 0 \end{bmatrix}, B \triangleq \begin{bmatrix} 0.3 & 0 \\ 0 & 0.3 \end{bmatrix}.$$

The known desired trajectory $x_d : [0, \infty) \to \mathbb{R}^2$ of the leader is

$$x_d(t) \triangleq [5\cos(0.2\pi t),\ 5\sin(0.4\pi t)]^\top, \tag{2–49}$$

while the leader's trajectory tracking error $e_0 : [0, \infty) \to \mathbb{R}^2$ is

$$e_0(t) \triangleq x_d(t) - x_0(t). \tag{2–50}$$

The leader's tracking error in (2–50) can be globally exponentially regulated using the following controller:

$$u_0(t) \triangleq B^{-1}(\dot{x}_d(t) - Ax_0(t) + k_0 e_0(t)), \tag{2–51}$$

where $k_0 > 0$.

Lemma 2.3. *The controller of the leader provided in* (2–51) *ensures* (2–50) *is globally exponentially regulated and* $x_0, u_0 \in \mathcal{L}_\infty$ *provided the desired trajectory satisfies* $x_d, \dot{x}_d \in \mathcal{L}_\infty$, *Assumption 2.1 is satisfied, the right pseudo inverse of the control effectiveness matrix, i.e.,* B, *exists, and* k_0 *is selected such that* $k_0 > 0$.

Proof. See Appendix A.3. ■

All simulations are 12 seconds long and use an integration time-step of 1.00×10^{-5} seconds. Additionally, all ETC and STC simulations used the following parameters, which originate from Algorithm 2.1: $k_0 = 3\ s^{-1}$, $\delta = 3 \times 10^7$, $\kappa = 1.00 \times 10^{-2}$, $\rho = 4.87 \times 10^5$, $\gamma = 1.54 \times 10^5$, $k_1 = 2.78 \times 10^3$, $k_2 = 1.78 \times 10^3$, $k_3 = 1.00 \times 10^3$, $k = 1.07 \times 10^4$, $\theta = 1.00 \times 10^3\ m^2 \cdot s^{-1}$, $\phi_1 = 1.00 \times 10^3\ s^{-1}$, $\phi_2 = 7.80 \times 10^6\ s^{-1}$, $\phi_3 = 37.87\ s^{-1}$, $M_1 = 800\ m$, $M_2 = 800\ m$, $M_3 = 800\ m$, $M_4 = 800\ m$, and $M_5 = 800\ m$.

2.6.1 Benchmark Simulation

As a benchmark, the MAS is first simulated by using an event-triggered approach, where all followers are designed as cooperative agents for the entire simulation. Figure 2-1 depicts two networks, where the network on the left consists only of cooperative followers while the network on the right consists of both cooperative and Byzantine followers. The blue square denotes the leader agent, the orange circles denote the cooperative followers, and the red triangles denote the Byzantine followers. The network used in the benchmark simulation is depicted by the left topology in Figure 2-1, and Figures 2-2 and 2-3 display the results. The x's denote the starting position of each agent in Figure 2-2.

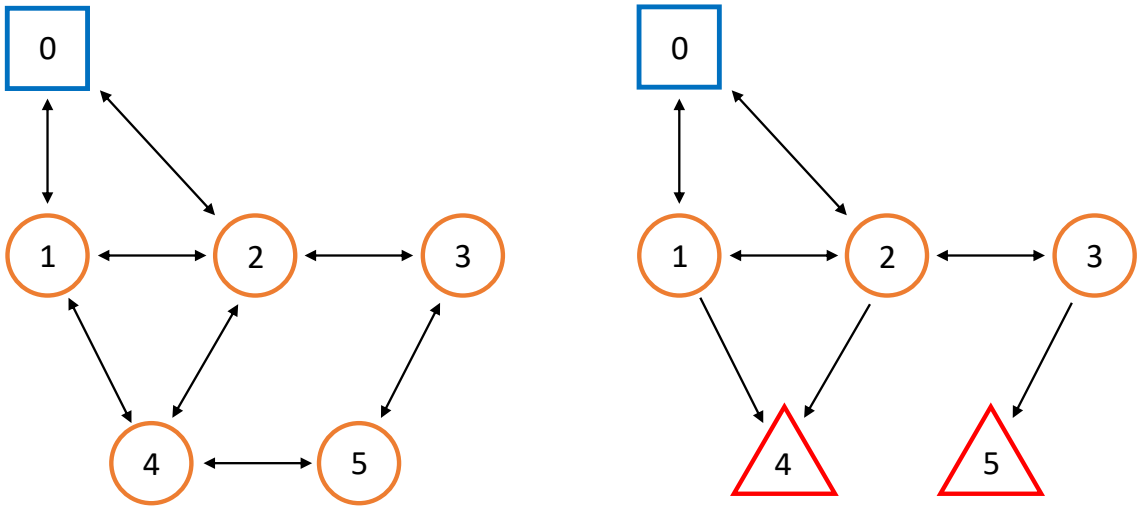

Figure 2-1. Illustration of the network topologies used in the simulations.

Figure 2-2 displays a planar view of the MAS trajectories for the ETC method with cooperative agents. Figure 2-3 presents the norm of the tracking errors of the followers and leader as quantified by (2–2) and (2–50), respectively. In Figure 2-3, the followers connected to the leader experience smaller tracking errors than the followers that are not connected to the leader. The maximum steady state tracking errors of Followers $1-5$ are 0.41 m, 0.46 m, 0.68 m, 0.59 m, and 0.72 m, respectively. Moreover, the maximum steady state velocities of Followers $1-5$ are 7.38 m/s, 7.34 m/s, 7.27 m/s, 7.39 m/s, and

7.22 m/s, respectively. The time instances a follower sent information to a neighbor were measured throughout the simulation. The minimum time difference between consecutive communication instances for all followers was 6.00×10^{-5} s, which implies that all followers must be equipped with radios capable of broadcasting at approximately 16.67 kHz.

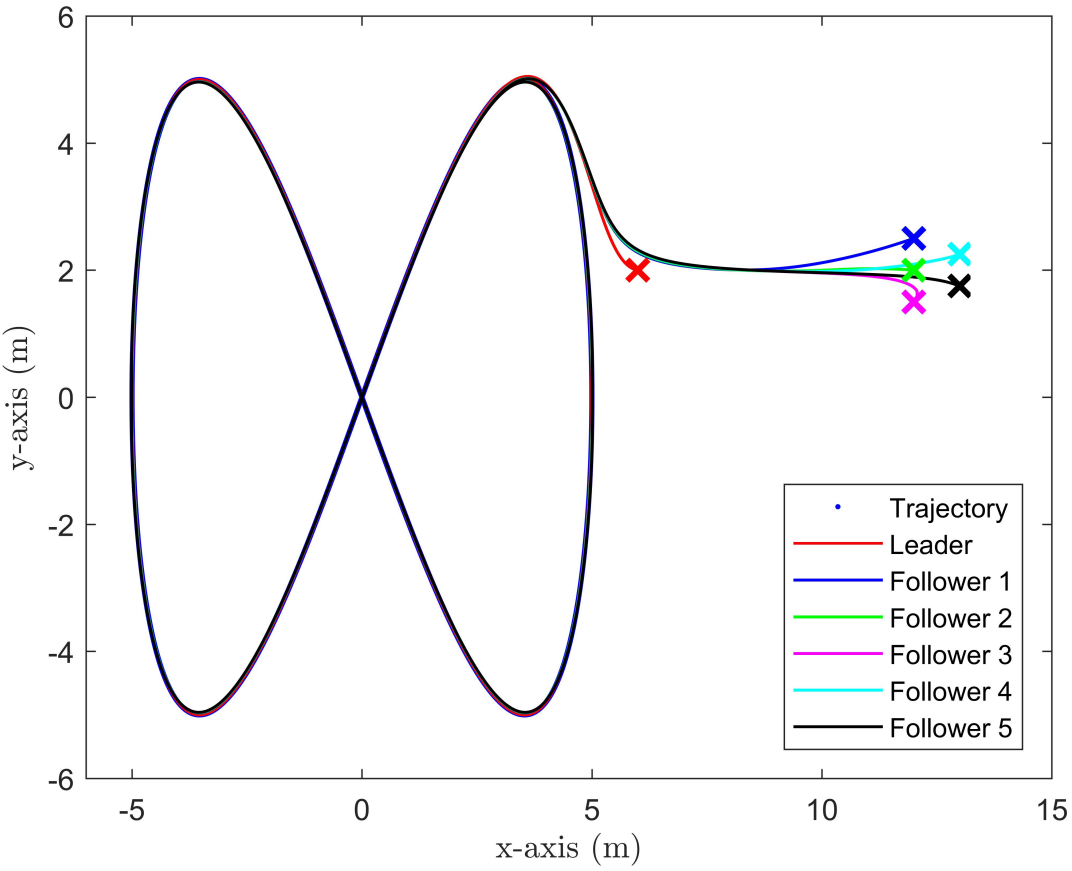

Figure 2-2. Planar trajectories of the MAS using ETC with purely cooperative agents.

2.6.2 ETC Simulation with Byzantine Adversaries

The next simulation is similar to the benchmark, except two originally cooperative followers are converted into Byzantine agents. Specifically, Follower 4 is converted into a Type II Byzantine agent at time $t = 9$ seconds, and Follower 5 is converted into a Type I Byzantine agent at time $t = 5$ seconds. For $t \geq 9$ seconds, Follower 4 executes the controller $u_4(t) = [50, \ -50]^\top$, and for $t \geq 5$ seconds, Follower 5 communicates state

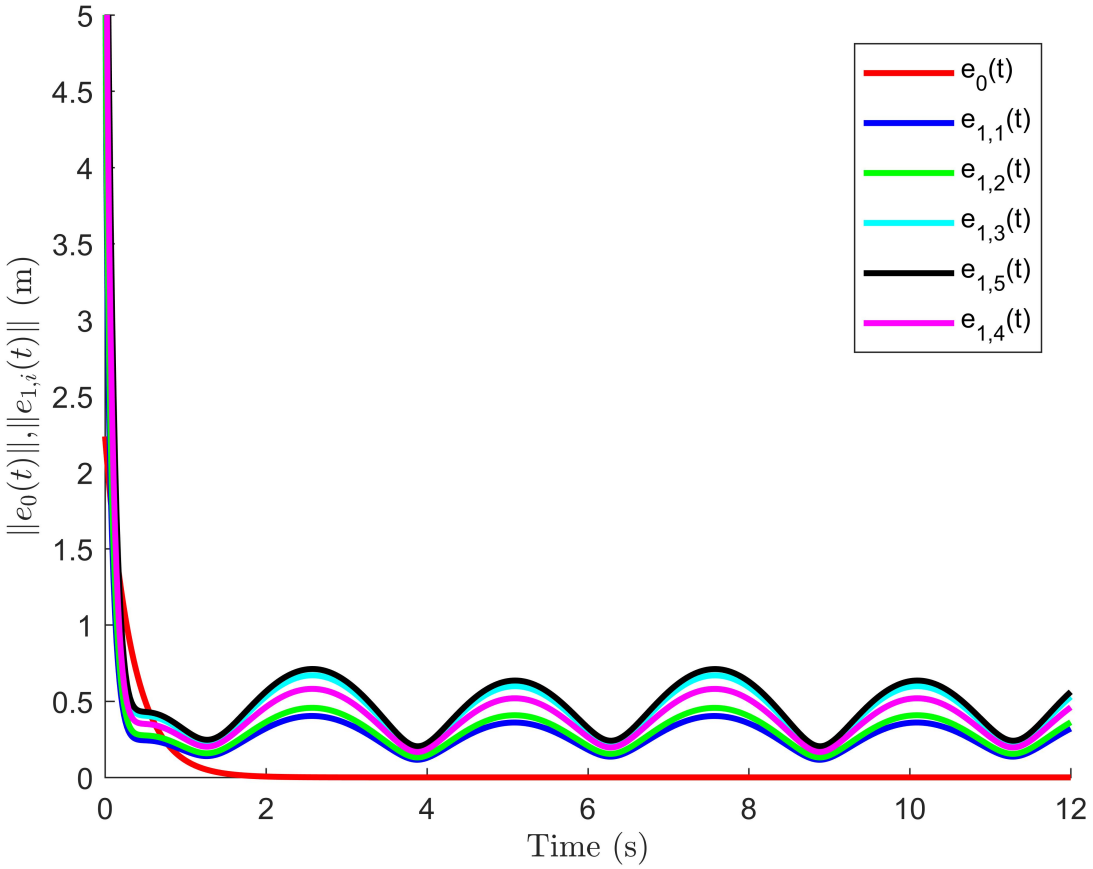

Figure 2-3. Norm of the tracking errors for the MAS using ETC with purely cooperative agents.

information about itself to its neighbors according to $x_{5,i}(t) = e^{100I_2(t-5)}x_5(t)$, where $x_{5,i}(t)$ denotes the position of Follower 5 within the global coordinate frame at time $t \geq 5$ that is communicated to neighbor i. The objective of the remaining cooperative followers is to identify any potential Byzantine neighbors, remove the Byzantine agent's influence from their controllers, and synchronize their trajectories to the leader's trajectory. Successful execution of this protocol will transform the communication topology from the left network to the right network in Figure 2-1.

Figure 2-4 demonstrates that the cooperative followers satisfied the objective, where Follower 1 and Follower 2 each detected the Type II Byzantine agent at $t = 9.04$ seconds and Follower 3 detected the Type I Byzantine agent at $t = 5.02$ seconds. As

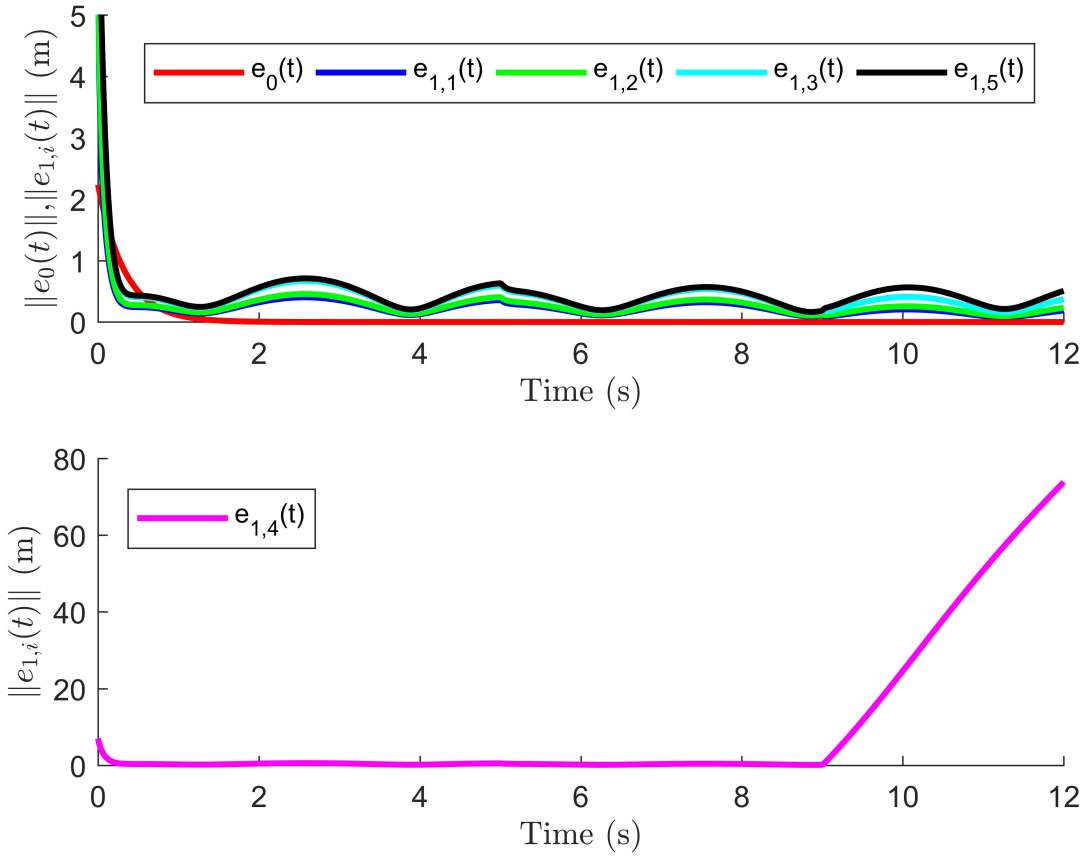

Figure 2-4. Norm of the tracking errors for the MAS using ETC with cooperative and Byzantine agents in the network.

seen in Figure 2-4, the followers connected to the leader experience smaller tracking errors than followers that are not connected to the leader. The maximum steady state tracking errors of Followers $1-3$ are 0.41 m, 0.46 m, and 0.68 m, respectively. Moreover, the maximum steady state velocities of Followers $1-3$ are 7.58 m/s, 7.75 m/s, 11.57 m/s, respectively. The minimum time difference between consecutive communication instances for all followers was 6.00×10^{-5} s. Followers 4 and 5 are Byzantine adversaries, where their behaviors cannot be guaranteed. Therefore, their steady state tracking error and maximum steady state velocity are not included. When compared to the benchmark simulation results, the cooperative followers in this simulation obtain the same steady

state tracking errors and similar maximum steady state velocities. Therefore, the ETC method obtained similar performance to the Benchmark result.

2.6.3 STC Simulation with Byzantine Adversaries

This simulation is identical to the one in Section 2.6.2, except the STC method from Section 2.5 is used instead. Figure 2-5 demonstrates that the cooperative followers satisfied the objective, where Follower 1 and Follower 2 detected the Type II Byzantine agent at $t = 9.001$ seconds and Follower 3 detected the Type I Byzantine agent at $t = 5.001$ seconds. As depicted in Figure 2-5, the followers connected to the leader experience smaller tracking errors than followers that are not connected to the leader. The maximum steady state tracking errors of Followers $1 - 3$ are 0.40 m, 0.46 m, and 0.67 m, respectively. Moreover, the maximum steady state velocities of Followers $1 - 3$ are 7.25 m/s, 7.31 m/s, 7.70 m/s, respectively. The minimum time difference between consecutive communication instances for all followers was 2.00×10^{-5} s.

When compared to the ETC results with Byzantine agents, the cooperative followers in the STC simulation obtain similar steady state tracking errors and maximum steady state velocities. While the same θ parameter was used between simulations, further investigation of the effect θ has on communication is needed for the ETC and STC approaches. The results of such a study are provided in the following subsection.

2.6.4 Communication Frequency vs. Performance Study

In this section, six simulations are performed for the ETC and STC strategies under the same parameters as the previous simulations, except θ is varied to investigate the trade-off between communication frequency and steady state consensus errors. Furthermore, an additional reference simulation is performed to enable comparison between the ETC and STC results. The reference simulation is performed under the same parameters as the previous simulations except all agents communicate at the same fixed rate of 10 kHz. A communication rate of 10 kHz for a 12 second simulation results in 1.20×10^5 reference event-times, i.e., reference communication instances.

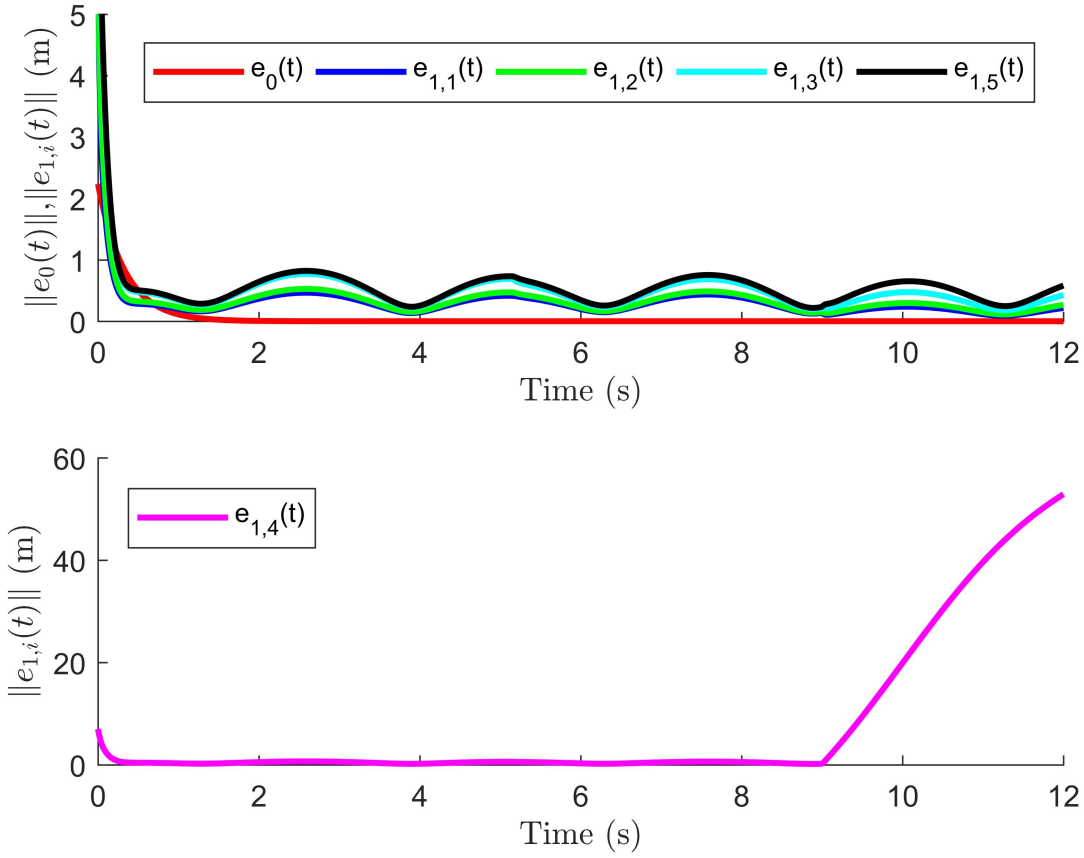

Figure 2-5. Norm of the tracking errors for the MAS using STC with cooperative and Byzantine agents in the network.

Tables 2-1 and 2-2 summarize the results of the ETC and STC simulations, respectively, where $\beta_{1,m}$ denotes the maximum steady state tracking error between Followers $1-3$, Min. Comm. Time denotes the minimum time difference between consecutive communication events over all followers, Comm. Fraction represents the amount of communication performed by an agent as determined by

$$\text{Comm. Fraction} \triangleq \frac{\text{Number of Event Times}}{\text{Number of Ref. Event Times}}, \tag{2–52}$$

and Comm. Max. Energy denotes the maximum amount of energy used by all followers to monitor and transmit data. According to [78], the energy $J_i : [0, \infty) \to \mathbb{R}_{\geq 0}$ consumed by follower i at time t to monitor and transmit data under an ETC approach is given

by $J_i(t) \triangleq \sum_{k \in \Gamma_i(t)} (c_1 + p_2 c_2) + c_3 t$, where $\Gamma_i(t) \triangleq \{k : t_k^i \leq t\}$, c_1 describes the cost associated to the packet overhead transmission, c_2 describes the cost per transmitted scalar, c_3 describes the cost of continuous monitoring, and p_2 denotes the number of transmitted scalars. Since the STC method does not require continuous monitoring of the trigger condition, where monitoring is done at the same time as transmission, the monitoring cost is negligible when compared to the ETC approach. Therefore, the energy consumption function for follower i using STC is $J_i(t) \triangleq \sum_{k \in \Gamma_i(t)} (c_1 + p_2 c_2)$. The parameters c_1 through c_3 denote fixed energy costs consumed per update. Since each follower transmits its state at the current event-time under the ETC approach, $p_2 = 2$ given $x_i(t) \in \mathbb{R}^2$. For STC, each follower transmits its state and future event-time at the current event-time. Hence, $p_2 = 3$ since $x_i(t) \in \mathbb{R}^2$ and $t_k^i \in \mathbb{R}_{\geq 0}$. The parameters used in the energy consumption functions are $c_1 = 38.4$ mJ, $c_2 = 3.2$ mJ, and $c_3 = 60$ mW, which are approximations obtained from power consumption values for a MicaZ using a ZigBee for wireless communication [78].

The * next to the Comm. Fraction of Follower 5 in Table 2-1 indicates that Follower 5 was not able to detect Follower 4 as a Byzantine neighbor. As seen in Tables 2-1 and 2-2, frequent communication results in high energy costs. Moreover, frequent communication leads to better tracking performance, where the cooperative followers can track the leader more closely. Tables 2-1 and 2-2 also indicate that the STC approach yields better performance than the ETC strategy relative to the same value of θ because of the more frequent communication by STC than ETC. However, ETC can yield comparable performance to STC while using less energy to communicate.

Table 2-1. Event-Triggered Communication Performance Summary

Simulation	1	2	3	4	5	6
$\theta(\ m^2 \cdot s^{-1})$	1.00×10^3	1.00×10^4	1.00×10^5	1.00×10^6	1.00×10^7	1.00×10^8
$\beta_{1,m}\ (m)$	0.68	0.69	0.78	0.81	0.86	1.15
Min. Comm. Time (s)	6.00×10^{-5}	1.00×10^{-4}	2.60×10^{-4}	2.90×10^{-4}	8.30×10^{-4}	6.70×10^{-3}
Comm. Max. Energy (J)	1.45×10^3	467.04	148.96	54.17	53.63	28.89
Foll. 1: Comm. Frac.	0.17	0.06	0.02	0.01	0.007	0.004
Foll. 2: Comm. Frac.	0.27	0.09	0.03	0.01	0.009	0.003
Foll. 3: Comm. Frac.	0.19	0.06	0.02	0.01	0.007	0.004
Foll. 4: Comm. Frac.	0.25	0.08	0.03	0.01	0.009	0.005
Foll. 5: Comm. Frac.	0.17	0.06	0.02	0.01	0.006	0.002*

Table 2-2. Self-Triggered Communication Performance Summary

Simulation	1	2	3	4	5	6
$\theta(\ m^2 \cdot s^{-1})$	1.00×10^3	1.00×10^4	1.00×10^5	1.00×10^6	1.00×10^7	1.00×10^8
$\beta_{1,m}\ (m)$	0.67	0.67	0.67	0.67	0.69	0.74
Min. Comm. Time (s)	2.00×10^{-5}	6.00×10^{-5}	2.10×10^{-4}	6.60×10^{-4}	2.10×10^{-3}	3.20×10^{-3}
Comm. Max. Energy (J)	7.49×10^4	2.37×10^4	7.50×10^3	2.37×10^3	749.90	237.22
Foll. 1: Comm. Frac.	8.28	2.62	0.83	0.26	0.08	0.03
Foll. 2: Comm. Frac.	13.02	4.12	1.30	0.41	0.13	0.04
Foll. 3: Comm. Frac.	9.47	2.99	0.95	0.30	0.09	0.03
Foll. 4: Comm. Frac.	11.83	3.74	1.18	0.37	0.12	0.04
Foll. 5: Comm. Frac.	8.28	2.62	0.83	0.26	0.08	0.03

CHAPTER 3
EVENT-TRIGGERED FORMATION CONTROL AND LEADER TRACKING WITH RESILIENCE TO BYZANTINE ADVERSARIES: A REPUTATION-BASED APPROACH

A distributed event-triggered controller is developed for FCLT with robustness to adversarial Byzantine agents for a class of heterogeneous control-affine MASs. Assuming each agent can accurately measure the state of a neighbor whenever the neighbor broadcasts its state, a reputation-based strategy is developed for each agent to detect Byzantine agent behaviors within their neighbor set and then selectively disregard Byzantine state information. Note that the reputation algorithm does not require model knowledge. Selectively ignoring Byzantine agents results in a time-varying graph topology. Nonsmooth dynamics also result from intermittent communication due to an event-triggered strategy, which facilitates the efficient use of resources. Nonsmooth Lyapunov methods are used to prove stability and FCLT of the MAS consisting of the remaining cooperative agents.

3.1 Agent Dynamics and Network Topology

Consider a heterogeneous MAS consisting of a single leader agent indexed by 0 and a set of $N \in \mathbb{Z}_{>0}$ follower agents indexed by $\mathcal{V}$. The uncertain nonlinear model for agent $i \in \mathcal{V} \cup \{0\}$ is

$$\dot{x}_i(t) \triangleq f_i(x_i(t)) + g_i(x_i(t))\, u_i(t) + d_i(t), \tag{3–1}$$

where $x_i : [0,\infty) \to \mathbb{R}^n$ denotes the position, $\dot{x}_i : [0,\infty) \to \mathbb{R}^n$ denotes the velocity, $f_i : \mathbb{R}^n \to \mathbb{R}^n$ denotes the uncertain drift dynamics, $g_i : \mathbb{R}^n \to \mathbb{R}^{n\times m}$ denotes the known control effectiveness matrix, $u_i : [0,\infty) \to \mathbb{R}^m$ denotes the control input, and $d_i : [0,\infty) \to \mathbb{R}^n$ denotes an exogenous disturbance for agent i. Let $\mathcal{B} : [0,\infty) \to 2^{\mathcal{V}}$ define the time-varying set of Byzantine agents and $\mathcal{C} : [0,\infty) \to 2^{\mathcal{V}}$ define the time-varying set of cooperative agents, where $\mathcal{B}(t) \cap \mathcal{C}(t) = \varnothing$ and $\mathcal{B}(t) \cup \mathcal{C}(t) = \mathcal{V}$ for all $t \geq 0$. The following assumptions are made to facilitate the subsequent analysis.

Assumption 3.1. For each $i \in \mathcal{V} \cup \{0\}$, the uncertain drift dynamics f_i are class C^1 and bounded given a bounded argument, i.e., if $\|x(t)\| \leq \bar{c}_1$ for some $\bar{c}_1 \in \mathbb{R}_{>0}$, then $\|f_i(x(t))\| \leq \bar{c}_2$ for some $\bar{c}_2 \in \mathbb{R}_{>0}$.

Assumption 3.2. The control effectiveness matrix g_i is C^1, bounded given a bounded argument, and full-row rank for all $i \in \mathcal{V} \cup \{0\}$. Moreover, the right pseudo inverse of g_i is denoted by $g_i^+ : \mathbb{R}^n \to \mathbb{R}^{m \times n}$, where $g_i^+(\cdot) \triangleq g_i^\top(\cdot)\left(g_i(\cdot)\, g_i^\top(\cdot)\right)^{-1}$ is bounded given a bounded argument for each $i \in \mathcal{V} \cup \{0\}$.[1]

Assumption 3.3. The exogenous disturbance d_i is continuous and bounded in the sense that $\|d_i(t)\| \leq d_{i,\max}$ for all $t \geq 0$ and $i \in \mathcal{V} \cup \{0\}$, where $d_{i,\max} \in \mathbb{R}_{>0}$ is a known bounding constant.

Assumption 3.4. The leader is cooperative for all $t \geq 0$.[2]

Assumption 3.5. Agent i is capable of measuring its own position $x_i(t)$ for all $t \geq 0$ and all $i \in \mathcal{V} \cup \{0\}$.

Assumption 3.6. [37] The control and position of the leader are bounded, i.e., there exist $u_{0,\max}, x_{0,\max} \in \mathbb{R}_{>0}$ such that $\|u_0(t)\| \leq u_{0,\max}$ and $\|x_0(t)\| \leq x_{0,\max}$ for all $t \geq 0$.

Assumption 3.7. For each instant $t \geq 0$ that follower $j \in \mathcal{N}_i(t)$ broadcasts its state to follower i, follower i can accurately measure the state of follower j.

Let $x_{ij} : [0, \infty) \to \mathbb{R}_{\geq 0}$ be defined as $x_{ij}(t) \triangleq \|x_i(t) - x_j(t)\|$. Agent i can broadcast information to agent j if and only if $x_{ij}(t) \leq R_{C,i}$, where $R_{C,i} \in \mathbb{R}_{>0}$ denotes

[1] The assumption of a full row rank control influence matrix is potentially restrictive for some applications (e.g., underactuated systems) and is a topic for future investigation. For LTI systems with a full column rank control effectiveness matrix, the Algebraic Riccati Equation or Linear Matrix Inequalities can potentially be used to develop stabilizing controllers.

[2] In the absence of a manned leader, multiple leaders can be added to the MAS through the pinning matrix strategy to impart additional resilience to Byzantine adversaries. Assumption 3.4 can then be reduced to requiring that at least one leader is cooperative for all time.

the communication radius of agent i. Similarly, agent i can sense agent j if and only if $x_{ij}(t) \leq R_{S,i}$, where $R_{S,i} \in \mathbb{R}_{>0}$ denotes the sensing radius of agent i. Without loss of generality, let $R \triangleq \min_{i \in \mathcal{V}} \{R_{C,i}, R_{S,i}\} \in \mathbb{R}_{>0}$, where R is defined as the interaction radius of all agents in the MAS. The neighbor set of follower i is given by $\mathcal{N}_i(t) \triangleq \{j \in \mathcal{V} : x_{ij}(t) \leq R\}$, where followers i and $j \in \mathcal{N}_i(t)$ can both broadcast information to and sense each other. Followers i and j are said to be paired if and only if $i \in \mathcal{N}_j(t)$ and $j \in \mathcal{N}_i(t)$. Similarly, followers i and j are said to be connected if and only if $a_{ij}(t) \neq 0$ and $a_{ji}(t) \neq 0$.

Observe that follower i can be influenced by follower j if and only if $a_{ij}(t) \neq 0$. The influence relationships between the followers of the MAS are modeled by a time-varying, weighted, and undirected graph $\mathcal{G}(t) \triangleq (\mathcal{V}, \mathcal{E}(t), \mathcal{A}(t))$. Let $\mathcal{E}_C(t)$ denote the undirected edge set and $\mathcal{A}_C(t)$ denote the weighted adjacency matrix associated with all cooperative followers in $\mathcal{C}(t)$. Moreover, the sub-MAS consisting of only the cooperative followers is modeled by the time-varying, weighted, and undirected graph $\mathcal{G}_C(t) \triangleq (\mathcal{C}(t), \mathcal{E}_C(t), \mathcal{A}_C(t))$ and is referred to as the cooperative MAS (CMAS).

Assumption 3.8. The graph $\mathcal{G}_C(t)$ is connected for all $t \geq 0$, and $b_i(t) > 0$ for some $i \in \mathcal{C}(t)$ for all $t \geq 0$.[3]

Remark 3.1. Assumptions 3.4 and 3.8 ensure that each cooperative agent has at least one cooperative neighbor for all $t \geq 0$, even in the presence of a DoS attack. Moreover, Assumptions 3.4 and 3.8 ensure that the Byzantine agents cannot enter the MAS in a manner that partitions $\mathcal{G}_C(t)$ for any $t \geq 0$.

[3] An alternative to Assumption 3.8 is to assume $\mathcal{G}_C(t)$ is connected for all time, upper bound the number of Byzantine adversaries within a network by $f \in \mathbb{Z}_{>0}$, use more than f leaders, and employ connectivity models like the $2f+1$ model described in [26].

3.2 Objectives

The FCLT goal is to design distributed controllers for all followers in the MAS that maneuver the followers to a desired formation while tracking the leader. However, as FCLT is taking place, some followers may transform into Byzantine agents as a result of operating within a contested environment, e.g., if they suffer cyber-attacks. The objective is to design distributed controllers for all followers $i \in \mathcal{V}$ governed by (3–1) that enable the cooperative followers to achieve FCLT while identifying Byzantine agents and removing all Byzantine influence from the CMAS. The distributed controllers are event-triggered to promote the efficient use of communication and sensing resources. Cooperative and Byzantine agents are managed through the edge weight policy, which is based on a reputation algorithm. The policy enables all agents to differentiate between cooperative and Byzantine neighbors, coordinate their motion by using only information from cooperative neighbors, and re-integrate agents into the CMAS once an agent converts from Byzantine to cooperative. The separation between communication and influence is made to enable the re-integration of remediated followers, which requires communication between cooperative-Byzantine pairs. The ability to reintegrate cooperative agents is key for defense against adversarial behaviors such as mobile jammers that can temporarily affect agents before moving on to jam other agents. To quantify the objective, let the FCLT error $e_{1,i} : [0, \infty) \to \mathbb{R}^n$ be defined as

$$e_{1,i}(t) \triangleq x_i(t) - x_0(t) - v_i, \tag{3–2}$$

where $v_i \in \mathbb{R}^n$ denotes the desired relative position between follower i and the leader.

Assumption 3.9. The relative position vector v_i is fixed for all $i \in \mathcal{V}$. Moreover, each follower knows v_i for all $i \in \mathcal{V}$, i.e., each follower knows the entire formation.

By allowing each follower to know v_i for all $i \in \mathcal{V}$, any rehabilitated agent can be re-integrated into any available formation vacancy, if there are multiple options. The FCLT

problem can be converted into a leader-follower consensus problem provided $v_i \triangleq 0_n$ for all $i \in \mathcal{V}$. The use of ETC also motivates the development of an estimator to provide continuous state estimates between communication events. The state estimation error of follower i is defined by $e_{2,i} : [0, \infty) \to \mathbb{R}^n$, where

$$e_{2,i}(t) \triangleq \hat{x}_i(t) - x_i(t) \tag{3–3}$$

such that $\hat{x}_i : [0, \infty) \to \mathbb{R}^n$ denotes the state estimate of x_i.

3.3 Controller Development

3.3.1 Trust Model

As Byzantine agents emerge in the MAS, the remaining cooperative followers require a method to identify their cooperative neighbors. Let $\tau_{ij} : [0, \infty) \to [0, 1]$ denote the piecewise constant trust that follower i has in follower $j \in \mathcal{N}_i(t)$, where 0 and 1 represent no trust and maximum trust, respectively. Each follower i can obtain state information from any neighbor j through communication and sensing, where the redundancy in state information is used to compute τ_{ij}. Let $x_{i,1} : [0, \infty) \to \mathbb{R}^n$ and $x_{i,2} : [0, \infty) \to \mathbb{R}^n$ denote the communicated and sensed, i.e., measured, state of follower i, respectively. The subscripts 1 and 2 denote the type of data, i.e., 1 refers to communicated data and 2 refers to sensed data, where both types of data describe the same quantity.

Let $\{t_k^j\}_{k=0}^{\infty} \subset \mathbb{R}_{\geq 0}$ be an increasing sequence of event-times determined by the event-trigger mechanism of follower j, where the event-time t_k^j denotes the k^{th} instance follower j broadcasts its state information to its neighbors, all of which are received simultaneously. Let $t_{\text{reset}} \in \mathbb{R}_{>0}$ be a user-defined parameter that denotes the length of time over which trust is determined. The trust follower i has in neighbor j is determined

by (cf., the motivating result in [37])

$$\tau_{ij}(t) \triangleq \begin{cases} 1, & |S_j| = 0 \\ \frac{1}{|S_j|} \sum\limits_{t_k^j \in S_j} e^{-s_1 \Psi_{ij}(t_k^j)}, & |S_j| \neq 0 \end{cases} \tag{3–4}$$

$$\Psi_{ij}\left(t_k^j\right) \triangleq \left\| x_{j,1}\left(t_k^j\right) - x_{j,2}\left(t_k^j\right) \right\|,$$

where $S_j \triangleq \{t_k^j \in \mathbb{R}_{\geq 0} : t - t_{\text{reset}} \leq t_k^j < t\}$, $x_{j,1}(t_k^j)$ and $x_{j,2}(t_k^j)$ denote the communicated and sensed version of the state of follower j at event-time t_k^j, respectively, and $s_1 \in \mathbb{R}_{>0}$ is a user-defined parameter that determines how fast trust decreases. Note that $\Psi_{ij}(t_k^j)$ measures the discrepancy in the state information follower i has about follower $j \in \mathcal{N}_i(t)$ at time t_k^j. Other trust models can be used instead of (3–4) provided agreement and disagreement between the communicated and sensed version of the state of follower j results in high and low trust, respectively. In (3–4), all agents begin with maximum trust. However, as discrepancies in the two-point authentication of follower j grow, the trust value of follower j decreases to zero. Conversely, the trust of follower j may increase given the discrepancies in the two-point authentication of follower j are negligible for each $t_k^j \in S_j$, i.e., if $\Psi_{ij}(t_k^j) \approx 0$ for each $t_k^j \in S_j$, then $\tau_{ij}(t) \approx 1$. In the event that follower $j \in \mathcal{N}_i(t)$ does not provide state information to follower i when required, i.e., $\Delta t_k^j \triangleq t_k^j - t_{k-1}^j > \Delta_j$, then $\Psi_{ij}(t_k^j) = \vartheta$, where $\Delta_j \in \mathbb{R}_{>0}$ is a user-defined parameter based on either a simulation/experimental study or an analysis-based derivation, and $\vartheta \in \mathbb{R}_{>0}$ is a user-defined penalty. Similarly, if the distance between follower $j \in \mathcal{N}_i(t)$ and follower i is beyond a user-defined threshold a time t_k^j, i.e., $r < \omega_{ij}(t_k^j) \triangleq \|x_i(t_k^j) - x_{j,2}(t_k^j)\| \leq R$, for $r \in (0, R)$, then $\Psi_{ij}(t_k^j) = \vartheta$.

Remark 3.2. Assumption 3.7 affords each agent access to ground-truth state information for each of its neighbors, where comparisons between the communicated and sensed states enable Type I Byzantine agent detection. Moreover, Type II Byzantine agents can abandon the MAS while potentially communicating true state information that could pull the remaining agents with them in their attempt to maintain connectivity.

Such a scenario may perturb and destabilize the MAS. Therefore, agent i requires access to accurate state information for each $j \in \mathcal{N}_i(t)$ that is $r-$close to $x_i(t)$ to ensure Type I and Type II Byzantine agent detection for each $i \in \mathcal{V}$.

Remark 3.3. By Assumption 3.7, follower i is able to measure the state of follower $j \in \mathcal{N}_i(t)$ each time follower j broadcasts its state. Therefore, Assumption 3.7 implies that the broadcast state of follower j is synchronized with the measured state of follower j. In practice, achieving synchronization between the broadcast and sensed states of follower j may be unattainable, where the sensed state may be obtained $\delta t > 0$ time units after the broadcast state is received. However, the s_1 parameter in (3–4) can be tuned to account for the asynchronous state information provided $\delta t > 0$ is small enough such that $\|x_{j,1}(t_k^j) - x_{j,2}(t_k^j + \delta t)\| \leq \epsilon(\delta t)$ for small $\epsilon(\delta t) > 0$. Future works aim at developing trust models that enable Byzantine agent detection through the use of asynchronous state information, where [79] and [80] serve as potential inroads.

3.3.2 Reputation Model

Because a Byzantine agent can provide different state information to each of its neighbors, each neighbor may have a different trust value for the same Byzantine agent. However, multiple trust values for a common neighbor can be consolidated into an overall reputation for the common neighbor. Let $\mathcal{N}_{ij}(t) \triangleq \mathcal{N}_i(t) \cap \mathcal{N}_j(t)$ denote the set of common neighbors shared between followers i and j. Motivated by [37], the continuous reputation $\zeta_{ij} : [0, \infty) \to \mathbb{R}_{\geq 0}$ follower i has for follower $j \in \mathcal{N}_i(t)$ is

$$\dot{\zeta}_{ij}(t) \triangleq \text{proj}\left(\eta_\tau\left(\tau_{ij}(t) - \zeta_{ij}(t)\right) + \sum_{n \in \mathcal{N}_{ij}(t)} \eta_\zeta \zeta_{in}(t)\left(\zeta_{nj}(t_k^n) - \zeta_{ij}(t)\right)\right), \tag{3–5}$$

where $\zeta_{ij}(0) = 1$ and $\text{proj}(\cdot)$ denotes the continuous projection operator defined in [81] that is used to ensure $\zeta_{ij}(t) \in [0, 1]$ for all $t \geq 0$. In (3–5), the parameters $\eta_\tau \in \mathbb{R}_{>0}$ and $\eta_\zeta \in \mathbb{R}_{\geq 0}$ allow the user to select whether the reputation model places more emphasis on measured information, i.e., $\tau_{ij}(t) - \zeta_{ij}(t)$, observed information, i.e., $\zeta_{in}(t)\left(\zeta_{nj}(t_k^n) - \zeta_{ij}(t)\right)$, or weighs both measured and observed information equally.

Like the trust model in (3–4), reputation values of 0 and 1 correspond to no and maximum reliability, respectively. At event-time t_k^n, follower i receives reputation values held by follower $n \in \mathcal{N}_i(t)$ for all followers $j \in \mathcal{N}_n(t)$, i.e., $\zeta_{nj}(t_k^n)$, where follower i computes $\zeta_{in}(t)(\zeta_{nj}(t_k^n) - \zeta_{ij}(t))$ over $n \in \mathcal{N}_{ij}(t)$. The measured information in (3–5) contributes towards the reputation held by follower i for follower j based on the trust measurements follower i has of follower j. The observed information in (3–5) contributes to the reputation held by follower i for follower j based on the reputation of follower j held by common neighbors $n \in \mathcal{N}_{ij}(t)$, which is weighted based on the corresponding reputation of follower $n \in \mathcal{N}_{ij}(t)$. Hence, a common neighbor $n_1 \in \mathcal{N}_{ij}(t)$ with a low reputation has less influence on the reputation of neighbor j than common neighbor $n_2 \in \mathcal{N}_{ij}(t) \setminus \{n_1\}$ with a higher reputation.

3.3.3 Edge Weight Policy

The edge weights of $\mathcal{G}(t)$ encode the degree of influence each neighbor $j \in \mathcal{N}_i(t)$ has on follower i. Since the objective is to achieve FCLT by the cooperative followers and the reputation model captures the degree of reliability of each follower, the edge weights can be continuously updated according to the reputation model. The edge weight $a_{ij}(t)$ is defined by

$$a_{ij}(t) \triangleq \begin{cases} \zeta_{ij}(t), & \zeta_{ij}(t) \geq \zeta_{\min} \text{ and } j \in \mathcal{N}_i(t) \\ 0, & \zeta_{ij}(t) < \zeta_{\min} \text{ or } j \notin \mathcal{N}_i(t), \end{cases} \tag{3–6}$$

where $\zeta_{\min} \in [0, 1]$ is a user-defined parameter that determines whether follower i categorizes follower $j \in \mathcal{N}_i(t)$ as cooperative or Byzantine.

The set of cooperative and Byzantine neighbors of follower i at time t are given by $\mathcal{C}_i(t) \triangleq \{j \in \mathcal{N}_i(t) : a_{ij}(t) \neq 0\}$ and $\mathcal{B}_i(t) \triangleq \mathcal{N}_i(t) \setminus \mathcal{C}_i(t)$, respectively. Remark 3.4 explains the time-varying nature of the cooperative and Byzantine neighbor sets. Furthermore, $\mathcal{B}(t) \triangleq \{j \in \mathcal{V} : j \in \mathcal{B}_i(t) \text{ for some } i \in \mathcal{V}\}$ and $\mathcal{C}(t) \triangleq \mathcal{V} \setminus \mathcal{B}(t)$. From (3–6), the edge weight $a_{ij}(t)$ is positive if follower j is a cooperative neighbor of follower i.

Conversely, edge weight $a_{ij}(t)$ is zero if followers i and j are not neighbors or if follower j is a Byzantine neighbor of follower i. Note that if $j \in \mathcal{B}_i(t)$, then follower j cannot influence follower i. However, follower i can still compute trust and reputation for follower $j \in \mathcal{N}_i(t)$, where follower j can be reintegrated into $\mathcal{C}_i(t)$ once $\zeta_{ij}(t) \geq \zeta_{\min}$ provided $j \in \mathcal{N}_i(t)$. This enables a remediated Byzantine agent to enter the CMAS and become cooperative neighbors with any cooperative agent. Hence, the information exchange and influence between agents are decoupled. Furthermore, if follower $j \in \mathcal{B}_i(t)$, then follower i will not communicate any true state information about itself to follower j until follower j becomes a cooperative neighbor of follower i. Note that the leader will only communicate state information to its cooperative neighbors by also using (3–6). Hence, cooperative state information is only communicated between cooperative agents.

Remark 3.4. The cooperative and Byzantine neighbor sets are time-varying because cooperative agents may be attacked within contested environments and converted into Byzantine agents. Moreover, it may be possible for operators to employ countermeasures to convert Byzantine agents back into cooperative agents. Hence, a follower may be initiated as cooperative, eventually become Byzantine, and then eventually become cooperative again. While the Byzantine neighbor set of a follower may be empty at some time, Assumption 3.8 ensures the cooperative neighbor set of each cooperative follower is never empty. This also implies that each cooperative agent cannot have all neighbors be Byzantine if there are at least two cooperative followers in the network. Relaxing Assumption 3.8 is the subject of future work.

3.3.4 Event-Triggered Control Development

The state estimate of agent $i \in \mathcal{V} \cup \{0\}$, which is synchronized among all agents $j \in \mathcal{N}_i(t) \cup \{i\}$, is generated by the zero-order hold

$$\hat{x}_i(t) \triangleq x_{i,1}\left(t_k^i\right), \; t \in \left[t_k^i, t_{k+1}^i\right). \tag{3–7}$$

According to (3–7), agent i samples its position at time t_k^i and broadcasts it to all agents $j \in \mathcal{N}_i(t)$. Each agent $j \in \mathcal{N}_i(t) \cup \{i\}$ equates the state estimate of agent i, i.e., $\hat{x}_i(t)$, to $x_i(t_k^i)$ for all time until the next broadcast event of agent i. Recall that $x_{i,1}(t)$ denotes the broadcast state of agent i at time t, which cooperative agents communicate accurately, i.e., $x_{i,1}(t_k^i) = x_i(t_k^i)$. Based on the subsequent stability analysis, the controller for follower $i \in \mathcal{V}$ is

$$u_i(t) \triangleq g_i^+(x_i(t))(k_1 z_i(t) + k_2 e_{2,i}(t)) \tag{3–8}$$

$$z_i(t) \triangleq \sum_{j \in \mathcal{N}_i(t)} a_{ij}(t)(\hat{x}_j(t) - \hat{x}_i(t) - v_j + v_i) + b_i(t)(v_i + \hat{x}_0(t) - \hat{x}_i(t)), \tag{3–9}$$

where $k_1 \triangleq \frac{1}{\Lambda_{\min}}\left(k_{1,1} + \frac{\rho_1^2}{\delta_1}\right) \in \mathbb{R}_{>0}$, $k_2 \triangleq k_{2,1} + \frac{\rho_2^2}{\delta_2} \in \mathbb{R}_{>0}$, $k_{1,1} \triangleq k_{1,2} + k_{1,3} \in \mathbb{R}_{>0}$, and $k_{1,2},\ k_{1,3},\ k_{2,1},\ \rho_1,\ \rho_2,\ \delta_1,\ \delta_2 \in \mathbb{R}_{>0}$ are parameters defined in Theorem 3.1. Note that $\Lambda_{\min} \in \mathbb{R}_{>0}$ is a parameter defined in Lemma 3.2, and $z_i : [0, \infty) \to \mathbb{R}^n$ is the estimate-based distributed FCLT control effort. The stacked form of (3–9) is defined by $Z \triangleq [z_1^\top(t), z_2^\top(t), ..., z_N^\top(t)]^\top \in \mathbb{R}^{nN}$.

The stacked error systems for the leader-follower relative position error in (3–2) and state estimation error in (3–3) are $E_1 \triangleq [e_{1,1}^\top(t), e_{1,2}^\top(t), ..., e_{1,N}^\top(t)]^\top \in \mathbb{R}^{nN}$ and $E_2 \triangleq [e_{2,1}^\top(t), e_{2,2}^\top(t), ..., e_{2,N}^\top(t)]^\top \in \mathbb{R}^{nN}$, respectively. Substituting (3–1)–(3–3), (3–8), and (3–9) into the time-derivative of (3–2) yields

$$\dot{e}_{1,i}(t) = f_i(x_i(t)) + k_1 \sum_{j \in \mathcal{N}_i(t)} a_{ij}(t)(e_{2,j}(t) - e_{2,i}(t)) + k_1 \sum_{j \in \mathcal{N}_i(t)} a_{ij}(t)(e_{1,j}(t) - e_{1,i}(t))$$
$$+ k_1 b_i(t) e_{2,0}(t) - k_1 b_i(t) e_{1,i}(t) - k_1 b_i(t) e_{2,i}(t) + k_2 e_{2,i}(t) + d_i(t) - \dot{x}_0(t). \tag{3–10}$$

Substituting (3–1)–(3–3) and (3–7)–(3–9) into the time-derivative of (3–3) yields

$$\dot{e}_{2,i}(t) = -f_i(x_i(t)) - k_1 \sum_{j \in \mathcal{N}_i(t)} a_{ij}(t)(e_{2,j}(t) - e_{2,i}(t)) - k_1 \sum_{j \in \mathcal{N}_i(t)} a_{ij}(t)(e_{1,j}(t) - e_{1,i}(t))$$
$$- k_1 b_i(t) e_{2,0}(t) + k_1 b_i(t) e_{1,i}(t) + k_1 b_i(t) e_{2,i}(t) - k_2 e_{2,i}(t) - d_i(t). \tag{3–11}$$

Substituting (3–10) and (3–11) into the time-derivative of E_1 and E_2, respectively, and compactly expressing the results with the Kronecker product yields

$$\dot{E}_1 = \widetilde{N} + N_d - k_1 \left(H\left(t\right) \otimes I_n\right) E_2 - k_1 \left(H\left(t\right) \otimes I_n\right) E_1 + k_1 \left(B\left(t\right) 1_N \otimes e_{2,0}\left(t\right)\right) + k_2 E_2, \tag{3–12}$$

$$\dot{E}_2 = -F\left(X\right) + k_1 \left(H\left(t\right) \otimes I_n\right) E_2 + k_1 \left(H\left(t\right) \otimes I_n\right) E_1 - k_1 \left(B\left(t\right) 1_N \otimes e_{2,0}\left(t\right)\right) - k_2 E_2 - D, \tag{3–13}$$

where $\widetilde{N} \triangleq F\left(X\right) - F\left(X_0\right) \in \mathbb{R}^{nN}$, $N_d \triangleq F\left(X_0\right) + D - \dot{X}_0 \in \mathbb{R}^{nN}$, $F\left(X\right) \triangleq \left[f_1^\top\left(x_1\left(t\right)\right), f_2^\top\left(x_2\left(t\right)\right), ..., f_N^\top\left(x_N\left(t\right)\right)\right]^\top \in \mathbb{R}^{nN}$, $F\left(X_0\right) \triangleq \left[f_1^\top\left(x_0\left(t\right)\right), f_2^\top\left(x_0\left(t\right)\right), ..., f_N^\top\left(x_0\left(t\right)\right)\right]^\top \in \mathbb{R}^{nN}$, $D \triangleq \left[d_1^\top\left(t\right), d_2^\top\left(t\right), ..., d_N^\top\left(t\right)\right]^\top \in \mathbb{R}^{nN}$, $X_0 \triangleq 1_N \otimes x_0\left(t\right) \in \mathbb{R}^{nN}$, $X \triangleq \left[x_1^\top\left(t\right), x_2^\top\left(t\right), ..., x_N^\top\left(t\right)\right]^\top \in \mathbb{R}^{nN}$, and $\mathbf{V} \triangleq \left[v_1^\top, v_2^\top, ..., v_N^\top\right]^\top \in \mathbb{R}^{nN}$. Given the dynamics in (3–1) and Assumptions 3.1–3.3, and 3.6, there exists a $c_1 \in \mathbb{R}_{>0}$ such that $\left\|N_d\right\| \leq c_1$. By Assumption 3.3, there exists a $c_2 \in \mathbb{R}_{>0}$ such that $\left\|D\right\| \leq c_2$. By Assumptions 3.1 and 3.6, there exists a $c_3 \in \mathbb{R}_{>0}$ such that $\left\|F\left(X_0\right)\right\| \leq c_3$. Using Assumption 3.9, there exists a $c_4 \in \mathbb{R}_{>0}$ such that $\left\|\mathbf{V}\right\| \leq c_4$. Using [82, Lemma 5], $\widetilde{N}$ can be bounded as $\left\|\widetilde{N}\right\| \leq \mu\left(\left\|E\right\|\right)\left\|E\right\| + c_5$, where $E\left(t\right) \triangleq \left[E_1^\top, E_2^\top\right]^\top \in \mathbb{R}^{2nN}$ denotes the MAS error, $\mu : \mathbb{R}_{\geq 0} \to \mathbb{R}_{\geq 0}$ is a positive, non-decreasing, and radially unbounded function, and $c_5 \in \mathbb{R}_{>0}$ is a bounding constant. Note that $E\left(0\right) = \left[E_1^\top\left(0\right), E_2^\top\left(0\right)\right]^\top$, where $E_k\left(0\right) = \left[e_{k,1}^\top\left(0\right), e_{k,2}^\top\left(0\right), ..., e_{k,N}^\top\left(0\right)\right]^\top$ for $k \in \{1, 2\}$.

Recall that the objective is to minimize $e_{1,i}\left(t\right)$ as given by (3–2) for each $i \in \mathcal{C}\left(t\right)$. However, E_1 and E_2 may contain error systems belonging to Byzantine agents, which cannot be controlled, may be unbounded, and may prevent the objective. Therefore, the FCLT error and the state estimation error are set to zero for all Byzantine agents, i.e., $e_{1,i}\left(t\right) \triangleq 0_n$ and $e_{2,i}\left(t\right) \triangleq 0_n$ for all $i \in \mathcal{B}\left(t\right)$, which allows the objective to apply only to the cooperative followers.

3.4 Stability Analysis

To facilitate the subsequent stability analysis, consider the following lemmas.

Lemma 3.1. *There exists a bounding constant* $\Lambda_{\max} \in \mathbb{R}_{>0}$ *such that* $\|H(t) \otimes I_n\| \leq \Lambda_{\max}$ *for all* $t \geq 0$.

Proof. See Appendix B.1. ■

Lemma 3.2. *If Assumptions 3.4, 3.7, and 3.8 are satisfied for all* $t \geq 0$, *then a bounding constant* $\Lambda_{\min} \in \mathbb{R}_{>0}$ *exists such that* $E_1^\top (H(t) \otimes I_n) E_1 \geq \Lambda_{\min} \|E_1\|^2$ *for all* $t \geq 0$.[4]

Proof. See Appendix B.2. ■

Furthermore, consider the following. Substituting (3–2), (3–3), and (3–9) for all $i \in \mathcal{V}$ into Z yields

$$Z = -(H(t) \otimes I_n) E_1 - (H(t) \otimes I_n) E_2 + (B(t) 1_N \otimes e_{2,0}(t)). \tag{3–14}$$

Using Lemma 3.1, (3–14), and Young's inequality, it follows that

$$-k_{1,3} \|E_1\|^2 \leq k_{1,3} \|E_2\|^2 - \frac{k_{1,3}}{(2\Lambda_{\max}^2 + \Lambda_{\max})} \|Z\|^2 + \frac{k_{1,3}}{\Lambda_{\max}} \|B(t) 1_N \otimes e_{2,0}(t)\|^2. \tag{3–15}$$

Note that (3–15) is a useful inequality that facilitates the development of the event-trigger mechanisms for the leader and the followers. Moreover, observe that

$$\|B(t) 1_N \otimes e_{2,0}(t)\|^2 \leq N b_{\max}^2 \|e_{2,0}(t)\|^2 \tag{3–16}$$

since $\|B(t)1_N \otimes e_{2,0}(t)\|^2 = \sum_{i \in \mathcal{V}} b_i^2(t) \|e_{2,0}(t)\|^2$ and $b_i(t) \in [0, b_{\max}]$ for all $t \geq 0$ and each $i \in \mathcal{V}$ by construction. The subsequent stability analysis uses several auxiliary

[4] The use of Assumption 3.7, the trust model in (3–4), reputation model in (3–5), and edge weight policy in (3–6) ensure Type I and Type II Byzantine agents are detected and removed from the CMAS.

parameters. Let

$$\begin{aligned}
\phi_1 &\triangleq \left(1 - \frac{1}{\kappa}\left(\frac{2\Lambda_{\max}+1}{2\Lambda_{\min}}\right)\right) k_{1,2} - \frac{1}{2} \\
&\quad - \frac{1}{\kappa}\left(k_{1,3} + \frac{\rho_1^2}{\delta_1}\right)\left(\frac{2\Lambda_{\max}+1}{2\Lambda_{\min}}\right) - \frac{k_2}{2\kappa}, \\
\phi_2 &\triangleq k_{2,1} - \frac{1}{2}, \quad \phi_3 \triangleq \frac{k_1}{2} + \frac{\kappa k_1}{2} + \frac{k_{1,3}}{\Lambda_{\max}}, \\
\phi_4 &\triangleq \frac{k_1}{2} + k_{1,3} + k_1\Lambda_{\max} + \frac{\kappa\left(2k_1\Lambda_{\max} + k_2\right)}{2}, \\
\phi_5 &\triangleq \frac{k_{1,3}}{(2\Lambda_{\max}^2 + \Lambda_{\max})}, \quad \phi_6 \triangleq \min\left\{\phi_1, \phi_2\right\}, \\
\delta^* &\triangleq \delta_1 + \delta_2 + c_0 + \varepsilon.
\end{aligned} \tag{3–17}$$

Note that κ, c_0, and ε are defined in Theorem 3.1. The set over which the stability analysis is performed is

$$\mathcal{D} \triangleq \left\{\xi \in \mathbb{R}^{2nN} : \|\xi\| < \inf \mu^{-1}\left(\left[\sqrt{\phi_6/4}, \infty\right)\right)\right\},$$

where, given a set $\Omega \subset \mathbb{R}$, the preimage $\mu^{-1}(\Omega) \subset \mathbb{R}$ is defined as $\mu^{-1}(\Omega) \triangleq \{\omega \in \mathbb{R} : \mu(\omega) \in \Omega\}$. The admissible set of initial conditions is

$$\mathcal{S}_{\mathcal{D}} \triangleq \left\{\xi \in \mathbb{R}^{2nN} : \|\xi\| < \frac{\sqrt{2}}{2} \inf \mu^{-1}\left(\left[\sqrt{\phi_6/4}, \infty\right)\right)\right\}.$$

Let $E_{\max} \triangleq \frac{\sqrt{2}}{2} \inf \mu^{-1}([\sqrt{\phi_6/4}, \infty))$, and recall that μ is a non-decreasing function. If $\|E\| < E_{\max}$, then $\mu(\|E\|) \leq \sqrt{\phi_6/4}$. In Appendices C.1 and C.2, an algorithm that summarizes the control strategy used by each agent to achieve the objective is presented. The algorithm is expressed with respect to follower i, and a similar algorithm follows for the leader. Recall that $\omega_{ij}(t_k^j) = \|x_i(t_k^j) - x_{j,2}(t_k^j)\|$ and $\Delta t_k^j = t_k^j - t_{k-1}^j$ as defined in Section 3.3.1.

Theorem 3.1. *The trust model in* (3–4)*, reputation model in* (3–5)*, edge weight policy in* (3–6)*, estimator in* (3–7)*, and controller in* (3–8) *and* (3–9) *ensure the MAS error E is*

uniformly ultimately bounded (UUB) in the sense that

$$\limsup_{t\to\infty} \|E\| \leq 2\sqrt{\frac{4c_5^2 + 2\delta^*}{\phi_6}}, \tag{3–18}$$

provided the leader broadcasts its state as dictated by the event-trigger mechanism in

$$t_{k+1}^0 \triangleq \inf\left\{t > t_k^0 : Nb_{\max}^2\phi_3 \left\|e_{2,0}\left(t\right)\right\|^2 \geq c_0\right\}, \tag{3–19}$$

each follower $i \in \mathcal{V}$ broadcasts its state as dictated by the event-trigger mechanism in

$$t_{k+1}^i \triangleq \inf\left\{t > t_k^i : \phi_4 \left\|e_{2,i}\left(t\right)\right\|^2 \geq \phi_5 \left\|z_i\left(t\right)\right\|^2 + \frac{\varepsilon}{N}\right\}, \tag{3–20}$$

Assumptions 3.1–3.9 are satisfied, the initial condition of the system is selected such that $E\left(0\right) \in \mathcal{S}_{\mathcal{D}}$, and the following sufficient user-defined parameter conditions are satisfied

$$\begin{aligned}
\kappa &> \frac{2\Lambda_{\max}+1}{2\Lambda_{\min}}, \quad k_{1,3} > 0, \quad k_{2,1} > \frac{1}{2}, \quad \rho_1 \geq c_1, \\
\rho_2 &\geq c_2 + c_3, \quad c_0 > 0, \quad \delta_1 > 0, \quad \delta_2 > 0, \quad \varepsilon > 0, \\
k_{1,2} &> \frac{2\kappa\Lambda_{\min}}{2\left(\kappa\Lambda_{\min} - \Lambda_{\max}\right) - 1}\left(\frac{1}{2} + \frac{k_2}{2\kappa} + \frac{1}{\kappa}\left(k_{1,3} + \frac{\rho_1^2}{\delta_1}\right)\left(\frac{2\Lambda_{\max}+1}{2\Lambda_{\min}}\right)\right),
\end{aligned}$$

$$\sqrt{\left(8c_5^2 + 4\delta^*\right)/\phi_6} < \frac{\sqrt{2}}{2}\inf \mu^{-1}\left(\left[\sqrt{\phi_6/4}, \infty\right)\right). \tag{3–21}$$

Proof. Consider the candidate Lyapunov function $V_1 : \mathcal{D} \to \mathbb{R}_{\geq 0}$ defined as

$$V_1\left(E\left(t\right)\right) \triangleq \frac{1}{2}E_1^\top E_1 + \frac{1}{2}E_2^\top E_2, \tag{3–22}$$

which can be bounded as

$$\alpha_1\left(\|E\|\right) \leq V_1\left(E\left(t\right)\right) \leq \alpha_2\left(\|E\|\right), \tag{3–23}$$

where $\alpha_1,\ \alpha_2 : \mathbb{R}_{\geq 0} \to \mathbb{R}_{\geq 0}$ are user-defined class $\mathcal{K}$ functions. Without loss of generality, let $\alpha_1 (\|E\|) \triangleq \frac{1}{2} \|E\|^2$ and $\alpha_2 (\|E\|) \triangleq \|E\|^2$. Suppose $g : [0, \infty) \to \mathbb{R}^{2nN}$ is a Filippov solution to the differential inclusion $\dot{g}(t) \in K[h](g(t))$, where $g(t) = E(t)$, the mapping $K[\cdot]$ provides a calculus for computing Filippov's differential inclusion as defined in [75], and $h : \mathbb{R}^{2nN} \to \mathbb{R}^{2nN}$ is defined as $h(g(t)) = \left[\dot{E}_1^\top, \dot{E}_2^\top\right]^\top$. The time-derivative of V_1 exists almost everywhere (a.e.), i.e., for almost all $t \in [0, \infty)$, and

$$\dot{V}_1 (g(t)) \overset{a.e.}{\in} \dot{\tilde{V}}_1 (g(t)), \tag{3–24}$$

where $\dot{\tilde{V}}_1 (g(t))$ is the generalized time-derivative of V_1 along the Filippov trajectories of $\dot{g}(t) = h(g(t))$. By [76, Equation 13], $\dot{\tilde{V}}_1 (g(t)) \triangleq \bigcap_{\xi \in \partial V_1 (g(t))} \xi^\top \begin{bmatrix} K[h]^\top (g(t)), & 1 \end{bmatrix}^\top$, where $\partial V_1 (g(t))$ denotes the Clarke generalized gradient of $V_1 (g(t))$. Since $V_1 (g(t))$ is continuously differentiable in $g(t)$, $\partial V_1 (g(t)) = \{\nabla V_1 (g(t))\}$, where ∇ denotes the gradient operator. The generalized time-derivative of (3–22) is

$$\dot{\tilde{V}}_1 (g(t)) \subseteq E^\top (t) K[h](g(t)). \tag{3–25}$$

Using the calculus of $K[\cdot]$ from [75], (3–25), and simplifying the substitution of (3–12) and (3–13) into the generalized time-derivative of (3–22) yields

$$\begin{aligned}
\dot{\tilde{V}}_1 (g(t)) \subseteq & \left\{ E_1^\top \widetilde{N} + E_1^\top N_d - E_2^\top F(X) - E_2^\top D \right\} \\
& + k_1 E_2^\top K[(H(t) \otimes I_n) E_2] + k_1 E_2^\top K[(H(t) \otimes I_n)] E_1 + k_2 E_1^\top K[E_2] \\
& - k_1 E_1^\top K[(H(t) \otimes I_n) E_2] - k_1 E_1^\top K[(H(t) \otimes I_n)] E_1 - k_2 E_2^\top K[E_2] \\
& + k_1 E_1^\top K[(B(t) 1_N \otimes e_{2,0}(t))] - k_1 E_2^\top K[(B(t) 1_N \otimes e_{2,0}(t))],
\end{aligned} \tag{3–26}$$

where set addition is defined by the Minkowski sum. Adding and subtracting $E_2^\top F(X_0)$ and using (3–24), Lemma 3.1, Lemma 3.2, $\|N_d\| \leq c_1$, $\|D\| \leq c_2$, $\|F(X_0)\| \leq c_3$, $\|\mathbf{V}\| \leq c_4$, $\|\widetilde{N}\| \leq \mu(\|E\|)\|E\| + c_5$, and Young's inequality, (3–26) can be upper bounded

as

$$\dot{V}_1(E(t)) \overset{a.e.}{\leq} \frac{1}{2}\|E_1\|^2 + 2\mu^2(\|E\|)\|E\|^2 + 2c_5^2 + c_1\|E_1\| + \frac{1}{2}\|E_2\|^2$$
$$+ 2k_1\Lambda_{\max}\|E_1\|\|E_2\| - k_1\Lambda_{\min}\|E_1\|^2 + c_3\|E_2\|$$
$$+ k_1\|E_1\|\|B(t)1_N \otimes e_{2,0}(t)\| + k_2\|E_1\|\|E_2\| + k_1\Lambda_{\max}\|E_2\|^2$$
$$+ k_1\|E_2\|\|B(t)1_N \otimes e_{2,0}(t)\| - k_2\|E_2\|^2 + c_2\|E_2\|. \tag{3–27}$$

Since $\rho_1 \geq c_1$ and $\rho_2 \geq c_2 + c_3$ by the hypothesis of Theorem 3.1, one has that $\left(c_1 - \frac{\rho_1^2}{\delta_1}\|E_1\|\right)\|E_1\| \leq \delta_1$ and $\left(c_2 + c_3 - \frac{\rho_2^2}{\delta_2}\|E_2\|\right)\|E_2\| \leq \delta_2$. Using these bounds, $k_1 = \frac{1}{\Lambda_{\min}}\left(k_{1,1} + \frac{\rho_1^2}{\delta_1}\right)$, $k_{1,1} = k_{1,2} + k_{1,3}$, $k_2 = k_{2,1} + \frac{\rho_2^2}{\delta_2}$, (3–15), Young's inequality, the inequality in (3–16), and the auxiliary parameters in (3–17), (3–27) can be upper bounded by

$$\dot{V}_1(E(t)) \overset{a.e.}{\leq} -\frac{\phi_6}{2}\|E\|^2 - \left(\frac{\phi_6}{2} - 2\mu^2(\|E\|)\right)\|E\|^2 + 2c_5^2 + \delta^*$$
$$+ \sum_{i\in\mathcal{V}}\left(\phi_4\|e_{2,i}(t)\|^2 - \phi_5\|z_i(t)\|^2 - \frac{\varepsilon}{N}\right)$$
$$+ Nb_{\max}^2\phi_3\|e_{2,0}(t)\|^2 - c_0, \tag{3–28}$$

where satisfying the parameter conditions in (3–21) ensures $\phi_i > 0\ \forall i \in \{1, 2, ..., 6\}$. Based on (3–28), the event-trigger mechanism for the leader is given by (3–19), and the event-trigger mechanism for each follower $i \in \mathcal{V}$ is given by (3–20). Since each agent provides state feedback according to the event-trigger mechanisms in (3–19) and (3–20), (3–28) can be upper bounded as

$$\dot{V}_1(E(t)) \overset{a.e.}{\leq} -\frac{\phi_6}{2}\|E\|^2 - \left(\frac{\phi_6}{2} - 2\mu^2(\|E\|)\right)\|E\|^2 + 2c_5^2 + \delta^*. \tag{3–29}$$

Using (3–23), one has that $\|E\| \leq \alpha_1^{-1}(\alpha_2(\|E\|))$ and $\alpha_2^{-1}(\alpha_1(\|E\|)) \leq \|E\|$, where $\alpha_1^{-1}(\alpha_2(\|E\|)) = \sqrt{2}\|E\|$ and $\alpha_2^{-1}(\alpha_1(\|E\|)) = \frac{\sqrt{2}}{2}\|E\|$ given the selected class $\mathcal{K}$ functions. Note that $\phi_6/2 - 2\mu^2(\|E\|) > 0$ provided $E_{\max} = \frac{\sqrt{2}}{2}\inf\mu^{-1}([\sqrt{\phi_6/4}, \infty)) >$

$\|E\|$. Moreover, $-(\phi_6/4)\|E\|^2 + 2c_5^2 + \delta^* \leq 0$ provided $\|E\| \geq \sqrt{(8c_5^2 + 4\delta^*)/\phi_6}$. It then follows that (3–29) can be upper bounded as $\dot{V}_1(E(t)) \overset{a.e.}{\leq} -\frac{\phi_6}{4}\|E\|^2$ for all $E_{\max} > \|E\| \geq \sqrt{(8c_5^2 + 4\delta^*)/\phi_6}$. Let $\mathcal{Z} \triangleq \{\xi \in \mathbb{R}^{2nN} : \|\xi\| \geq \sqrt{(8c_5^2 + 4\delta^*)/\phi_6}\}$. Since $\sqrt{(8c_5^2 + 4\delta^*)/\phi_6} < \frac{\sqrt{2}}{2}\inf \mu^{-1}([\sqrt{\phi_6/4}, \infty))$, it follows that $\dot{V}_1(E(t)) \overset{a.e.}{<} 0$ for all $E \in \mathcal{S}_{\mathcal{D}} \cap \mathcal{Z}$. If $E \in \mathcal{S}_{\mathcal{D}} \cap \mathcal{Z}^C$, then $\dot{V}_1(E(t)) \overset{a.e.}{\leq} -\frac{\phi_6}{4}\|E\|^2 + 2c_5^2 + \delta^*$, which may allow $V_1(E(t))$ to grow. However, E will exit $\mathcal{Z}^C$ before exiting $\mathcal{S}_{\mathcal{D}}$, and, therefore, flow into $\mathcal{S}_{\mathcal{D}} \cap \mathcal{Z}$. It then follows that $\mathcal{S}_{\mathcal{D}}$ is forward invariant, where initializing the MAS such that $E(0) \in \mathcal{S}_{\mathcal{D}}$ ensures E is uniformly ultimately bounded with the ultimate bound presented in (3–18).

The state, state estimate, control signal, FCLT error, and state estimation error are shown to be bounded for each agent. Since $E \in \mathcal{L}_\infty$, it follows that $E_1 \in \mathcal{L}_\infty$ and $E_2 \in \mathcal{L}_\infty$ given the definition of E. Since $E_1 \in \mathcal{L}_\infty$, $e_{1,i}(t) \in \mathcal{L}_\infty$ for all $i \in \mathcal{V}$ given the definition of E_1. From Assumption 3.6, $x_0(t) \in \mathcal{L}_\infty$. Since $e_{1,i}(t) \in \mathcal{L}_\infty$, $v_i \in \mathcal{L}_\infty$, and $x_0(t) \in \mathcal{L}_\infty$, (3–2) implies $x_i(t) \in \mathcal{L}_\infty$ for each $i \in \mathcal{V}$.

Since $E_2 \in \mathcal{L}_\infty$, $e_{2,i}(t) \in \mathcal{L}_\infty$ for all $i \in \mathcal{V}$ given the definition of E_2. Since $x_i(t) \in \mathcal{L}_\infty$ and $e_{2,i}(t) \in \mathcal{L}_\infty$, (3–3) implies $\hat{x}_i(t) \in \mathcal{L}_\infty$ for all $i \in \mathcal{V}$. Since $x_0(t) \in \mathcal{L}_\infty$ by Assumption 3.6, (3–7) implies $\hat{x}_0(t) \in \mathcal{L}_\infty$. Since $\hat{x}_i(t) \in \mathcal{L}_\infty$ for all $i \in \mathcal{V} \cup \{0\}$, $a_{ij}(t) \in [0,1]$ for all $t \geq 0$ and each $i, j \in \mathcal{V}$ by construction, $v_i \in \mathcal{L}_\infty$ for all $i \in \mathcal{V}$ by design, and $b_i(t) \in [0, b_{\max}]$ for all $t \geq 0$ and each $i \in \mathcal{V}$ by construction, (3–9) implies $z_i(t) \in \mathcal{L}_\infty$ for each $i \in \mathcal{V}$. Since $z_i(t) \in \mathcal{L}_\infty$, $e_{2,i}(t) \in \mathcal{L}_\infty$, $x_i(t) \in \mathcal{L}_\infty$, and $g_i^+(x_i(t)) \in \mathcal{L}_\infty$ by Assumption 3.2, it follows that (3–8) implies $u_i(t) \in \mathcal{L}_\infty$ for all $i \in \mathcal{V}$. ■

Remark 3.5. With respect to (3–21), c_0 is a user-defined parameter that determines the rate at which the leader broadcasts its state to its neighbors. Moreover, c_0 is used to uniformly lower bound the difference between consecutive broadcast events performed by the leader away from zero. Similarly, ε is a user-defined parameter used to uniformly lower bound the difference between consecutive broadcast events for each follower $i \in \mathcal{V}$ away from zero.

Remark 3.6. Based on the definition of ϕ_1 and ϕ_2 in (3–17), ϕ_6 can be increased by increasing $k_{1,2}$ and $k_{2,1}$ provided $k_{1,2}$ and κ are selected according to (3–21). Given $E(0)$, select ϕ_6 such that $E(0) \in \mathcal{S}_{\mathcal{D}}$. Observe that $\sqrt{(8c_5^2 + 4\delta^*)/\phi_6}$ decreases with increasing ϕ_6, where c_5 and δ^* are fixed. Furthermore, since μ is a non-decreasing function, it follows that $\mu^{-1}([\sqrt{\phi_6/4}, \infty))$ is non-decreasing with respect to ϕ_6. Hence, $\sqrt{(8c_5^2 + 4\delta^*)/\phi_6} < \frac{\sqrt{2}}{2} \inf \mu^{-1}([\sqrt{\phi_6/4}, \infty))$ can be satisfied for some ϕ_6.

The event-trigger mechanisms in (3–19) and (3–20) are now shown to be free from Zeno behavior.

Theorem 3.2. *The difference between consecutive broadcast times generated by the event-trigger mechanism of the leader in* (3–19) *is uniformly lower bounded by*

$$t_{k+1}^0 - t_k^0 \geq \frac{1}{b_{\max}\theta_{0,\max}} \sqrt{\frac{c_0}{N\phi_3}} \tag{3–30}$$

for all $k \in \mathbb{Z}_{\geq 0}$, *where* $\theta_{0,\max} \in \mathbb{R}_{>0}$ *is a user-defined parameter selected such that* $\|f_0(x_0(t))\| + \|g_0(x_0(t))\| \|u_0(t)\| + \|d_0(t)\| \leq \theta_{0,\max}$.

Proof. See Appendix B.3. ■

Theorem 3.3. *The difference between consecutive broadcast times generated by the event-trigger mechanism of follower* $i \in \mathcal{V}$ *in* (3–20) *is uniformly lower bounded by*

$$t_{k+1}^i - t_k^i \geq \frac{1}{k_2} \ln\left(\frac{k_2}{\theta_{i,\max}} \sqrt{\frac{\varepsilon}{N\phi_4}} + 1\right) \tag{3–31}$$

for all $k \in \mathbb{Z}_{\geq 0}$, *where* $\theta_{i,\max} \in \mathbb{R}_{>0}$ *is a user-defined parameter selected such that* $\|f_i(x_i(t))\| + k_1 \|z_i(t)\| + \|d_i(t)\| \leq \theta_{i,\max}$.

Proof. See Appendix B.4. ■

3.5 Simulation Example

A simulation study is included to validate the developed approach. The simulated MAS consists of five follower agents and a single leader agent. The initial positions of each agent are $x_0(0) = [500\ 10]^\top$, $x_1(0) = [465\ -51]^\top$, $x_2(0) = [566\ -52]^\top$,

$x_3(0) = [417\ \ -103]^\top$, $x_4(0) = [518\ \ -104]^\top$, and $x_5(0) = [619\ \ -105]^\top$. The uncertain drift dynamics[5] and known control effectiveness matrix of agent i are $f_i(x_i(t)) \triangleq [\bar{a}_{1i}\psi(x_{1i}(t)) + \bar{a}_{2i},\ \bar{a}_{3i} + \bar{a}_{4i}\psi(x_{2i}(t))]^\top \in \mathbb{R}^2$ and

$$g_i(x_i(t)) \triangleq \begin{bmatrix} \cos(\varphi_i(t)) & -\sin(\varphi_i(t)) \\ \sin(\varphi_i(t)) & \cos(\varphi_i(t)) \end{bmatrix} \in \mathbb{R}^{2\times 2},$$

respectively, where $x_i(t) \triangleq [x_{1i}(t)\ \ x_{2i}(t)]^\top \in \mathbb{R}^2$, $\bar{a}_i \triangleq [\bar{a}_{1i}\ \bar{a}_{2i}\ \bar{a}_{3i}\ \bar{a}_{4i}]^\top \in \mathbb{R}^4$, $\psi(x) \triangleq \frac{1}{\sigma\sqrt{2\pi}}\exp\left(-\frac{x^2}{2\sigma^2}\right) \in \mathbb{R}_{>0}$, and $\varphi_i(t) \triangleq \arctan\left(\frac{x_{2i}(t)}{x_{1i}(t)}\right) \in \mathbb{R}$ such that $\arctan(\cdot)$ is the four quadrant inverse tangent, i.e., $\texttt{atan2}(\cdot)$ with respect to MATLAB. The uncertain drift dynamics coefficients for each agent are $\bar{a}_0 \triangleq [1\ 1\ 1\ 1]^\top$, $\bar{a}_1 \triangleq [1\ 1.5\ 3\ 2]^\top$, $\bar{a}_2 \triangleq [0.5\ 0.5\ 1.9\ 0.7]^\top$, $\bar{a}_3 \triangleq [1.5\ 2.1\ 1.2\ 0.5]^\top$, $\bar{a}_4 \triangleq [3\ 1.75\ 1.15\ 3]^\top$, and $\bar{a}_5 \triangleq [2\ 1\ 1\ 1.6]^\top$. The exogenous disturbance acting on all agents is random, drawn from a normal distribution, and scaled by $d_{\text{mag}} \in \mathbb{R}_{>0}$, which is subsequently defined. The relative position vectors defining the desired formation are $v_1 \triangleq [-50\ \ -50]^\top$, $v_2 \triangleq [50\ \ -50]^\top$, $v_3 \triangleq [-100\ \ -100]^\top$, $v_4 \triangleq [0\ \ -100]^\top$, and $v_5 \triangleq [100\ \ -100]^\top$. The known desired trajectory $x_d : [0,\infty) \to \mathbb{R}^2$ of the leader is

$$x_d(t) \triangleq 500[\cos\left(2\pi 10^{-2}t\right)\ \ \sin\left(2\pi 10^{-2}t\right)]^\top,$$

while the leader's trajectory tracking error $e_0 : [0,\infty) \to \mathbb{R}^2$ is defined as $e_0(t) \triangleq x_d(t) - x_0(t)$. The leader's tracking error can be globally exponentially regulated using the following controller:

$$u_0(t) \triangleq g_0^+(x_0(t))(-f_0(x_0(t)) + \dot{x}_d(t) + k_{0,1}e_0(t) + k_{0,2}\text{sgn}(e_0(t))),$$

[5] The leader knows its drift dynamics while the followers do not know their drift dynamics.

where $k_{0,1} \in \mathbb{R}_{>0}$ and $k_{0,2} \in \mathbb{R}_{>0}$ are user-defined parameters. The simulation is 50 time units long and uses an integration time-step of 1.00×10^{-3} time units. The following parameters are used to generate the simulation results: $b_{\max} = 1.25$, $\vartheta = 10$, $\sigma = 100$, $R = 110$, $k_{0,1} = 1$, $k_{0,2} = 0.25$, $d_{\text{mag}} = 0.03$, $c_1 = 3$, $c_2 = 1$, $c_3 = 0.008$, $\Lambda_{\min} = 1$, $\Lambda_{\max} = 10$, $\rho_1 = 4$, $\delta_1 = 0.25$, $\rho_2 = 2.008$, $\delta_2 = 0.25$, $\kappa = 105$, $k_{1,3} = 1$, $k_{2,1} = 1$, $k_{1,2} = 15.74$, $\varepsilon = 10^6$, $c_0 = 10^4$, $N = 5$, $s_1 = 5$, $t_{\text{reset}} = 1$, $\Delta_i = 0.125$ for each $i \in \{1, 2, ..., 5\}$, $\eta_\tau = 70$, $\eta_\zeta = 70$, and $\zeta_{\min} = 0.95$. The adjacency matrix of the communication graph of the followers and the leader pinning matrix are

$$\mathcal{A} = \begin{bmatrix} 0 & 0 & 1 & 1 & 0 \\ 0 & 0 & 0 & 1 & 1 \\ 1 & 0 & 0 & 1 & 0 \\ 1 & 1 & 1 & 0 & 1 \\ 0 & 1 & 0 & 1 & 0 \end{bmatrix}$$

and $B(t) = b_{\max} \cdot \text{diag}(1\ 1\ 0\ 0\ 0)$, respectively.

Figures 3-1 and 3-2 display the simulation results. The simulation subjected the MAS to at most two Byzantine agents, where Follower 3 was converted to a Type II Byzantine agent for $t \in [10, 40]$ time units, and Follower 5 was converted to a Type I Byzantine agent for $t \in [13, 40]$ time units. Follower 3 does not communicate with its neighbors during $t \in [10, 40]$. For $t \in [10, 30]$, Follower 3 was first maneuvered to $[225, 150]$ in an attempt to strain the network and destabilize the CMAS. For $t \in [30, 40]$, Follower 3 was maneuvered towards the CMAS, where it was converted back to a cooperative follower for $t > 40$ time units.[6]

[6] An adversary may corrupt a cooperative agent and cause it to abandon the CMAS. However, it may be possible to execute countermeasures to convert the Byzantine agent back into a cooperative agent. In such a case, it may be desirable to maneuver the cooperative agent back into the formation formed by the remaining cooperative agents.

The controller used to maneuver Follower 3 to $[225, 150]$ and then back to the CMAS is identical in form to that of the leader, where exact model knowledge was used only for the purpose of moving the follower away from the CMAS and simulating unanticipated behavior of an initial member of the CMAS. The communication protocol used by Follower 5 during $t \in [13, 40]$ was $x_{5,1}(t) = -0.1 \cdot x_5(t)$, i.e., the communicated information was negative one-tenth the true state of Follower 5. Since Follower 5 remained with the CMAS for $t \in [13, 40]$, its tracking error $e_{1,5}(t)$ is similar to that of the cooperative followers.

The cooperative followers, i.e., Followers 1, 2, and 4, satisfied the objective for all time, even in the presence of the Byzantine adversaries. Followers 3 and 5 also satisfied the objective during their periods of cooperation. Figure 3-1 depicts the trust, reputation, and edge weights of the neighbors of Follower 4, which illustrates the Byzantine behavior of Followers 3 and 5. Since Followers 1 and 2 are cooperative agents for all time, they communicate true state information about themselves to Follower 4, which results in maximum trust, reputation, and edge weight values for all time. Conversely, Followers 3 and 5 are Byzantine for $t \in [10, 40]$ and $t \in [13, 40]$, respectively, which results in their zero trust, reputation, and edge weight values with respect to Follower 4 during their Byzantine status. The trust, reputation, and edge weight figures for Followers 1, 2, 3, and 5 are omitted since they are similar to those of Follower 4. Figure 3-1 shows that Follower 4 detected the Byzantine behavior of Followers 3 and 5 at $t = 10$ and $t = 13$, respectively. As a result of the detected Byzantine behavior, the trust that Follower 4 had in Followers 3 and 5 decreased to 0, which caused the corresponding reputation values and edge weights to decrease to 0. Figure 3-1 also shows that Follower 4 detected cooperative behavior from Followers 3 and 5 at $t > 40$ and $t > 40$, respectively, which caused the trust, reputation, and edge weights of Followers 3 and 5, with respect to Follower 4, to increase to 1.

Figure 3-2 depicts the event-times for the leader and each follower for the first 2.5 time units of the simulation, where a 0, or white space, denotes no communication and a 1, or blue line, denotes a communication event. The first 2.5 time units of the simulation are shown, rather than entire simulation, to better exhibit the intermittency in communication. The average difference between consecutive event-times for the entire simulation for the leader and Followers 1–5 are 0.0282 time units, 0.0144 time units, 0.0136 time units, 0.0016 time units, 0.0141 time units, and 0.0197 time units, respectively. The minimum difference between consecutive event-times for the leader and Followers 1–5 are 0.028 time units, 0.002 time units, 0.002 time units, 0.001 time units, 0.003 time units, and 0.003 time units, respectively.

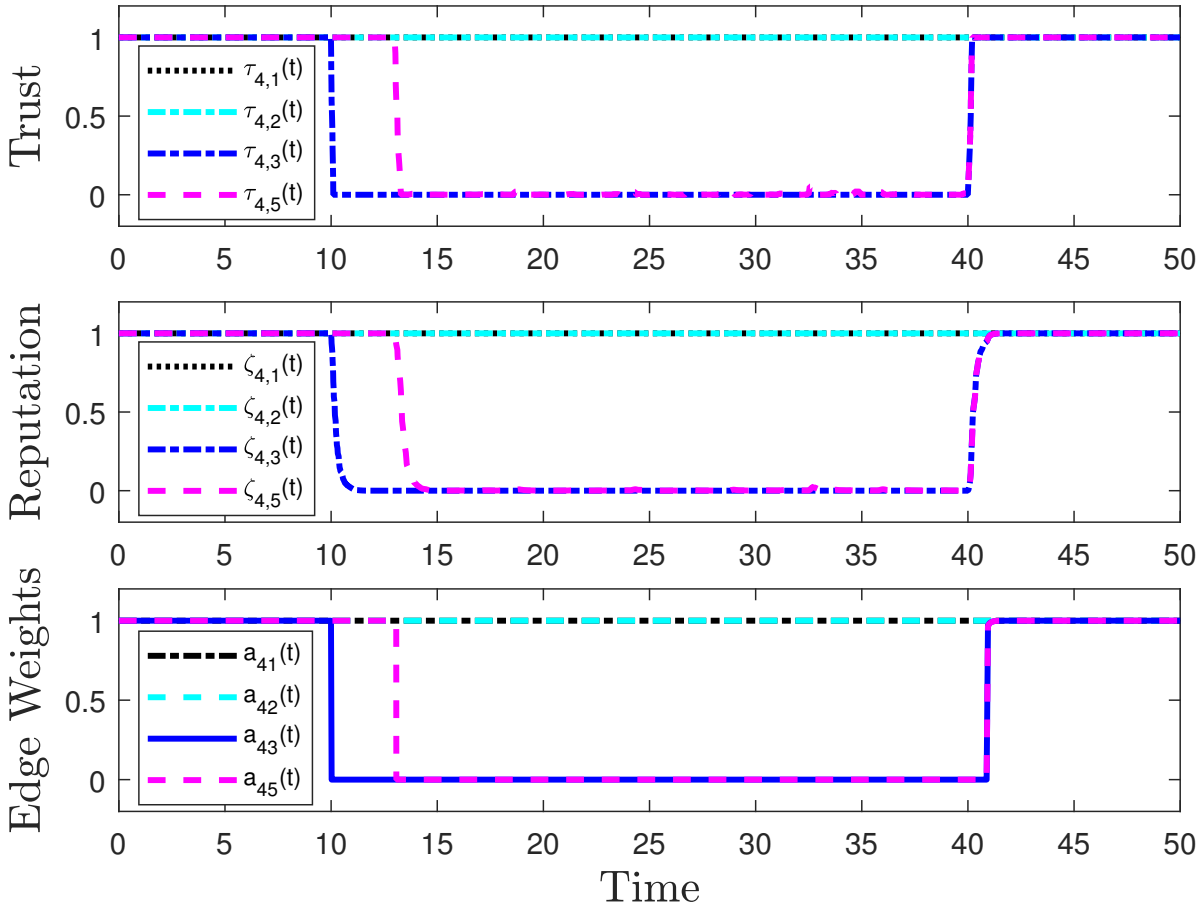

Figure 3-1. Trust, reputation, and edge weight values that Follower 4 has for its neighbors.

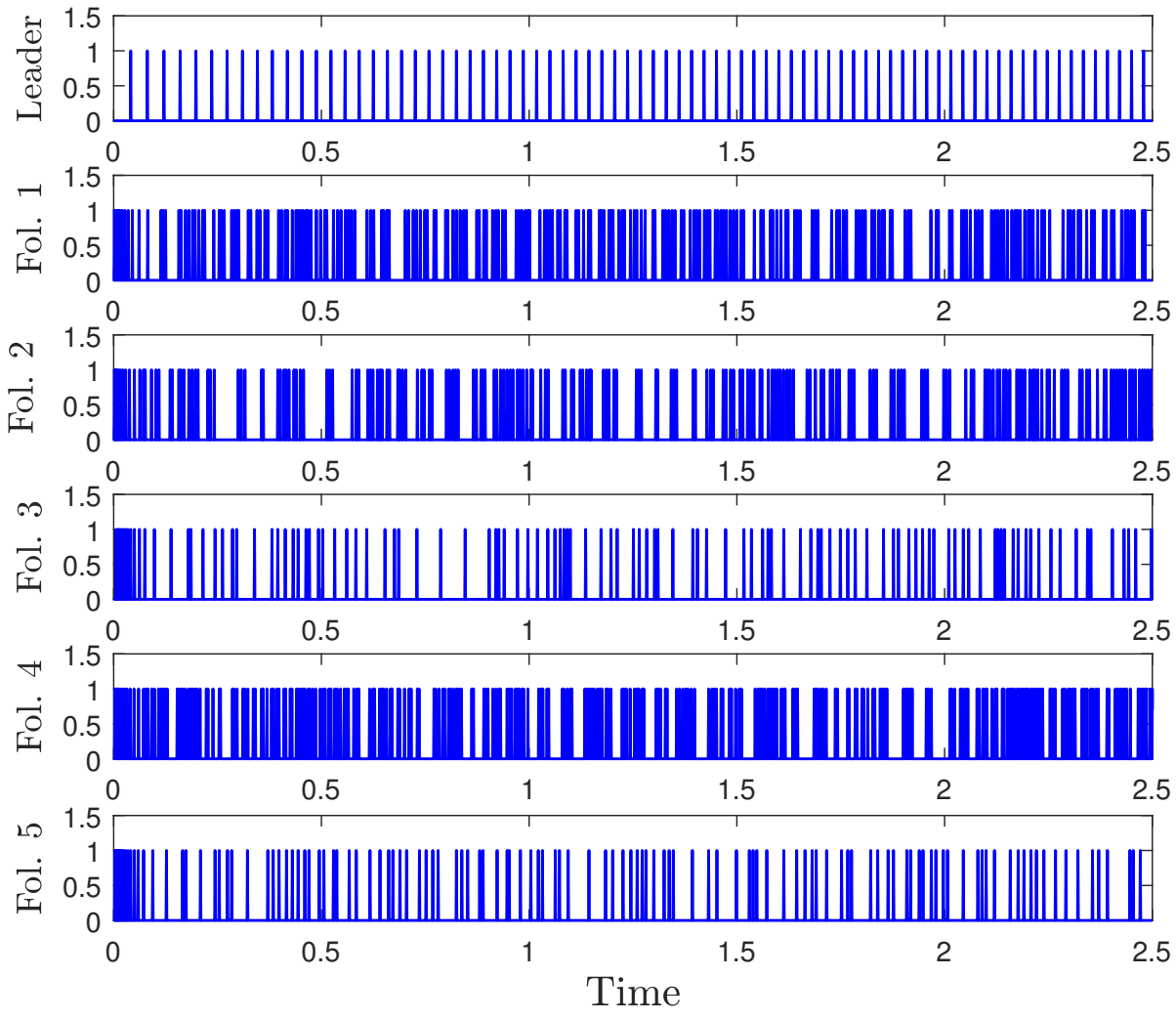

Figure 3-2. Illustration of the event-times for the leader and each follower during the first 2.5 time units of the simulation.

CHAPTER 4
CONSENSUS OVER CLUSTERED NETWORKS WITH ASYNCHRONOUS INTER-CLUSTER COMMUNICATION

Within this chapter, the consensus problem for a C-MAS is investigated. Given a MAS, the agents are organized into disjoint clusters, where each cluster forms a connected network. The agents that are within the same cluster can communicate continuously with their neighbors. Between some cluster pairs, there exists an inter-cluster that enables the relay of information between the two clusters. Agents that have neighbors in clusters different from their own can communicate intermittently and asynchronously with their different-cluster neighbors. The goal of each agent in the C-MAS is to converge to an agreement value by sharing local information of a continuous-time homogeneous process. Note that the intermittent communication events of the continuous-time process are inherently hybrid. Therefore, a unique coupling between a static consensus protocol and a hybrid consensus protocol is designed. The closed-loop network model is presented using a hybrid systems framework. The consensus problem is then recast into a set stability problem and sufficient conditions of the consensus set are presented through leveraging a Lyapunov-based stability analysis.

4.1 Cluster and Inter-Cluster Subgraphs

In this section, notation for the particular graph used in this chapter is introduced. The nodes in $\mathcal{V}$ can be grouped into $M \in \mathbb{Z}_{>0}$, $M < N$, disjoint clusters indexed by $[M]$ and defined by the cluster set $\mathcal{C} \triangleq \{\mathcal{V}_1, \mathcal{V}_2, ..., \mathcal{V}_M\}$, where $\mathcal{C}$ is a partition of $\mathcal{V}$. Specifically, $\mathcal{C}$ being a partition of $\mathcal{V}$ means $\mathcal{V}_p \subset \mathcal{V}$ for all $p \in [M]$, $\mathcal{V}_p \cap \mathcal{V}_q = \varnothing$ for each distinct $p, q \in [M]$, and $\cup_{p\in[M]}\mathcal{V}_p = \mathcal{V}$. Note that a cluster can contain a single node, i.e., $|\mathcal{V}_p| = 1$. Each cluster induces a subgraph of $\mathcal{G}$. The induced subgraph of cluster p is given by $\mathcal{G}[\mathcal{V}_p] \triangleq (\mathcal{V}_p, \mathcal{E}[\mathcal{V}_p], \mathscr{A}[\mathcal{V}_p])$, where $\mathcal{E}[\mathcal{V}_p] \triangleq \{(i,k) \in \mathcal{E} : i, k \in \mathcal{V}_p\}$ and $\mathscr{A}[\mathcal{V}_p] \in \mathbb{R}^{|\mathcal{V}_p|\times|\mathcal{V}_p|}$ is determined from $\mathcal{E}[\mathcal{V}_p]$ and the edge weights in $\mathscr{A}$. Let $S \subset \mathcal{V}$. The induced subgraph of S with respect to $\mathcal{G}$, i.e., $\mathcal{G}[S]$, is undirected given $\mathcal{G}$ is undirected and the construction of $\mathcal{E}[S]$. In this work, we only consider $S \subset \mathcal{V}$ such that $\mathcal{G}[S]$ is

connected. The induced inter-cluster subgraph of $\mathcal{G}$ between distinct clusters p and q is given by $\mathcal{G}[\mathcal{V}_{pq}] \triangleq (\mathcal{V}_{pq}, \mathcal{E}[\mathcal{V}_{pq}], \mathscr{A}[\mathcal{V}_{pq}])$, where $\mathcal{V}_{pq} \triangleq \{i \in \mathcal{V}_p : (i,k) \in \mathcal{E}, k \in \mathcal{V}_q\} \cup \{i \in \mathcal{V}_q : (i,k) \in \mathcal{E}, k \in \mathcal{V}_p\}$, $\mathcal{E}[\mathcal{V}_{pq}] \triangleq \{(i,k) \in \mathcal{E} : i,k \in \mathcal{V}_{pq}$ and $(i,k) \notin \mathcal{E}[\mathcal{V}_p] \cup \mathcal{E}[\mathcal{V}_q]\}$, and $\mathscr{A}[\mathcal{V}_{pq}] \in \mathbb{R}^{|\mathcal{V}_{pq}| \times |\mathcal{V}_{pq}|}$ is determined from $\mathcal{E}[\mathcal{V}_{pq}]$ and the edge weights in $\mathscr{A}$. Figure 4-1 shows an example of an undirected graph $\mathcal{G}$ with three cluster subgraphs, i.e., $\mathcal{G}[\mathcal{V}_1]$, $\mathcal{G}[\mathcal{V}_2]$, and $\mathcal{G}[\mathcal{V}_3]$, and two inter-cluster subgraphs, i.e., $\mathcal{G}[\mathcal{V}_{12}]$ and $\mathcal{G}[\mathcal{V}_{23}]$. The union of all cluster and inter-cluster subgraphs is equal to the graph $\mathcal{G}$. In this particular example, we have that $\mathcal{V}_1 \cup \mathcal{V}_2 \cup \mathcal{V}_3 = \mathcal{V}$, where $\mathcal{V}_{12}$ connects two nodes from $\mathcal{V}_1$ to a single node in $\mathcal{V}_2$. Similarly, $\mathcal{V}_{23}$ connects two nodes from $\mathcal{V}_3$ to a single node in $\mathcal{V}_2$.

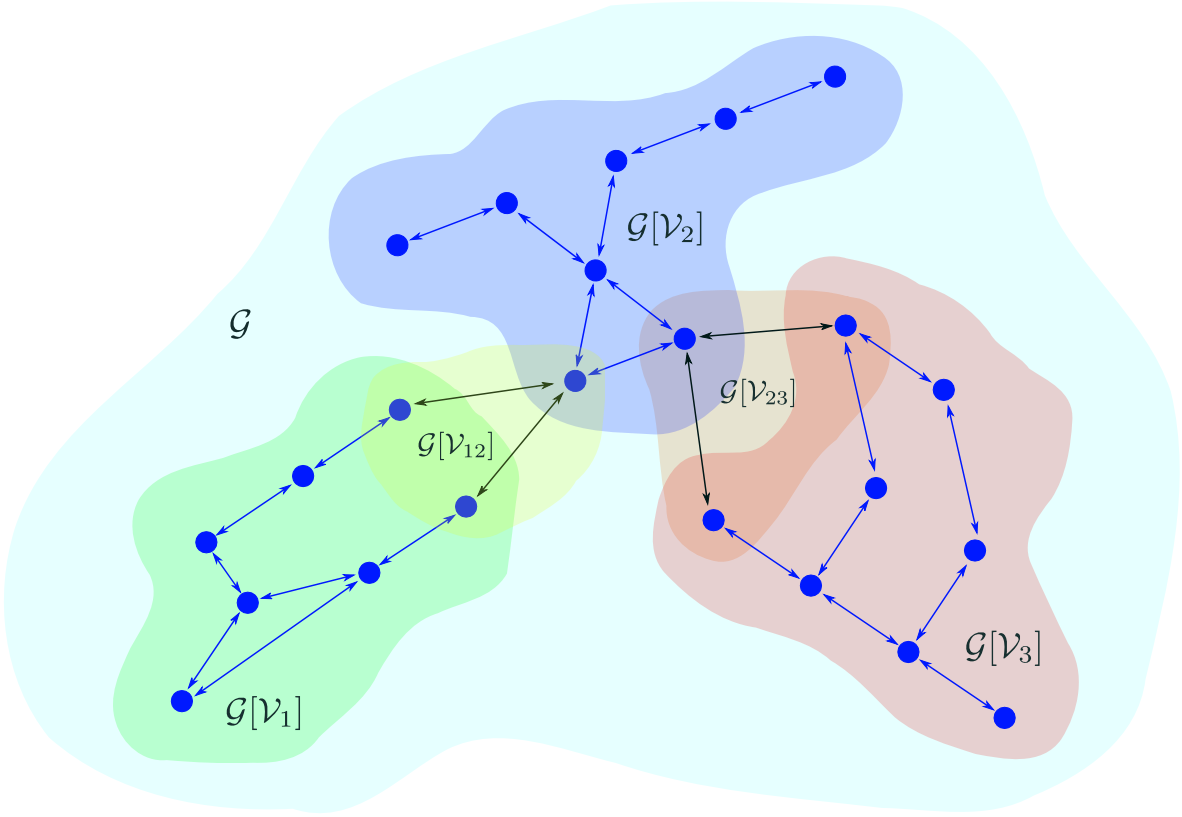

Figure 4-1. Example of a clustered MAS with three clusters and two inter-clusters.

To simplify the development, this chapter only focus on clustered graph structures with at most one inter-cluster subgraph between any two distinct cluster subgraphs. Hence, given M cluster subgraphs, there are $M^* \in \{0, ..., M(M-1)/2\}$ inter-cluster

subgraphs. The inter-cluster subgraphs can be indexed by $[M^*]$, where every $pq \in [M] \times [M]$ uniquely corresponds to some $r \in [M^*]$ through the use of an enumeration.[1] Therefore, for all $pq \in [M] \times [M]$ there exists an $r \in [M^*]$, where we now refer to inter-cluster pq as inter-cluster r, i.e., $\mathcal{V}^r \triangleq \mathcal{V}_{pq}$. Note that $\mathcal{G}[\mathcal{V}_{pq}] = \mathcal{G}[\mathcal{V}^r]$ if and only if $\mathcal{V}_{pq} = \mathcal{V}^r$. Hence, given a cluster set $\mathcal{C}$, the cluster subgraphs of $\mathcal{G}$ are denoted by $\mathcal{G}[\mathcal{V}_p]$ for $p \in [M]$, and the inter-cluster subgraphs of $\mathcal{G}$ are denoted by $\mathcal{G}[\mathcal{V}^r]$ for $r \in [M^*]$. By construction, the union graph composed from all cluster and inter-cluster subgraphs is equal to $\mathcal{G}$. A MAS composed of N agents that is divided into clusters according to some cluster set $\mathcal{C}$ is henceforth referred to as a *clustered MAS*. Each subgraph may have an adjacency matrix with size that is different from $N \times N$. To facilitate the subsequent analysis, we now construct an $N \times N$ augmented adjacency matrix for each subgraph of $\mathcal{G}$. The augmented adjacency matrix of $\mathcal{G}[S]$ is defined by $\mathsf{A}[S] \triangleq [\mathsf{a}_{ik}] \in \mathbb{R}^{N \times N}$, where $\mathsf{a}_{ik} \triangleq a_{ik}$ if $(i,k) \in \mathcal{E}[S]$ and $\mathsf{a}_{ik} \triangleq 0$ otherwise. Hence, the augmented adjacency matrix of cluster p is denoted by $\mathsf{A}[\mathcal{V}_p]$. Similarly, the augmented adjacency matrix of inter-cluster r is denoted by $\mathsf{A}[\mathcal{V}^r]$. The augmented adjacency matrix corresponding to the union of all clusters is defined by $\mathsf{A}_0 \triangleq \sum_{p \in [M]} \mathsf{A}[\mathcal{V}_p]$. The Laplacian matrix of the union of all cluster subgraphs is defined by $L_0 \triangleq \mathsf{diag}(\mathsf{A}_0 \cdot 1_N) - \mathsf{A}_0 \in \mathbb{R}^{N \times N}$. The Laplacian matrix of inter-cluster $r \in [M^*]$ is defined by $L_r \triangleq \mathsf{diag}(\mathsf{A}[\mathcal{V}^r] \cdot 1_N) - \mathsf{A}[\mathcal{V}^r] \in \mathbb{R}^{N \times N}$. It can then be shown that $L = L_0 + \sum_{r \in [M^*]} L_r$.

4.2 Problem Statement

Consider a C-MAS composed of N agents in the node set $\mathcal{V}$, where each agent is assigned to one cluster for all time. Each agent computes a homogeneous process[2] such that the local version of the process for i^{th} agent evolves according to the following

[1] A bijective mapping from $[M] \times [M]$ to $[M^*]$.

[2] Homogeneous process means that all agents in the C-MAS interact with the same system. In the LTI system in (4–1), the A and B matrices are the same for all agents.

continuous-time differential equation

$$\dot{x}_i = Ax_i + Bu_i, \tag{4–1}$$

where $x_i : [0, \infty) \to \mathbb{R}^n$ denotes the state, $A \in \mathbb{R}^{n\times n}$ denotes the known state matrix, $B \in \mathbb{R}^{n\times d}$ denotes the known control effectiveness matrix, and $u_i : [0, \infty) \to \mathbb{R}^d$ denotes the control input.

Assumption 4.1. For all $i \in \mathcal{V}$ and $t \geq 0$, agent i can measure its state, $x_i(t)$.

As indicated in Section 4.1, the underlying communication network is modeled through a partitioning of the node set $\mathcal{V}$ to form disjoint clusters with inter-cluster links leading to the following assumption.

Assumption 4.2. Let M connected cluster subgraphs and $M^* \geq M - 1$ connected inter-cluster subgraphs be given.

In this work, the C-MAS under consideration is such that all agents in each cluster can communicate continuously with their neighbors within the same cluster, while all agents contained in each inter-cluster can only communicate intermittently with their neighbors within the same inter-cluster. More precisely, for each $p \in [M]$ and $i \in \mathcal{V}_p$, the process state of agent i, namely $x_i(t)$, is broadcast to all agents $k \in \mathcal{N}_i \cap \mathcal{V}_p$ for all $t \in \mathbb{R}_{\geq 0}$. However, for each $r \in [M^*]$ and $i \in \mathcal{V}^r$, the state of agent i is broadcast to each agent $k \in \mathcal{N}_i \cap \mathcal{V}^r$ only at isolated times. Specifically, let $\{t_w^r\}_{w=1}^{\infty}$ be an increasing sequence of broadcast times, where t_w^r denotes the w^{th} instance that the state of agent $i \in \mathcal{V}^r$ is broadcast to all agents $k \in \mathcal{N}_i \cap \mathcal{V}^r$ for each $i \in \mathcal{V}^r$. For each inter-cluster $r \in [M^*]$, let $0 < T_1^r \leq T_2^r$ denote lower and upper bounds, respectively, for the difference between consecutive broadcast times in $\{t_w^r\}_{w=1}^{\infty}$, i.e.,

$$T_1^r \leq t_{w+1}^r - t_w^r \leq T_2^r \tag{4–2}$$

for all $w \in \mathbb{Z}_{\geq 1}$ and $t_1^r \leq T_2^r$. For conciseness, let $\mathcal{N}_i^0 \triangleq \mathcal{N}_i \cap \mathcal{V}_p$ such that $\mathcal{V}_p$ denotes the cluster of agent i, and $\mathcal{N}_i^q \triangleq \mathcal{N}_i \cap \mathcal{V}^q$ for $q \in [M^*]$. Therefore, $\mathcal{N}_i^0$ contains the neighbors

of agent i that are in the same cluster as agent i, and $\mathcal{N}_i^q$ contains the neighbors of agent i that are in inter-cluster q.

The objective is to design a distributed controller for each agent $i \in \mathcal{V}$ that ensures $\{x_i\}_{i\in\mathcal{V}}$ achieves consensus through the use of the communication graph $\mathcal{G}$ whose cluster subgraphs and inter-cluster subgraphs undergo continuous communication and intermittent communication, respectively. Let the disagreement between the state of agent i and the average state of the C-MAS be defined by $e_i : [0, \infty) \to \mathbb{R}^n$ such that

$$e_i \triangleq x_i - \frac{1}{N}\sum_{\ell\in\mathcal{V}} x_\ell. \tag{4–3}$$

The C-MAS is said to achieve consensus if $e_i = e_k$ for all $i, k \in \mathcal{V}$. From the construction of (4–3), for each $i, k \in \mathcal{V}$, $e_i = e_k \iff x_i = x_k$. Moreover, the difference in the state of agents $i, k \in \mathcal{V}$ can be alternatively expressed as

$$e_k - e_i = x_k - x_i. \tag{4–4}$$

4.3 Consensus Control Design and Hybrid System Modeling

The broadcast times of inter-cluster r are determined by discrete time instances governed by the set of points $\{t_w^r\}_{w=1}^{\infty}$. Following our previous work in [61], a timer state $\tau_r : [0, \infty) \to [0, T_2^r]$ is defined whose hybrid dynamics are given by[3]

$$\begin{aligned} \dot{\tau}_r &= -1, \qquad && \tau_r \in [0, T_2^r] \\ \tau_r^+ &\in [T_1^r, T_2^r], && \tau_r = 0, \end{aligned} \tag{4–5}$$

where $0 < T_1^r \leq T_2^r$ are the constraints on the broadcast times given in (4–2). At each timer reset, i.e., when $\tau_r = 0$, the w^{th} broadcast time corresponding to the agents in $\mathcal{G}[\mathcal{V}^r]$ is set equal to the current time.

[3] Timers like (4–5) can also be developed for each agent to enable intermittent state broadcasting within clusters.

Remark 4.1. The graph $\mathcal{G}$ does not represent continuous communication between adjacent agents, but rather, the underlying graph of potential communications. Figure 4-1 represents a 3 cluster system wherein the agents communicate continuously within their own clusters. Moreover, when $\tau_r = 0$, a communication instance occurs for inter-cluster r.

Suppose agent i is assigned to cluster p, i.e., $i \in \mathcal{V}_p$. The information coming into each agent may occur at drastically different time instances, namely, both continuously and intermittently. The consensus controller of agent i is, therefore, designed as

$$u_i \triangleq K\left(\eta_i + \sum_{r\in[M^*]} \eta_{i,r}\right), \tag{4–6}$$

where $K \in \mathbb{R}^{d\times n}$ is a to be designed matrix, $\eta_i : [0,\infty) \to \mathbb{R}^n$ defines agent i's control component corresponding to state information coming from cluster p, and $\eta_{i,r} : [0,\infty) \to \mathbb{R}^n$ defines agent i's control component corresponding to state information coming from inter-cluster r. With respect to agent i, the component of (4–6) that uses the continuously available state information from same-cluster neighbors is given by the following static controller

$$\eta_i \triangleq \sum_{k\in\mathcal{N}_i^0} a_{ik}(x_k - x_i). \tag{4–7}$$

Similarly, the component in (4–6) that uses the intermittently available state information from neighbors in inter-cluster r evolves according to the sample-and-hold dynamics given by the following hybrid system

$$\begin{aligned} \dot{\eta}_{i,r} &= 0_n, && \tau_r \in [0, T_2^r] \\ \eta_{i,r}^+ &= \sum_{k\in\mathcal{N}_i^r} a_{ik}(x_k - x_i), && \tau_r = 0. \end{aligned} \tag{4–8}$$

Recall that $\mathcal{N}_i^r = \mathcal{N}_i \cap \mathcal{V}^r$, which denotes the set of neighbors of agent i that are in inter-cluster r. We now derive the closed-loop error system for the local consensus error of agent i as defined in (4–3). Substituting (4–1) and (4–6) into the time derivative

of (4–3) yields

$$\dot{e}_i = Ae_i + BK\left(\eta_i - \frac{1}{N}\sum_{\ell\in\mathcal{V}}\eta_\ell\right) + BK\sum_{r\in[M^*]}\left(\eta_{i,r} - \frac{1}{N}\sum_{\ell\in\mathcal{V}}\eta_{\ell,r}\right). \tag{4–9}$$

To facilitate the subsequent stability analysis for the closed-loop C-MAS, let $e \triangleq [e_1^\top, e_2^\top, ..., e_N^\top]^\top \in \mathbb{R}^{nN}$ denote the stacked consensus error, $\eta \triangleq [\eta_1^\top, \eta_2^\top, ..., \eta_N^\top]^\top \in \mathbb{R}^{nN}$ denote the cluster control components, $\theta_r \triangleq [\eta_{1,r}^\top, \eta_{2,r}^\top, ..., \eta_{N,r}^\top]^\top \in \mathbb{R}^{nN}$ denote the control components for inter-cluster r, $\Theta \triangleq [\theta_1^\top, \theta_2^\top, ..., \theta_{M^*}^\top]^\top \in \mathbb{R}^{nNM^*}$ denote the control components for all inter-clusters, and $\tau \triangleq [\tau_1, \tau_2, ..., \tau_{M^*}]^\top \in \mathcal{T} \triangleq [0, T_2^1] \times ... \times [0, T_2^{M^*}]$ denote the stacked timer states for all inter-clusters. Moreover, recall that $L_C \in \mathbb{R}^{N\times N}$ denotes the Laplacian of the complete graph on N nodes. It follows from (4–9) that the stacked consensus error dynamics are given by

$$\dot{e} = (I_N \otimes A)\, e + \frac{1}{N}(L_C \otimes BK)\,\eta + \frac{1}{N}(L_C \otimes BK)\sum_{r\in[M^*]}\theta_r. \tag{4–10}$$

Substituting (4–4) and (4–7) into η for all $i \in \mathcal{V}$ yields

$$\eta = -(L_0 \otimes I_n)\, e. \tag{4–11}$$

Substituting (4–11) into (4–10) yields

$$\dot{e} = \bar{A}e + \bar{B}\sum_{r\in[M^*]}\theta_r,\ \bar{A} \triangleq (I_N \otimes A) - \frac{1}{N}(L_C L_0 \otimes BK),\ \bar{B} \triangleq \frac{1}{N}(L_C \otimes BK). \tag{4–12}$$

Note that the stacked consensus error denoted by e is naturally a continuous-time system. Therefore, at each jump, which occurs when $\tau_r = 0$ for some $r \in [M^*]$, the closed-loop dynamics of the stacked consensus error are updated as $e^+ = e$. Next, observe that substituting (4–8) into the time derivative of θ_r for all $i \in \mathcal{V}$ and $r \in [M^*]$ yields

$$\dot{\theta}_r = 0_{nN}. \tag{4–13}$$

At jumps, i.e., when $\tau_r = 0$ for some $r \in [M^*]$, the substitution of (4–4) and (4–8) into θ_r for all $i \in \mathcal{V}$ and $r \in [M^*]$ yields

$$\theta_r^+ = -\left(L_r \otimes I_n\right) e. \tag{4–14}$$

To further facilitate the development, the following variables are introduced. Let

$$\tilde{\theta}_r \triangleq -\left(L_r \otimes I_n\right) e - \theta_r \tag{4–15}$$

and $\widetilde{\Theta} \triangleq \left[\tilde{\theta}_1^\top, \tilde{\theta}_2^\top, ..., \tilde{\theta}_{M^*}^\top\right]^\top \in \mathbb{R}^{nNM^*}$. Substituting (4–12) and (4–13) into the time derivative of (4–15) yields

$$\dot{\tilde{\theta}}_r = -\left(L_r \otimes I_n\right) \bar{A} e - \left(L_r \otimes I_n\right) \bar{B} \sum_{\ell \in [M^*]} \theta_\ell. \tag{4–16}$$

Substituting $e^+ = e$ and (4–14) into the time difference of (4–15) for $r \in [M^*]$ yields

$$\tilde{\theta}_r^+ = 0_{nN}. \tag{4–17}$$

Substituting (4–15) into (4–12) and (4–16) yields

$$\dot{e} = \left(\bar{A} - \bar{B}\bar{L}\right) e - \bar{B}\left(1_{M^*}^\top \otimes I_{nN}\right) \widetilde{\Theta}, \tag{4–18}$$

and

$$\dot{\tilde{\theta}}_r = -\left(L_r \otimes I_n\right)\left(\bar{A} - \bar{B}\bar{L}\right) e + \left(L_r \otimes I_n\right) \bar{B}\left(1_{M^*}^\top \otimes I_{nN}\right) \widetilde{\Theta}, \tag{4–19}$$

respectively, where

$$\bar{L} \triangleq \sum_{\ell \in [M^*]} \left(L_\ell \otimes I_n\right).$$

The closed-loop C-MAS hybrid dynamics denoted by $\mathcal{H}$ are now constructed. Let $\xi \triangleq [e^\top, \widetilde{\Theta}^\top, \tau^\top]^\top \in \mathcal{X}$ denote the C-MAS state variable, where $\mathcal{X} \triangleq \mathbb{R}^{nN} \times \mathbb{R}^{nNM^*} \times \mathcal{T}$ denotes the state space of the hybrid system. Furthermore, let $z \triangleq [e^\top, \widetilde{\Theta}^\top]^\top \in \mathbb{R}^{nN} \times \mathbb{R}^{nNM^*}$. The flow set of the hybrid system is defined as $C \triangleq \mathcal{X}$, and the flow map $f : \mathcal{X} \to \mathcal{X}$ is

defined as

$$f(\xi) \triangleq \begin{bmatrix} \mathbf{A}z \\ -1_{M^*} \end{bmatrix}, \tag{4–20}$$

where

$$\mathbf{A} \triangleq \begin{bmatrix} \bar{A} - \bar{B}\bar{L} & -\mathbf{A}^* \\ -\mathbf{L}\left(1_{M^*} \otimes \left(\bar{A} - \bar{B}\bar{L}\right)\right) & \mathbf{L}\left(1_{M^*} \otimes \mathbf{A}^*\right) \end{bmatrix}$$

$$\mathbf{A}^* \triangleq \bar{B}\left(1_{M^*}^\top \otimes I_{nN}\right),\ \mathbf{L} \triangleq \text{diag}\left(L_1 \otimes I_n, ..., L_{M^*} \otimes I_n\right).$$

Let $\kappa_1 \triangleq nN(1 + M^*)$, and observe that $\mathbf{A} \in \mathbb{R}^{\kappa_1 \times \kappa_1}$. The jump set is given by $D \triangleq \cup_{r\in[M^*]} D_r$, where $D_r \triangleq \{\xi \in \mathcal{X} : \tau_r = 0\}$. When $\tau_r = 0$, a jump for the r^{th} inter-cluster occurs, where e is mapped to itself by $e^+ = e$, $\tilde{\theta}_r$ is mapped to 0_{nN} by (4–17), and τ_r is mapped to some $\nu_r \in [T_1^r, T_2^r]$ by (4–5). For $k \in [M^*] \setminus \{r\}$, the variables e, $\tilde{\theta}_k$, and τ_k evolve according to (4–18), (4–19), and (4–5), respectively. The jump map $G : \mathcal{X} \rightrightarrows \mathcal{X}$ is defined as

$$\begin{aligned} G(\xi) &\triangleq \left\{G_r(\xi) : \xi \in D_r,\ r \in [M^*]\right\}, \\ G_r(\xi) &\triangleq \begin{bmatrix} e \\ \left[\tilde{\theta}_1^\top, ..., \tilde{\theta}_{r-1}^\top, 0_{nN}^\top, \tilde{\theta}_{r+1}^\top, ..., \tilde{\theta}_{M^*}^\top\right]^\top \\ \left[\tau_1, ..., \tau_{r-1}, [T_1^r, T_2^r], \tau_{r+1}, ..., \tau_{M^*}\right]^\top \end{bmatrix}. \end{aligned} \tag{4–21}$$

Due to the definition of G, the solutions to the hybrid system $\mathcal{H}$ are inherently non-unique. Nevertheless, using hybrid systems analysis, it will be shown that, under certain sufficient conditions, the subsequently defined consensus set $\mathcal{A}$ is globally exponentially stable. With respect to the objective, the set to stabilize is given by

$$\mathcal{A} \triangleq \left\{\xi \in \mathcal{X} : \forall_{i,k\in\mathcal{V}}\ e_i = e_k,\ \forall_{p,q\in[M^*]}\ \tilde{\theta}_p = \tilde{\theta}_q\right\}, \tag{4–22}$$

for the hybrid system $\mathcal{H}$ with data (C, f, D, G). Using (4–8), it can be shown that if $e_i = e_k$ for all $i, k \in \mathcal{V}$, then $\tilde{\theta}_r = 0_{nN}$ for each $r \in [M^*]$. Hence, stabilizing (4–22) is equivalent to having the C-MAS achieve consensus.

4.4 Stability Analysis

Before introducing the main results, two supporting lemmas are presented.

Lemma 4.1. *(cf. [83, Lemma 3.5]) Let* $0 < T_1^r \leq T_2^r$ *for each* $r \in [M^*]$*. Every* $\phi \in \mathcal{S}_{\mathcal{H}}$ *satisfies the following.*

- ϕ is complete, i.e., dom ϕ is unbounded.
- For each $(t, j) \in$ dom ϕ, $(\frac{j}{N} - 1)T_1^{\min} \leq t \leq \frac{j}{N}T_2^{\max}$, where $T_1^{\min} \triangleq \min_{r\in[M^*]}\{T_1^r\}$ and $T_2^{\max} \triangleq \max_{r\in[M^*]}\{T_2^r\}$.
- For all $j \in \mathbb{Z}_{\geq 0}$ such that $(t_{(j+1)N}, (j+1)N)$, $(t_{jN}, jN) \in$ dom ϕ, $t_{(j+1)N} - t_{jN} \in [T_1^{\max}, T_2^{\max}]$.

Lemma 4.2. *Assumption 4.2 is satisfied if and only if the graph* $\mathcal{G}$ *is connected.*

Proof. $(\Longrightarrow)$ By Assumption 4.2, the graph $\mathcal{G}$ consists of M connected clusters and at least $M - 1$ connected inter-clusters, where there is at most one inter-cluster between each pair of distinct clusters by construction. We can then build a line graph-like structure, where the nodes and edges of a line graph on M nodes correspond to clusters and inter-clusters, respectively. Since the line graph-like structure forms a connected graph, we see that the union graph $\mathcal{G}$ is connected.

$(\Longleftarrow)$ Recall that $\mathcal{G}$ is undirected by construction. Since $\mathcal{G}$ is connected, the graph can be partitioned into $M < N$ connected clusters and at least $M - 1$ connected inter-clusters. Note that clusters consisting of a single node are vacuously connected. ■

Next, we present useful objects that aid the stability analysis. Let $U \triangleq I_N - \frac{1}{N}1_N 1_N^\top \in \mathbb{R}^{N\times N}$, where

$$U = \frac{1}{N}\begin{bmatrix} N-1 & -1 & \cdots & -1 \\ -1 & N-1 & \cdots & -1 \\ \vdots & \vdots & \ddots & \vdots \\ -1 & -1 & \cdots & N-1 \end{bmatrix}$$

and $U^2 = U$ [84]. Recall that $L \in \mathbb{R}^{N\times N}$ denotes the Laplacian of the C-MAS. Since $\mathcal{G}$ is connected by Lemma 4.2 and undirected by construction, L is symmetric and positive semi-definite. Since L is symmetric, L is diagonalizable, where $L = SDS^{-1}$ such that $S \in \mathbb{R}^{N\times N}$ is an orthonormal eigenvector matrix and $D \in \mathbb{R}^{N\times N}$ is a diagonal eigenvalue matrix. Let $\lambda_1, \lambda_2, ..., \lambda_N$ denote the eigenvalues of L, and recall that $0 = \lambda_1 < \lambda_2 \leq ... \leq \lambda_N$ for a connected and undirected graph $\mathcal{G}$. Let $s_i \in \mathbb{R}^N$ denote the i^{th} eigenvector of L that corresponds to λ_i and $\Psi \triangleq [s_2, s_3, ..., s_N] \in \mathbb{R}^{N\times(N-1)}$. Note that $U = \Psi\Psi^\top$ and $\Psi^\top\Psi = I_{N-1}$ [84]. Let $\kappa_2 \triangleq n(N-1)(1+M^*)$, $\bar{\Psi} \triangleq \Psi \otimes I_n \in \mathbb{R}^{nN\times n(N-1)}$, and $\widetilde{\Psi} \triangleq I_{(1+M^*)} \otimes \bar{\Psi} \in \mathbb{R}^{\kappa_1\times\kappa_2}$. For $z \in \mathbb{R}^{nN(1+M^*)}$, observe that

$$\begin{aligned} \|\widetilde{\Psi}^\top z\|^2 &= z^\top\widetilde{\Psi}\widetilde{\Psi}^\top z \\ &= z^\top\widetilde{\Psi}I_{\kappa_2}\widetilde{\Psi}^\top z \\ &= z^\top\widetilde{\Psi}\widetilde{\Psi}^\top\widetilde{\Psi}\widetilde{\Psi}^\top z \\ &= \|(I_{1+M^*} \otimes (U \otimes I_n))z\|^2. \end{aligned} \tag{4–23}$$

Hence, $\|\widetilde{\Psi}^\top z\|$ measures the distance of z to $\mathcal{A}$. Recalling that $\xi = [z^\top, \tau^\top]^\top$, we henceforth write $|\xi|_{\mathcal{A}} = \|\widetilde{\Psi}^\top z\|$.

Theorem 4.1. *Suppose Assumptions 4.1 and 4.2 are satisfied. Given $0 < T_1^r \leq T_2^r$ for all $r \in [M^*]$, the set $\mathcal{A}$ is globally exponentially stable for the hybrid system $\mathcal{H}$ with data in* (4–20) *and* (4–21) *if there exists a scalar $\sigma > 0$, gain matrix $K \in \mathbb{R}^{d\times n}$, and symmetric positive definite matrices $P \in \mathbb{R}^{n(N-1)\times n(N-1)}$ and $Q_r \in \mathbb{R}^{n(N-1)\times n(N-1)}$ for each $r \in [M^*]$ such that*

$$M(\tau) \triangleq \widetilde{\mathbf{A}}^\top R(\tau) + R(\tau)\widetilde{\mathbf{A}} - \widetilde{R}(\tau) < 0_{\kappa_2\times\kappa_2} \ \forall \tau \in \mathcal{T}, \tag{4–24}$$

where $\widetilde{\mathbf{A}} \triangleq \widetilde{\Psi}^\top\mathbf{A}\widetilde{\Psi}$, $R(\tau) \triangleq$ diag$(P, Q_1e^{\sigma\tau_1}, ..., Q_{M^*}e^{\sigma\tau_{M^*}})$, and $\widetilde{R}(\tau) \triangleq$ diag$(0 \cdot P, \sigma Q_1e^{\sigma\tau_1}, ..., \sigma Q_{M^*}e^{\sigma\tau_{M^*}})$.

Proof. Inspired by [84], let the Lyapunov function $V : \mathcal{X} \to \mathbb{R}_{\geq 0}$ be defined as

$$V(\xi) \triangleq z^\top\widetilde{\Psi}R(\tau)\widetilde{\Psi}^\top z. \tag{4–25}$$

Let $\alpha_1 \triangleq \lambda_{\min}(R(0_{M^*})) \in \mathbb{R}_{>0}$ and $\alpha_2 \triangleq \lambda_{\max}(R(T_2)) \in \mathbb{R}_{>0}$ denote the minimum and maximum eigenvalues of $R(\tau)$, respectively, where $T_2 \triangleq [T_2^1, T_2^2, ..., T_2^{M^*}]^\top \in \mathbb{R}^{M^*}$. Recalling that $|\xi|_{\mathcal{A}} = \|\widetilde{\Psi}^\top z\|$ and using the definitions of α_1 and α_2, we can bound (4–25) as

$$\alpha_1 |\xi|_{\mathcal{A}}^2 \leq V(\xi) \leq \alpha_2 |\xi|_{\mathcal{A}}^2. \tag{4–26}$$

During flows, the change in V is given by $\langle \nabla V(\xi), f(\xi) \rangle$ for each $\xi \in C$. Hence, it follows that

$$\begin{aligned}
\langle \nabla V(\xi), f(\xi) \rangle =& 2z^\top \widetilde{\Psi} R(\tau) \widetilde{\Psi}^\top \mathbf{A} z + z^\top \widetilde{\Psi} \dot{R}(\tau) \widetilde{\Psi}^\top z \\
=& 2z^\top \widetilde{\Psi} R(\tau) \widetilde{\Psi}^\top \mathbf{A} \Big(I_{\kappa_1} - \widetilde{\Psi}\widetilde{\Psi}^\top + \widetilde{\Psi}\widetilde{\Psi}^\top \Big) z + z^\top \widetilde{\Psi} \dot{R}(\tau) \widetilde{\Psi}^\top z \\
=& z^\top \widetilde{\Psi} \Big[\widetilde{\mathbf{A}}^\top R(\tau) + R(\tau) \widetilde{\mathbf{A}} - \widetilde{R}(\tau) \Big] \widetilde{\Psi}^\top z \\
&+ 2z^\top \widetilde{\Psi} R(\tau) \widetilde{\Psi}^\top \mathbf{A} \left(I_{\kappa_1} - \widetilde{\Psi}\widetilde{\Psi}^\top \right) z,
\end{aligned} \tag{4–27}$$

where $\dot{R}(\tau) = -\widetilde{R}(\tau)$. Since $\mathcal{G}$ is connected by Lemma 4.2, $s_1 = 1_N$ is the eigenvector of L that corresponds to the 0 eigenvalue. Since $\{s_i\}_{i=1}^N$ is an orthonormal basis for $\mathbb{R}^N$, L_C and L_r for $r \in [M^*]$ are symmetric, zero row sum matrices, and $\Psi^\top 1_N = 0_{N-1}$, it follows that

$$\widetilde{\Psi} R(\tau) \widetilde{\Psi}^\top \mathbf{A} \left(I_{\kappa_1} - \widetilde{\Psi}\widetilde{\Psi}^\top \right) = 0_{\kappa_1 \times \kappa_1}. \tag{4–28}$$

Next, let $\zeta \triangleq -\sup\{\lambda_{\max}(M(\nu)) : \nu \in \mathcal{T}\}$, where $\zeta > 0$ since $M(\tau)$, as defined in (4–24), is negative definite for all $\tau \in \mathcal{T}$. Using ζ and (4–28), we see that (4–27) can be upper bounded

$$\langle \nabla V(\xi), f(\xi) \rangle \leq -\zeta z^\top \widetilde{\Psi}\widetilde{\Psi}^\top z. \tag{4–29}$$

Substituting $|\xi|_{\mathcal{A}} = \|\widetilde{\Psi}^\top z\|$ and the right inequality in (4–26) into (4–29) yields

$$\begin{aligned}
\langle \nabla V(\xi), f(\xi) \rangle \leq& -\zeta z^\top \widetilde{\Psi}\widetilde{\Psi}^\top z \\
=& -\zeta |\xi|_{\mathcal{A}}^2 \leq -\frac{\zeta}{\alpha_2} V(\xi).
\end{aligned} \tag{4–30}$$

During jumps, the change in V is given by $V(g) - V(\xi)$ for each $\xi \in D$ and $g \in G(\xi)$. Without loss of generality, suppose $\tau_q = 0$ for some $q \in [M^*]$. From (4–21), it follows that

$$\begin{aligned} V(g) - V(\xi) =& (e^+)^\top \bar{\Psi} P \bar{\Psi}^\top (e^+) + \sum_{r \in [M^*]} (\tilde{\theta}_r^+)^\top \bar{\Psi} Q_r e^{\sigma \tau_r^+} \bar{\Psi}^\top (\tilde{\theta}_r^+) \\ & - e^\top \bar{\Psi} P \bar{\Psi}^\top e - \sum_{r \in [M^*]} \tilde{\theta}_r^\top \bar{\Psi} Q_r e^{\sigma \tau_r} \bar{\Psi}^\top \tilde{\theta}_r \\ =& (\tilde{\theta}_q^+)^\top \bar{\Psi} Q_q e^{\sigma \tau_q^+} \bar{\Psi}^\top (\tilde{\theta}_q^+) - \tilde{\theta}_q^\top \bar{\Psi} Q_q e^{\sigma \tau_q} \bar{\Psi}^\top \tilde{\theta}_q \\ =& - \tilde{\theta}_q^\top \bar{\Psi} Q_q \bar{\Psi}^\top \tilde{\theta}_q \leq 0. \end{aligned} \tag{4–31}$$

Therefore, $V(g) - V(\xi) \leq 0$ for each $\xi \in D$ and $g \in G(\xi)$. Next, for each $\phi \in \mathcal{S}_{\mathcal{H}}$, select $(t, j) \in \text{dom } \phi$, and let $0 = t_0 \leq t_1 \leq ... \leq t_{j+1} \leq t$ satisfy

$$\text{dom } \phi \bigcap ([0, t_{j+1}] \times \{0, 1, ..., j\}) = \bigcup_{s=0}^{j} ([t_s, t_{s+1}] \times \{s\}).$$

For each $s \in \{0, 1, ..., j\}$ and for almost all $r \in [t_s, t_{s+1}]$, $\phi(r, s) \in C$. It can then be seen that for each $s \in \{0, 1, ..., j\}$ and for almost all $r \in [t_s, t_{s+1}]$

$$\frac{d}{dr} V(\phi(r, s)) \leq -\frac{\zeta}{\alpha_2} V(\phi(r, s)). \tag{4–32}$$

Integrating both sides of (4–32) yields

$$V(\phi(t_{s+1}, s)) \leq \exp\left(-\frac{\zeta}{\alpha_2}(t_{s+1} - t_s)\right) V(\phi(t_s, s)) \tag{4–33}$$

for each $s \in \{0, 1, ..., j\}$. Similarly, for each $s \in \{0, 1, ..., j\}$, $\phi(t_s, s-1) \in D$, one has that

$$V(\phi(t_s, s)) - V(\phi(t_s, s-1)) \leq 0 \tag{4–34}$$

for all $s \in \{0, 1, ..., j\}$. Using (4–33) and (4–34), it follows that

$$V(\phi(t, j)) \leq \exp\left(-\frac{\zeta}{\alpha_2} t\right) V(\phi(0, 0)). \tag{4–35}$$

For any $(t, j) \in \text{dom } \phi$, substituting (4–26) into (4–35) yields

$$|\phi(t,j)|_{\mathcal{A}} \leq \sqrt{\frac{\alpha_2}{\alpha_1}} \exp\left(-\frac{\zeta}{2\alpha_2} t\right) |\phi(0,0)|_{\mathcal{A}}. \tag{4–36}$$

Using Lemma 4.1, it follows that $t = \varepsilon t + (1-\varepsilon)t \geq \varepsilon t + (1-\varepsilon)(\frac{j}{N} - 1)T_1^{\min}$, where $\varepsilon \in (0,1)$. Let

$$\alpha \triangleq \min\left\{\frac{\zeta\varepsilon}{2\alpha_2}, \frac{\zeta(1-\varepsilon)T_1^{\min}}{2N\alpha_2}\right\},$$
$$\kappa \triangleq \sqrt{\frac{\alpha_2}{\alpha_1}} \exp\left(\frac{\zeta(1-\varepsilon)T_1^{\min}}{2\alpha_2}\right).$$

Observe that

$$-\frac{\zeta}{2\alpha_2}\left(\varepsilon t + (1-\varepsilon)\left(\frac{j}{N} - 1\right)T_1^{\min}\right)$$
$$\leq -\min\left\{\frac{\zeta\varepsilon}{2\alpha_2}, \frac{\zeta(1-\varepsilon)T_1^{\min}}{2N\alpha_2}\right\}(t+j) + \frac{\zeta(1-\varepsilon)T_1^{\min}}{2\alpha_2}.$$

Therefore, (4–36) can be upper bounded as

$$|\phi(t,j)|_{\mathcal{A}} \leq \kappa e^{-\alpha(t+j)} |\phi(0,0)|_{\mathcal{A}}. \tag{4–37}$$

By Lemma 4.1, every maximal solution of $\mathcal{H}$ is complete. Hence, $\mathcal{A}$ is globally exponential stable for $\mathcal{H}$. Lastly, since (4–35) implies V is globally exponential stable, (4–25) implies $z \in \mathcal{L}_\infty$. Since $z \in \mathcal{L}_\infty$, the definition of z can be used to conclude that $e_i \in \mathcal{L}_\infty$ and $\tilde{\theta}_r \in \mathcal{L}_\infty$ for all $i \in \mathcal{V}$ and all $r \in [M^*]$. Therefore, $u_i \in \mathcal{L}_\infty$ for all $i \in \mathcal{V}$ through the use of (4–4), (4–6)–(4–8), (4–15), and the definition of θ_r. ■

Remark 4.2. It can be shown that the hybrid system $\mathcal{H}$ satisfies the hybrid basic conditions.[4] Moreover, since the consensus set $\mathcal{A}$ in (4–22) is globally exponentially stable, and, indeed, uniformly globally asymptotically stable, it follows that the consensus set is

[4] A hybrid system $\mathcal{H} = (C, f, D, G)$ satisfies the hybrid basic conditions if the sets C and D are closed, the single valued mapping $f : \mathbb{R}^n \to \mathbb{R}^n$ is continuous, and the set valued mapping $G : \mathbb{R}^n \rightrightarrows \mathbb{R}^n$ is well-posed.

robustly practically asymptotically stable to small perturbations, see [63, Lemma 7.20] for more information on robustness of hybrid systems.

The bilinear matrix inequality (BMI) in (4–24) must be satisfied for all $\tau \in \mathcal{T}$ to ensure the result in Theorem 4.1. Hence, given matrices P and Q_r for $r \in [M^*]$, one must verify that these matrices satisfy (4–24) for infinitely many points, i.e., for each $\tau \in \mathcal{T}$. However, one can leverage the BMI's structure to construct an equivalent BMI that is a convex combination of (4–24) evaluated at two subsequently defined endpoints. Hence, satisfying (4–24) at these endpoints ensures (4–24) is satisfied for all $\tau \in \mathcal{T}$. Before presenting the equivalent BMI, the following objects are introduced. For each $r \in [M^*]$, let the function $\vartheta_r : [0, T_2^r] \to [0, 1]$ be defined as

$$\vartheta_r(w) \triangleq \frac{\exp(\sigma w) - \exp(\sigma T_2^r)}{1 - \exp(\sigma T_2^r)}. \tag{4–38}$$

Also, let $\epsilon \in [0, 1]$, $\nu \triangleq [\nu_1, ..., \nu_{M^*}]^\top$, $\bar{\nu} \triangleq [\epsilon, \nu^\top]^\top$, $T_2 = [T_2^1, T_2^2, ..., T_2^{M^*}]^\top$, $\widetilde{Q}(\nu) \triangleq \operatorname{diag}(Q_1 e^{\sigma\nu_1}, ..., Q_{M^*} e^{\sigma\nu_{M^*}})$, $\overline{R}(\nu) \triangleq \operatorname{diag}(\vartheta_1(\nu_1), ..., \vartheta_{M^*}(\nu_{M^*})) \otimes I_{n(N-1)}$, and $\mathcal{R}(\bar{\nu}) \triangleq \operatorname{diag}(\epsilon I_{n(N-1)}, \overline{R}(\nu))$.

Proposition 4.1. *Let $0 < T_1^r \leq T_2^r$ for each $r \in [M^*]$. The inequality in* (4–24) *holds if there exists a scalar $\sigma > 0$ and symmetric positive definite matrices P and Q_r for each $r \in [M^*]$ satisfying $M(0_{M^*}) < 0_{\kappa_2 \times \kappa_2}$ and $M(T_2) < 0_{\kappa_2 \times \kappa_2}$, where*

$$M(\nu) = \mathcal{R}(\bar{\nu}) M(0_{M^*}) + (I_{\kappa_2} - \mathcal{R}(\bar{\nu})) M(T_2). \tag{4–39}$$

Proof. From (4–38), it follows that for each $r \in [M^*]$

$$\exp(\sigma w) = \vartheta_r(w) + (1 - \vartheta_r(w)) \exp(\sigma T_2^r). \tag{4–40}$$

Using $\widetilde{Q}(\nu)$, ν, and (4–40), it follows that

$$\widetilde{Q}(\nu) = \overline{R}(\nu) \widetilde{Q}(0_{M^*}) + \left(I_{n(N-1)M^*} - \overline{R}(\nu)\right) \widetilde{Q}(T_2). \tag{4–41}$$

Using the definition of $M(\nu)$ from Theorem 4.1, it can be seen that

$$\begin{aligned} M(\nu) =& R(\nu)\widetilde{\Psi}^{\top}\mathbf{A}\widetilde{\Psi} + \widetilde{\Psi}^{\top}\mathbf{A}^{\top}\widetilde{\Psi}R(\nu) - \widetilde{R}(\nu) \\ =& 2R(\nu)\widetilde{\Psi}^{\top}\mathbf{A}\widetilde{\Psi} - \widetilde{R}(\nu) \end{aligned} \tag{4–42}$$

and, using the definitions of $R(\nu)$ and $\widetilde{R}(\nu)$ from Theorem 4.1, one has

$$2R(\nu)\widetilde{\Psi}^{\top}\mathbf{A}\widetilde{\Psi} - \widetilde{R}(\nu) = 2\text{diag}\left(P, \widetilde{Q}(\nu)\right)\widetilde{\Psi}^{\top}\mathbf{A}\widetilde{\Psi} - \text{diag}\left(0_{nN\times nN}, \sigma\widetilde{Q}(\nu)\right). \tag{4–43}$$

Substituting $1 = \epsilon + (1-\epsilon)$, (4–41) and (4–42) into (4–43) yields (4–39). ■

Remark 4.3. Using Proposition 4.1, we can satisfy the BMI in (4–24) for all $\tau \in \mathcal{T}$ provided $M(0_{M^*})$ and $M(T_2)$ are negative definite.

4.5 Simulation Example

For the simulation, consider a C-MAS composed of 16 agents that is partitioned into 3 clusters and 2 inter-clusters. Each agent computes a homogeneous process that is modeled by (4–1) and

$$A \triangleq \begin{bmatrix} 0 & 1 \\ -\frac{k}{m} & -\frac{c}{m} \end{bmatrix}, \quad B \triangleq \begin{bmatrix} 0 \\ \frac{1}{m} \end{bmatrix}, \tag{4–44}$$

which denote the state space representation of a spring-mass-damper system. For this simulation, the spring constant, mass, and damping coefficient are selected as $k = 1.5$, $m = 1$, and $c = 0.7$, respectively. Figure 4-2 depicts the C-MAS, where $\mathcal{V}_1 \triangleq \{1,2,3,4,5\}$, $\mathcal{V}_2 \triangleq \{6,7,8,9,10\}$, $\mathcal{V}_3 \triangleq \{11,12,13,14,15,16\}$, $\mathcal{V}^1 \triangleq \{1,3,10\}$, and $\mathcal{V}^2 \triangleq \{9,14\}$. The green, orange, and blue nodes correspond to the cluster sets given by $\mathcal{V}_1$, $\mathcal{V}_2$, and $\mathcal{V}_3$, respectively. The inter-clusters are denoted by the purple blobs, where inter-cluster 1 is defined by $\mathcal{V}^1$, and inter-cluster 2 is defined by $\mathcal{V}^2$. The simulation was conducted with the Hybrid Systems Toolbox in MATLAB [85]. The network communication parameters are: $T_1^1 = 0.1$, $T_1^2 = 0.2$, $T_2^1 = 1.3$, $T_2^2 = 1.2$, and $\sigma = 10$. The controller gain matrix was set to $K = [-0.14, 0.5]$, which was selected using pole placement and $-0.6 \pm i$ as desired eigenvalues. It can shown that K satisfies the BMI in (4–39), more specifically,

it can be shown that there exist matrices P, Q_r for each $r \in [M^*]$ and scalar $\sigma > 0$ such that (4–39) holds. Each element in $e(0)$ and $\widetilde{\Theta}(0)$ was randomly drawn from a uniform distribution over $[-5, 5]$. Moreover, each timer was initialized such that $\tau_r(0) = T_2^r$ for $r \in \{1, 2\}$. Figure 4-3 illustrates the simulation results and demonstrates that the consensus objective is achieved. In particular, the top plot shows the norm of the consensus error for each agent in the C-MAS. The middle plot shows the evolution of the timer states for the two inter-clusters. The bottom plot shows the evolution of the Lyapunov function V, which was computed with (4–25).

With respect to Figure 4-3, the first 20 time units of the simulation are presented since the norm of the errors in the top subplot converge below 0.05 for all $t \geq 20$. In the middle subplot, once the timer state τ_r reaches 0, the timer state is randomly reset by drawing a new initial condition from a uniform distribution over $[T_1^r, T_2^r]$. The asynchronous communication in the C-MAS is depicted by the distinct instances that the inter-cluster communication timers reach 0.

In the bottom subplot, the large initial values of V are caused by the large P, Q_1, and Q_2 matrices used to satisfy the bilinear matrix inequality in (4–24). The P, Q_1, and Q_2 matrices are omitted since they are each a 30×30 matrix. The breakout window in the bottom plot depicts the end behavior of V, which shows that the value of the Lyapunov function tends to zero as time increases. Note that the parameters T_1^r, T_2^r for $r \in [M^*]$ must be selected so that both the BMI in (4–39) is satisfied and the Lyapunov function is non-increasing.

Based on Remark 4.2, a second simulation was performed, where each agent in the C-MAS was subjected to a sinusoidal disturbance with a magnitude of 0.05 and a phase drawn from a uniform distribution on $[0, 1]$. Note that the simulation parameters are the same as in the nominal case. Figure 4-4 outlines the simulation results, which demonstrates that the C-MAS achieved practical consensus. The top plot shows the norm of the consensus error for each agent in the C-MAS when subjected to a

sinusoidal disturbance. The bottom plot shows the evolution of the timer states for the two inter-clusters.

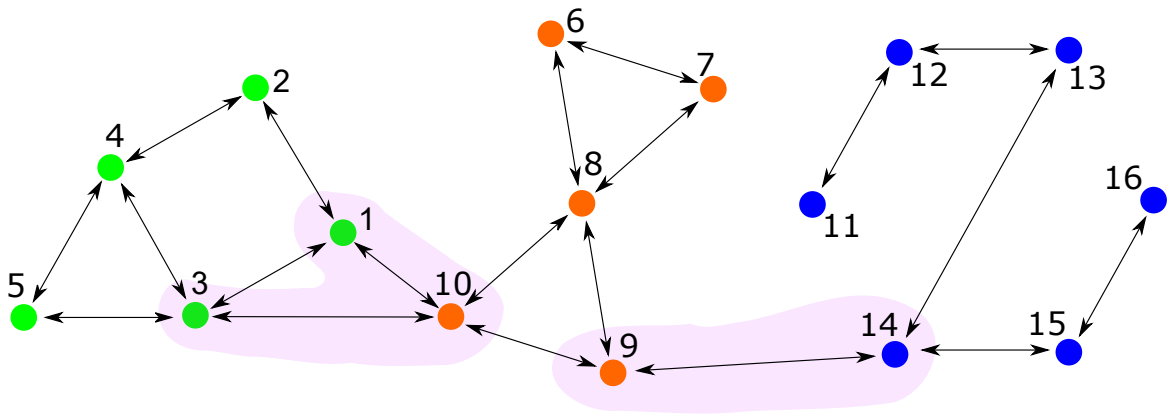

Figure 4-2. Coupling topology consisting of three clusters and two inter-clusters.

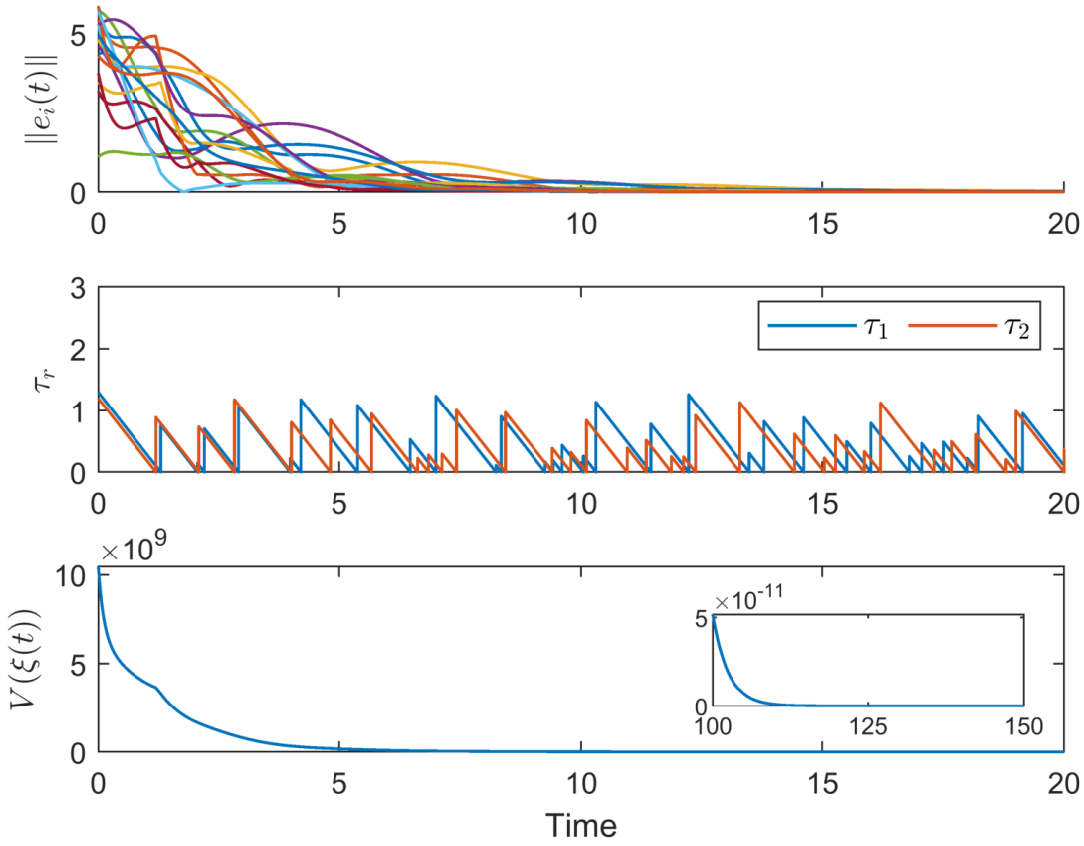

Figure 4-3. Simulation plots of the consensus errors, timer trajectories, and Lyapunov function for the C-MAS in a disturbance-free setting.

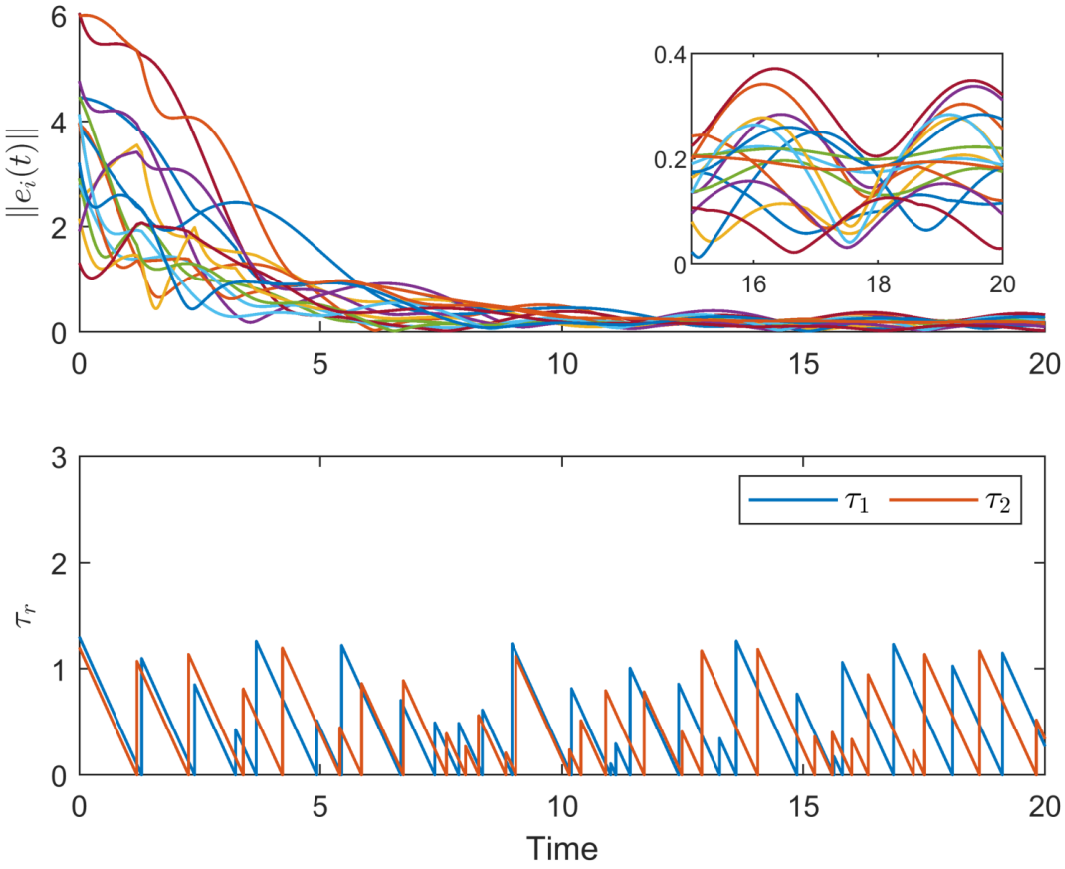

Figure 4-4. Simulation plots of the consensus errors and timer trajectories for the C-MAS while subjected to a sinusoidal disturbance.

CHAPTER 5
EVENT/SELF-TRIGGERED MULTI-AGENT SYSTEM RENDEZVOUS WITH GRAPH MAINTENANCE

This chapter explores the rendezvous problem for a MAS with distance-limited, intermittent communication and sensing. A framework is provided that characterizes a family of distributed event-triggered controllers leveraging non-singular edge-potentials to achieve approximate rendezvous while maintaining an initially connected distance-limited graph. The proposed framework excludes the possibility of Zeno behavior and accommodates the development of self-triggered controllers. The combination of continuous and impulsive dynamics results in a hybrid system, where the closed-loop dynamics of the MAS are presented and analyzed using hybrid differential inclusions. The approximate rendezvous problem is recast into a set stabilization problem and sufficient conditions of the rendezvous set are obtained through a Lyapunov-based analysis.

5.1 Graphs Revisited

In this section, the reader is reminded of notions from graph theory, and notation that is unique to this chapter is introduced. Let $\mathcal{V}$ be a finite non-empty set of cardinality N, and let n be a fixed positive integer. The *configuration space over* $\mathcal{V}$ is defined as $\texttt{Conf}(\mathcal{V}) \triangleq (\mathbb{R}^n)^{\mathcal{V}}$. The *configuration of particles in* $\mathbb{R}^n$ is referred to as $\mathbf{x} \triangleq (x_p)_{p\in\mathcal{V}} \in \texttt{Conf}(\mathcal{V})$. For $R > 0$, the *R-threshold graph* $\mathcal{G}_R(\mathbf{x})$ on a configuration $\mathbf{x}$ is the undirected graph with vertex set $\mathcal{V}$ and edge set $\mathcal{E}_R(\mathbf{x})$ defined by setting $pq \in \mathcal{E}_R(\mathbf{x})$ if and only if $\|x_p - x_q\| \leq R$, where $pq \triangleq \{p, q\}$ for all $p, q \in \mathcal{V}$, $p \neq q$. Recall, for any graph $\mathcal{G} = (\mathcal{V}, \mathcal{E})$, a path in $\mathcal{G}$ connecting a vertex p to a vertex q is a sequence of vertices $(v_0 = p, \ldots, v_k = q)$ where $k \in \mathbb{Z}_{\geq 0}$ and $v_{s-1}v_s \in \mathcal{E}$ for all $s = 1, 2, ..., k$. The graph $\mathcal{G}$ is connected, if every two vertices $p, q \in \mathcal{V}$ may be connected by a path in $\mathcal{G}$. The *neighborhood* $\mathcal{N}_p$ of a vertex $p \in \mathcal{V}$ is the set of all $q \in \mathcal{V}$ with $pq \in \mathcal{E}$. The *degree* of p is $d_p \triangleq |\mathcal{N}_p|$ and $\Delta(\mathcal{G})$ denotes the maximum degree in $\mathcal{G}$. Let $\mathcal{A} \triangleq [a_{pq}] \in \mathbb{R}^{\mathcal{V}\times\mathcal{V}}$ denote the adjacency matrix of $\mathcal{G}$, where $a_{pq} = 1$ if and only if $pq \in \mathcal{E}$ and $a_{pq} = 0$ otherwise.

Within this work, no self-loops are considered. Therefore, $a_{pp} \triangleq 0$ for all $p \in \mathcal{V}$. The degree matrix Δ of $\mathcal{G}$ is the diagonal matrix whose p-th diagonal entry is $\sum_{q\in\mathcal{V}} a_{pq}$. The Laplacian matrix of $\mathcal{G}$ is defined as $\mathbf{L} \triangleq \Delta - \mathcal{A} \in \mathbb{R}^{\mathcal{V}\times\mathcal{V}}$. More generally, if $c = [c_{pq}] \in \mathbb{R}^{\mathcal{V}\times\mathcal{V}}$ is a non-negative symmetric matrix, the weighted Laplacian is defined as $\mathbf{L}_c \triangleq \Delta_c - \mathcal{A}_c$, where $\Delta_c \triangleq \Delta \odot c$ and $\mathcal{A}_c \triangleq \mathcal{A} \odot c$, and known to be positive semidefinite. Let $\lambda_i(\mathbf{L}_c)$ denote the eigenvalues of $\mathbf{L}_c$ in non-decreasing order, and let $\lambda_i(\mathcal{G}) \triangleq \lambda_i(\mathbf{L})$. If $\mathcal{G}$ is connected then $\lambda_1(\mathcal{G}) = 0$ is a simple eigenvalue, and $\lambda_2(\mathcal{G})$, known as the *Fiedler value* of $\mathcal{G}$, is positive. Also, $\lambda_N(\mathbf{L}_c)$ coincides with the operator norm $\|\mathbf{L}_c\|$, since $\mathbf{L}_c$ is self-adjoint.

5.2 Hybrid Systems Revisited

In this section, elements from the hybrid systems framework of [63] are reviewed, and notation used in this chapter is presented. A hybrid differential inclusion $\mathcal{H}$ takes the form [63]:

$$\mathcal{H}\colon \begin{cases} \dot{z} \in F(z), & z \in C, \textit{ (flow constraint)} \\ z^+ \in G(z), & z \in D, \textit{ (jump constraint)} \end{cases} \tag{5–1}$$

where $F : C \rightrightarrows \mathbb{R}^n$, $C \subset \mathbb{R}^n$ are the *flow map and set*; and $G : D \rightrightarrows \mathbb{R}^n$, $D \subset \mathbb{R}^n$ are the *jump map and set*, respectively, and z^+ indicates the value of the state after a jump. Solutions of $\mathcal{H}$ evolve continuously over the flow set according to the dynamics given by the flow map, and are allowed to execute discrete jumps over the jump set, constrained to the sets specified by the jump map. Formally, a set $A \subset \mathbb{R}_{\geq 0} \times \mathbb{Z}_{\geq 0}$ is a *hybrid time domain*, if there is a non-decreasing sequence of non-negative reals $(t_j)_{j=0}^m$, $m \in \mathbb{Z}_{\geq 0} \cup \{\infty\}$, $t_0 = 0$, $t_m \in \mathbb{R}_{\geq 0} \cup \{\infty\}$, such that $A = \cup_{j=1}^m (I_j \times \{j-1\})$, where all the I_j, $j < m$ are of the form $[t_{j-1}, t_j]$, and I_m is of the form[1] $[t_{m-1}, t_m]$ or $[t_{m-1}, t_m)$ when $m < \infty$. Let $(t_j)_{j=0}^m$ denote the *jump sequence* of the time domain A. A *hybrid arc* ϕ is a function $\phi : \operatorname{dom}\phi \to \mathbb{R}^n$, where (1) $\operatorname{dom}\phi \subset \mathbb{R}_{\geq 0} \times \mathbb{Z}_{\geq 0}$ is a hybrid time domain with jump

[1] Note $t_m = \infty$ is allowed when $m < \infty$; for $m = \infty$ there is no t_m.

sequence $(t_j)_{j=0}^m$; and (2) ϕ is a locally absolutely continuous function of I_j, for every j. A *solution* of $\mathcal{H}$ is a hybrid arc ϕ such that, for all $j > 0$, (1) $\phi(t, j-1) \in C$ for almost all $t \in [t_{j-1}, t_j]$, and $\dot{\phi}(t, j-1) = f(\phi(t, j-1))$ for almost all $t \in I_j$ (the *flow condition*); and (2) $\phi(t_{j-1}, j-1) \in D$ and $\phi(t_{j-1}, j) \in G(\phi(t_{j-1}, j-1))$ (the *jump condition*). A solution ϕ to $\mathcal{H}$ is called *maximal* if ϕ cannot be extended, that is: if ψ is a solution with $\operatorname{dom}\phi \subseteq \operatorname{dom}\psi$, which coincides with ϕ on $\operatorname{dom}\phi$, then $\psi = \phi$. A solution ϕ is called *complete* if $\operatorname{dom}\phi$ is unbounded.

Definition 5.1. A solution ϕ of $\mathcal{H}$ is said to be t*-complete* if the sequence (t_j) is unbounded.[2]

5.3 Problem Formulation and Controller Design

Consider a cooperative MAS composed of $N \in \mathbb{Z}_{>0}$ agents indexed by a set $\mathcal{V}$, with states $x_p \in \mathbb{R}^n$, $p \in \mathcal{V}$. Any two agents $p, q \in \mathcal{V}$ are capable of exchanging information with each other whenever the distance between them does not exceed $R > 0$. Then, the possible connections among the agents are encoded by the R-threshold graph $\mathcal{G}_R(\mathbf{x})$. For each $p \in \mathcal{V}$, the model of agent p is a fully actuated single integrator, $\dot{x}_p = u_p$, where $u_p \in \mathbb{R}^n$ denotes a control input.

Assumption 5.1. The initial R-threshold graph, $\mathcal{G} \triangleq \mathcal{G}_R(\mathbf{x}(0))$, is connected, and every edge pq in $\mathcal{E} \triangleq \mathcal{E}_R(\mathbf{x}(0))$ satisfies $\|x_p - x_q\| < R$.

Assumption 5.2. For each $p \in \mathcal{V}$ and $q \in \mathcal{N}_p$, agent p is capable of measuring $x_p - x_q$ for all $t \geq 0$.

Definition 5.2. Let $\nu > 0$. The MAS is in a state of ν-approximate rendezvous if $\|x_p - x_q\| \leq \nu$ for all $p, q \in \mathcal{V}$.

A distributed controller is developed for driving the MAS to ν-approximate rendezvous while maintaining the initial graph structure throughout the process, in the

[2] Clearly, a t-complete solution is complete.

sense that $\mathcal{E} \subseteq \mathcal{E}_R(\mathbf{x}(t))$ holds for all $t \geq 0$. The developed controller limits communications and/or sensing to edges of the graph $\mathcal{G}$ to remove the need for continual monitoring of their R-neighborhood. Instead, each agent can rely on peer-to-peer communication with a fixed set of neighbors that was established at time $t = 0$, as long as this communication can be guaranteed. In addition, any properties of the communication graph, such as the spectrum of $\mathbf{L}_{\mathcal{G}}$, may be computed in advance at time $t = 0$.

5.3.1 Potential Functions

Inspired by [54], edge-potentials are employed to preserve the edges of configurations $\mathbf{x}$, which support a given graph $\mathcal{G} = (\mathcal{V}, \mathcal{E})$ in the sense that $\mathcal{E} \subseteq \mathcal{E}_R(\mathbf{x})$. Let $r : \mathbb{R}_{\geq 0} \to \mathbb{R}_{\geq 0}$ be a non-decreasing continuous function with $r(0) > 0$. Furthermore, let $P : \mathbb{R}_{\geq 0} \to \mathbb{R}_{\geq 0}$ be given by

$$P(\rho) \triangleq \int_0^\rho r(s)sds, \quad \rho \in \mathbb{R}_{\geq 0}. \tag{5–2}$$

The potential $V_{pq} : \texttt{Conf}(\mathcal{V}) \to \mathbb{R}_{\geq 0}$ for each $pq \in \mathcal{E}$ is

$$V_{pq}(\mathbf{x}) \triangleq P\left(\|x_p - x_q\|\right) \,,\; w_{pq} \triangleq r\left(\|x_p - x_q\|\right), \tag{5–3}$$

noting $V_{pq} = V_{qp}$, and that $w \triangleq [w_{pq}] \in \mathbb{R}_{\geq 0}^{\mathcal{V}\times\mathcal{V}}$ is a state-dependent symmetric matrix. The function r is specified as follows. First, $\varepsilon \in \mathbb{R}$ is selected so that $\widetilde{R} \triangleq R(1-\varepsilon)$ satisfies

$$R > \widetilde{R} > \tfrac{2}{3}R \;\Leftrightarrow\; \tfrac{1}{3} > \varepsilon > 0. \tag{5–4}$$

Next, let $\mu, \omega > 0$, and let $r(s)$ be selected as

$$r(s) \triangleq \mu \cdot \begin{cases} 1, & s \in [0, \widetilde{R}] \\ 1 + \omega(s^2 - \widetilde{R}^2), & s \in [\tilde{R}, R] \\ 1 + \omega(R^2 - \widetilde{R}^2), & s \geq R. \end{cases} \tag{5–5}$$

After some algebra, one can obtain

$$\omega \geq \frac{2\,|\mathcal{E}|\,(1-\varepsilon)^2}{R^2\varepsilon^2(2-\varepsilon)^2} \implies |\mathcal{E}|\,P(\widetilde{R}) \leq P(R). \tag{5–6}$$

Selecting ω according to (5–6) is required for graph maintenance (see Theorem 5.1). As in [54, Proposition 3.2], $\widetilde{R}$ plays the role of a safe communication distance below which the edge potential is the usual square of the distance. The goal is to prove that the initial graph will be preserved if all its edges are initially safe. However, our design differs from those considered in [54] in that r ramps up quadratically in the unsafe zone $[\widetilde{R}, R]$, whereas the latter are either held constant or grow linearly there, which results in lower bounds on the buffer: $\varepsilon \geq 1 - |\mathcal{E}|^{-1/2}$ for constant r and $\varepsilon \geq 1 - (\frac{2}{3|\mathcal{E}|-1})^{1/3}$ for linearly growing r. In contrast, our design enables the selection of a small enough ε at initialization.

5.3.2 Hybrid Controller and Closed-Loop Dynamics

Let $\mathcal{X} \triangleq \mathtt{Conf}(\mathcal{V}) \times \mathtt{Conf}(\mathcal{V}) \times [0,\infty)^{\mathcal{V}}$ denote the *extended configuration space* of the MAS. The controller of agent $p \in \mathcal{V}$ is designed as $u_p \triangleq \eta_p$, where $\eta_p \in \mathbb{R}^n$, $\tau_p \in \mathbb{R}$ are auxiliary variables subject to the following closed-loop dynamics:

$$\mathcal{H}\colon \begin{cases} \dot{x}_p = \eta_p, & \\ \dot{\tau}_p = 1,\ \dot{\eta}_p = 0_n, & \mathbf{T}_p(\boldsymbol{\xi}) > 0 \\ \tau_p^+ = 0,\ \eta_p^+ = \displaystyle\sum_{q\in\mathcal{N}_p} w_{pq}\,(x_q - x_p)\,, & \mathbf{T}_p(\boldsymbol{\xi}) = 0, \end{cases} \tag{5–7}$$

where:

1. $\boldsymbol{\xi} \triangleq [\mathbf{x}^\top, \boldsymbol{\eta}^\top, \boldsymbol{\tau}^\top]^\top \in \mathcal{X}$, $\boldsymbol{\eta} \triangleq (\eta_p)_{p\in\mathcal{V}} \in \mathtt{Conf}(\mathcal{V})$ denotes the stacked vector of auxiliary variables η_p, and $\boldsymbol{\tau} \triangleq (\tau_p)_{p\in\mathcal{V}} \in [0,\infty)^{\mathcal{V}}$ is a vector of *personal clocks*, each of which resets whenever the agent triggers, i.e., $\mathbf{T}_p = 0$.
2. The *triggers*, $\mathbf{T}_p\colon \mathcal{X} \to \mathbb{R}$, $p \in \mathcal{V}$ are continuous functions satisfying $\mathbf{T}_p(\boldsymbol{\xi}^+) > 0$ for all $p \in \mathcal{V}$ whenever $\mathbf{T}_q(\boldsymbol{\xi}) = 0$ for *any* $q \in \mathcal{V}$,

and where it is understood that $x_p^+ = x_p$, $\eta_p^+ = \eta_p$ and $\tau_p^+ = \tau_p$ hold for any jump not triggered by the jump condition of agent p. All functions of $\mathbf{x}$ will be regarded as functions of $\boldsymbol{\xi}$. Also, for any particular value of $\boldsymbol{\xi}$, the projection of $\boldsymbol{\xi}$ to the first component of $\mathcal{X}$ is denoted by $\mathbf{x}(\boldsymbol{\xi})$. Since the $\mathbf{T}_p$ are continuous, the sets

$$C \triangleq \bigcap_{p\in\mathcal{V}} [\mathbf{T}_p > 0] \ , \ D \triangleq \overline{C} \cap \bigcup_{p\in\mathcal{V}} [\mathbf{T}_p = 0] \ , \tag{5–8}$$

—the flow and jump sets of $\mathcal{H}$—are open and closed[3] , respectively, with $\overline{C} \subseteq C \cup D$. Both the flow and jump maps are single-valued and continuous, and solutions to the flow equations are global and unique.

Lemma 5.1. *Every initial condition $\phi(0,0) \in \overline{C}$ determines one and only one maximal solution ϕ of the hybrid system $\mathcal{H}$ given in* (5–7)*. Moreover, every maximal solution of $\mathcal{H}$ is either t-complete or Zeno.*

Proof. By [63, Proposition 2.10], and due to the preceding observations, maximal solutions of $\mathcal{H}$ are complete. The condition on the triggers gives $G(D) \subset D^{\complement}$, implying no solution of $\mathcal{H}$ has a pair of consecutive jumps. ■

5.3.3 MAS Control Objective

A configuration $\mathbf{x}$ is a *rendezvous state*, if $x_p = x_q$ for all $p, q \in \mathcal{V}$. The set $\Delta_{\mathcal{V}}$ of all rendezvous states is a linear subspace of $\mathtt{Conf}(\mathcal{V})$. Henceforth, let $\mathbf{x} = \tilde{\mathbf{x}} + \mathbf{x}^{\perp}$ denote the orthogonal decomposition of $\mathbf{x}$ with $\tilde{\mathbf{x}} \in \Delta_{\mathcal{V}}$ and $\mathbf{x}^{\perp} \in \Delta_{\mathcal{V}}^{\perp}$, and let $\Delta\mathbf{x} \triangleq (x_p - x_q)_{pq\in\mathcal{E}}$. It can be shown that:

$$\tilde{\mathbf{x}} = \mathbb{1}_N \otimes \tfrac{1}{N} \textstyle\sum_{p\in\mathcal{V}} x_p, \ \tfrac{1}{\sqrt{N}} \|\mathbf{x}^{\perp}\| \leq \|\Delta\mathbf{x}\|_{\infty} \leq \sqrt{2}\|\mathbf{x}^{\perp}\|. \tag{5–9}$$

[3] Continuous pre-images of open/closed sets are open/closed, respectively.

Achieving rendezvous is equivalent to globally[4] stabilizing the set $\mathcal{R} \triangleq \{\boldsymbol{\xi} \in \mathcal{X} : \|\Delta\mathbf{x}\|_\infty = 0\}$. Moreover, ν-approximate rendezvous is achieved whenever $\|\Delta\mathbf{x}\|_\infty \leq \nu$. Therefore, it suffices to show that every trajectory of $\mathcal{H}$ satisfying Assumption 5.1 is eventually contained in the set

$$\mathcal{R}_\nu \triangleq \{\boldsymbol{\xi} \in \mathcal{X} : \|\Delta\mathbf{x}\|_\infty \leq \nu\}. \tag{5–10}$$

In addition, the maintenance of the initial communication graph is required. To this end, if $\mathcal{G} = (\mathcal{V}, \mathcal{E})$ is a connected graph, for any $\rho > 0$, let

$$\mathcal{C}_\rho(\mathcal{G}) \triangleq \{\boldsymbol{\xi} \in \mathcal{X} : \mathcal{E} \subseteq \mathcal{E}_\rho(\mathbf{x})\}, \tag{5–11}$$

and note Assumption 5.1 means $\boldsymbol{\xi}(0) \in \operatorname{int}(\mathcal{C}_R(\mathcal{G}))$. Given an initial configuration $\mathbf{x}(0)$ satisfying Assumption 5.1, the initial condition $\boldsymbol{\xi}(0) = \phi(0,0)$ is set to satisfy

$$\phi(0,0) = (\mathbf{x}(0), (\mathbf{L}_w \otimes I_n)\mathbf{x}(0), 0), \tag{5–12}$$

and a controller is provided—that is, the values of ε, μ, ω are determined—to guarantee $\boldsymbol{\xi}(t) \in \mathcal{C}_R(\mathcal{G})$ for all $t \geq 0$, for the corresponding maximal solution ϕ of $\mathcal{H}$.

5.4 Graph Maintenance and t-Completeness

The edge weights w_{pq} in (5–3) give rise to the weighted graph Laplacian matrix of the MAS, $\mathbf{L}_w$, defined in Section 5.1, using the weights w_{pq} introduced in (5–3). Set

$$\boldsymbol{\zeta} \triangleq -(\mathbf{L}_w \otimes I_n)\,\mathbf{x} - \boldsymbol{\eta}. \tag{5–13}$$

Writing $\boldsymbol{\zeta} = (\zeta_p)_{p\in\mathcal{V}} \in \mathtt{Conf}(\mathcal{V})$, observe that

$$\zeta_p = \textstyle\sum_{q\in\mathcal{N}_p} w_{pq}\,(x_q - x_p) - \eta_p \tag{5–14}$$

[4] Over the space of configurations with connected communication graphs.

is the error between the instantaneous consensus term over $\mathcal{N}_p$ and the sampled consensus term for agent p.

Definition 5.3. Let $\mathbf{T}_p \colon \mathcal{X} \to \mathbb{R}$, $p \in \mathcal{V}$ be a continuously differentiable function, let $\sigma \in (0, 1]$, and let

$$f_p(\boldsymbol{\xi}) \triangleq \|\eta_p\|^2 - \|\zeta_p\|^2 + \sigma K \widetilde{R}^2 \,, \; K \triangleq \tfrac{\lambda_2^2(\mathcal{G})\mu^2}{2N}. \tag{5–15}$$

$\mathbf{T}_p$ is an *admissible trigger*, if $\mathbf{T}_p \leq f_p$ throughout $\mathcal{X}$ and there exist $\mathfrak{h}, \mathfrak{m} > 0$ such that (a) $\mathbf{T}_p(\boldsymbol{\xi}^+) \geq \mathfrak{h}$ at each jump of $\mathcal{H}$; and (b) $\frac{\mathrm{d}}{\mathrm{d}t}\mathbf{T}_p \geq -\mathfrak{m}$ holds along any solution of $\mathcal{H}$.

Note that admissibility implies agent p must update η_p at some time earlier than dictated by the condition $f_p \leq 0$, which is only state-dependent (and not time-dependent). Also, the parameter σ, to be determined later, allows the user to control the degree of rendezvous approximation (see Theorem 5.2).

Theorem 5.1. *Given $\widetilde{R} = R(1-\varepsilon)$ satisfying* (5–4) *and a connected graph $\mathcal{G}$, if $\{\mathbf{T}_p\}_{p\in\mathcal{V}}$ is a collection of admissible triggers, then every solution of $\mathcal{H}$ satisfying* (5–12) *and initiating from $\mathcal{C}_{\widetilde{R}}(\mathcal{G})$ remains in $\mathcal{C}_R(\mathcal{G})$, is t-complete, and the controllers u_p are bounded for all time.*

Proof. Using (5–3), define the *total potential* $V_{\mathcal{G}} \colon \mathcal{X} \to \mathbb{R}_{\geq 0}$ as

$$V_{\mathcal{G}}(\boldsymbol{\xi}) \triangleq \sum_{p\in\mathcal{V}} \sum_{q\in\mathcal{N}_p} V_{pq}(\mathbf{x}) = 2 \sum_{pq\in\mathcal{E}} V_{pq}(\mathbf{x}). \tag{5–16}$$

Note that $V_{\mathcal{G}}(\boldsymbol{\xi}) = 0$ for $\boldsymbol{\xi} \in \mathcal{R}$ and $V_{\mathcal{G}}(\boldsymbol{\xi}) > 0$ otherwise. Let $\phi : \operatorname{dom}\phi \to \mathcal{X}$ be a solution of $\mathcal{H}$ with initial condition $\phi(0,0) \in \mathcal{C}_{\widetilde{R}}(\mathcal{G})$. With a slight abuse of notation, let $\boldsymbol{\xi} = \phi(t,j)$ for $(t,j) \in \operatorname{dom}\phi$. First, it will be shown that $\dot{V}_{\mathcal{G}}(\boldsymbol{\xi}) \leq 0$ whenever $\|x_p - x_q\| \geq \widetilde{R}$ for some $pq \in \mathcal{E}$. During flows, the change in $V_{\mathcal{G}}$ is given by $\dot{V}_{\mathcal{G}}(\boldsymbol{\xi}) = \langle \nabla V_{\mathcal{G}}(\boldsymbol{\xi}), F(\boldsymbol{\xi})\rangle$, where F is the flow map of $\mathcal{H}$. It is known [53, Section 7.2] that $\nabla V_{\mathcal{G}}(\boldsymbol{\xi}) = 2(\mathbf{L}_w \otimes I_n)\mathbf{x}$ follows from (5–3). Therefore, substituting (5–13) yields

$$\begin{aligned}\dot{V}_{\mathcal{G}}(\boldsymbol{\xi}) &= 2\mathbf{x}^\top (\mathbf{L}_w \otimes I_n)^\top \boldsymbol{\eta} \\ &= -2\mathbf{x}^\top \left(\mathbf{L}_w^2 \otimes I_n\right)\mathbf{x} - 2\mathbf{x}^\top (\mathbf{L}_w \otimes I_n)\,\boldsymbol{\zeta}.\end{aligned}$$

Splitting the leading term and applying (5–13) twice yields

$$\begin{aligned}\dot{V}_{\mathcal{G}}(\boldsymbol{\xi}) &= -\mathbf{x}^\top \left(\mathbf{L}_w^2 \otimes I_n\right)\mathbf{x} - \|\boldsymbol{\zeta}\|^2 - \|\boldsymbol{\eta}\|^2 - 2\boldsymbol{\eta}^\top\boldsymbol{\zeta} - 2\mathbf{x}^\top\left(\mathbf{L}_w \otimes I_n\right)\boldsymbol{\zeta} \\ &= -\mathbf{x}^\top \left(\mathbf{L}_w^2 \otimes I_n\right)\mathbf{x} - \|\boldsymbol{\zeta}\|^2 - \|\boldsymbol{\eta}\|^2 - 2(\boldsymbol{\eta} + \left(\mathbf{L}_w \otimes I_n\right)\mathbf{x})^\top\boldsymbol{\zeta} \\ &= -\mathbf{x}^\top \left(\mathbf{L}_w^2 \otimes I_n\right)\mathbf{x} - \|\boldsymbol{\eta}\|^2 + \|\boldsymbol{\zeta}\|^2.\end{aligned} \tag{5–17}$$

By (5–3) and (5–5), $w_{pq} \geq \mu$ for all $pq \in \mathcal{E}$, which implies $\lambda_2(\mathbf{L}_w) \geq \mu\lambda_2(\mathcal{G})$. Together with (5–9), this yields

$$\begin{aligned}\dot{V}_{\mathcal{G}}(\boldsymbol{\xi}) &\leq -\lambda_2^2\left(\mathcal{G}\right)\mu^2\|\mathbf{x}^\perp\|^2 - \|\boldsymbol{\eta}\|^2 + \|\boldsymbol{\zeta}\|^2 \\ &\leq -\left(NK\|\Delta\mathbf{x}\|_\infty^2 + \|\boldsymbol{\eta}\|^2 - \|\boldsymbol{\zeta}\|^2\right).\end{aligned} \tag{5–18}$$

Using $\|\Delta\mathbf{x}\|_\infty \geq \widetilde{R}$, $\sigma K\widetilde{R}^2 \leq K\widetilde{R}^2$, and (5–15), one can obtain

$$\begin{aligned}\dot{V}_{\mathcal{G}}(\boldsymbol{\xi}) &\leq -\textstyle\sum_{p\in\mathcal{V}}(\sigma K\widetilde{R}^2 + \|\eta_p\|^2 - \|\zeta_p\|^2) \\ &\leq -\textstyle\sum_{p\in\mathcal{V}} f_p(\boldsymbol{\xi}) \leq -\sum_{p\in\mathcal{V}}\mathbf{T}_p(\boldsymbol{\xi}) \leq 0\end{aligned} \tag{5–19}$$

by the admissibility of the $\mathbf{T}_p$ and since all the $\mathbf{T}_p$ are non-negative during flows.

The maintenance of the edges of $\mathcal{G}$ is now shown. Proceeding by contradiction, let $(s_1, j_1) \in \operatorname{dom}\phi$ be a point with $\phi(s_1, j_1) \notin \mathcal{C}_R(\mathcal{G})$, and let

$$(s_0, j_0) \triangleq \sup\left\{(t,j) \in \operatorname{dom}\phi\colon (t,j) \leq (s_1, j_1),\ \phi(t,j) \in \mathcal{C}_{\widetilde{R}}(\mathcal{G})\right\}, \tag{5–20}$$

using the order on $\mathbb{R}^2$ given by $\mathbf{a} \leq \mathbf{b} \ \Leftrightarrow\ \mathbf{b} - \mathbf{a} \in \mathbb{R}^2_{\geq 0}$. Since $\operatorname{dom}\phi$ is closed in $\mathbb{R}^2$ under this order, $(s_0, j_0) \in \operatorname{dom}\phi$. Let $V_1 \triangleq V_{\mathcal{G}}(\phi(s_1, j_1))$ and $V_0 \triangleq V_{\mathcal{G}}(\phi(s_0, j_0))$. Also, note $j_0 \leq j_1$ and $s_0 \in [t_{j_0}, t_{j_0+1})$. Since $\mathbf{x}(\phi(t_{j+1}, j)) = \mathbf{x}(\phi(t_{j+1}, j+1))$ for all $j \geq 0$, the expression $\mathbf{z}(t) \triangleq \mathbf{x}(\phi(t,j))$ is a well-defined function of $t \in J \triangleq [s_0, s_1]$. Moreover, it is C^1-smooth at every $t \in J$ except for the points $t = t_j$, $j_0 \leq j \leq j_1$. Since $V_{\mathcal{G}}$ is a C^1-function of $\mathbf{x}$, the function $v(t) \triangleq V_{\mathcal{G}}(\mathbf{z}(t))$ is C^1-smooth at every $t \in J$ except for the points $t = t_j$, $j_0 \leq j \leq j_1$. Therefore, $V_1 - V_0 = v(s_1) - v(s_0) = \int_{s_0}^{s_1}\dot{v}(t)\mathrm{d}t$. Since $\phi(t,j) \notin \mathcal{C}_{\widetilde{R}}(\mathcal{G})$ for $t \in (s_0, s_1]$, the integrand is non-positive by (5–19), which results in $V_1 \leq V_0$. Since $\mathbf{x}$ evolves continuously with t and $\mathcal{C}_{\widetilde{R}}(\mathcal{G})$ is closed, one has that $\phi(s_0, j_0) \in \mathcal{C}_{\widetilde{R}}(\mathcal{G})$.

Therefore, by (5–6) and (5–16), $V_0 = 2\sum_{pq\in\mathcal{E}} V_{pq}(\phi(s_0, j_0)) \leq 2\,|\mathcal{E}|\,P(\widetilde{R}) \leq 2P(R)$. Since $\mathbf{x}(s_1)$ has at least one edge of length greater than R, $V_0 \leq 2P(R) < V_1$—contradiction. To prove the second assertion of the theorem, the t-completeness of a maximal solution ϕ is verified. By Lemma 5.1, a maximal solution $\phi : \operatorname{dom}\phi \to \mathcal{X}$ of $\mathcal{H}$ is either eventually continuous—in which case it is t-complete (and we are done)—or it has an infinite sequence of jump times t_j, $j \in \mathbb{Z}_{\geq 0}$. For each $p \in \mathcal{V}$, let J_p denote the set of indices $j > 0$ satisfying $\mathbf{T}_p(\phi(t_j, j-1)) = 0$, with the addition of the index $j = 0$. Fix a $p \in \mathcal{V}$ such that J_p is infinite, and denote the *hybrid jump times* $(t_j, j-1)$, $j \in J_p$ as $((t_i^p, j_i^p - 1))_{i=1}^{\infty}$, in increasing order. Also, let $t_0^p \triangleq 0$. Then, by Lemma 5.1, it suffices to find $\delta > 0$ such that $t_{i+1}^p - t_i^p \geq \delta$ for all $i \geq 0$. For each $i \geq 1$, $\mathbf{T}_p(\phi(t_i^p, j_i^p - 1)) = 0$ and $\mathbf{T}_p(\phi(t_i^p, j_i^p)) \geq \mathfrak{h}$ by Definition 5.3(a). Moreover, the continuity of $\mathbf{T}_p(\phi(t, j))$ during flows implies $t_{i+1}^p - t_i^p > 0$. Claim: $\delta = \mathfrak{h}/\mathfrak{m}$ satisfies our needs. Proceeding by contradiction, assume $t_{i+1}^p - t_i^p < \delta$. Substituting $\boldsymbol{\xi} = \phi(t_{i+1}^p, j_i^p)$ into $\mathbf{T}_p$, together with the continuity of $\dot{\mathbf{T}}_p(\phi(s, j_i^p))$ over all but finitely many $s \in [t_i^p, t_{i+1}^p]$, produces

$$\mathbf{T}_p(\boldsymbol{\xi}) = \int_{t_i^p}^{t_{i+1}^p} \dot{\mathbf{T}}_p(\phi(s, j_i^p))\mathtt{d}s \geq \mathfrak{h} - \mathfrak{m}\left(t_{i+1}^p - t_i^p\right) > 0, \tag{5–21}$$

contradicting the fact that $\boldsymbol{\xi}$ is a jump point for agent p. Finally, since $\|\Delta\mathbf{x}\|_\infty \leq R$ for all time, one can see that $w_{pq} \leq r(R)$ by (5–3), and $\|u_p\| = \|\eta_p\| \leq \Delta(\mathcal{G})Rr(R)$ by (5–5), for each $pq \in \mathcal{E}$ and $p \in \mathcal{V}$—hence bounded. ■

5.5 Stability Analysis

Theorem 5.2. *Let $\nu > 0$, $\widetilde{R} = R(1-\varepsilon)$ satisfy* (5–4)*, and $\mathcal{G}$ be a connected graph. Suppose $0 < \beta \leq \sigma K\widetilde{R}^2$ and $\{\mathbf{T}_p\}_{p\in\mathcal{V}}$ is a collection of admissible triggers such that, over solutions of $\mathcal{H}$ satisfying* (5–12) *and initiating from $\mathcal{C}_{\widetilde{R}}(\mathcal{G})$,*

$$\mathbf{T}_p + \sigma K\widetilde{R}^2 \leq f_p + \beta \tag{5–22}$$

holds for all $p \in \mathcal{V}$. Then, any such solution satisfies

$$\|\Delta\mathbf{x}(t)\|_\infty^2 \leq \tfrac{r(R)|\mathcal{E}|}{r(0)} \left(\|\Delta\mathbf{x}(0)\|_\infty^2 \, e^{-\frac{NKt}{r(R)|\mathcal{E}|}} + \sigma \widetilde{R}^2 \right). \tag{5–23}$$

In this sense, $\mathcal{R}_\nu$ is exponentially stable[5] *for $\sigma = \frac{\nu^2}{|\mathcal{E}|\widetilde{R}^2} \cdot \frac{r(0)}{r(R)}$. In particular, ν'-approximate rendezvous is achieved for every such maximal solution, for any $\nu' > \nu$.*

Proof. Let $\phi : \operatorname{dom}\phi \to \mathcal{X}$ be a maximal solution of $\mathcal{H}$ with initial condition $\phi(0,0) \in \mathcal{C}_{\widetilde{R}}(\mathcal{G})$. By Theorem 5.1, ϕ is t-complete. Consider the same total potential $V_\mathcal{G}(\boldsymbol{\xi})$ defined in (5–16). Using (5–2), (5–3), (5–5), and (5–16), $V_\mathcal{G}$ can be bounded as

$$r(0)\|\Delta\mathbf{x}\|^2 \leq V_\mathcal{G}(\boldsymbol{\xi}) \leq r(R)\|\Delta\mathbf{x}\|^2. \tag{5–24}$$

By (5–22), $\|\eta_p\|^2 - \|\zeta_p\|^2 \geq -\beta + \mathbf{T}_p$. Then, (5–18) yields

$$\begin{aligned} \dot{V}_\mathcal{G}(\boldsymbol{\xi}) &\leq -NK\|\Delta\mathbf{x}\|_\infty^2 - \textstyle\sum_{p\in\mathcal{V}} (-\beta + \mathbf{T}_p) \\ &\leq -NK\|\Delta\mathbf{x}\|_\infty^2 + N\beta. \end{aligned} \tag{5–25}$$

Combining (5–24) with $\|\Delta\mathbf{x}\| \leq \sqrt{|\mathcal{E}|}\|\Delta\mathbf{x}\|_\infty$ implies $V_\mathcal{G}(\boldsymbol{\xi}) \leq r(R)\,|\mathcal{E}|\,\|\Delta\mathbf{x}\|_\infty^2$. Then, (5–25) can be upper bounded as

$$\dot{V}_\mathcal{G}(\boldsymbol{\xi}) \leq -\tfrac{NK}{r(R)|\mathcal{E}|} V_\mathcal{G}(\boldsymbol{\xi}) + N\beta. \tag{5–26}$$

Since $V_\mathcal{G}$ only depends on $\mathbf{x}$ (5–16), and $\mathbf{x}$ evolves continuously under $\mathcal{H}$, $V_\mathcal{G}$ evolves continuously as well. By Theorem 5.1, $\dot{V}_\mathcal{G}(\boldsymbol{\xi})$, $\boldsymbol{\xi} = \phi(t,j)$ has only finitely many discontinuities in any bounded sub-interval of $\operatorname{dom}\phi$. Therefore, integrating (5–26) and recalling that $\beta \leq \sigma K \widetilde{R}^2$ yields

$$V_\mathcal{G}(\phi(t,j)) \leq V_\mathcal{G}(\phi(0,0))\mathrm{e}^{-\frac{NKt}{r(R)|\mathcal{E}|}} + \sigma r(R)\,|\mathcal{E}|\,\widetilde{R}^2, \tag{5–27}$$

[5] Recalling (5–9), Equation (5–23) implies the exponential stability of the ν-neighborhood of $\Delta_\mathcal{V}$ with respect to $\|\cdot\|$, in the same restricted sense.

where using the bounds of $V_{\mathcal{G}}$ in (5–24) and $\|\Delta\mathbf{x}\|_\infty \leq \|\Delta\mathbf{x}\| \leq \sqrt{|\mathcal{E}|}\|\Delta\mathbf{x}\|_\infty$ produces (5–23) for any $(t, j) \in \text{dom } \phi$. ■

5.6 Trigger Design

Lemma 5.2. *Let $\widetilde{R}, r, \omega$ satisfy the requirements in Section 5.3.1, and let $\mathcal{G}$ be a connected graph. If $\{\mathbf{T}_p\}_{p\in\mathcal{V}}$ is a collection of admissible triggers and ϕ is a solution of $\mathcal{H}$ with $\phi(0,0) \in \mathcal{C}_{\widetilde{R}}(\mathcal{G})$ satisfying* (5–12)*, then the following holds over every flow interval of agent p:*

$$\|\zeta_p(\phi(t,j))\| \leq Z\tau_p(\phi(t,j)), \tag{5–28}$$

where $Z \triangleq 2\Delta(\mathcal{G})\left(\mu\omega R^2 + \Delta(\mathcal{G})Rr(R)^2\right)$.

Proof. Using the notation from the proof of Theorem 5.1, consider any $t \in [t_i^p, t_{i+1}^p]$. By (5–7), η_p is constant over the interval $[t_i^p, t_{i+1}^p] \times \{j_i^p\} \subset \text{dom}\,\phi$. Furthermore, Theorem 5.1 and Equations (5–3)–(5–5) imply $\|x_p - x_q\| \leq R$ and $|w_{pq}| \leq r(R)$ for all $q \in \mathcal{N}_p$, respectively. It then follows that

$$\|\eta_p\| \leq d_p Rr(R) \leq \Delta(\mathcal{G})Rr(R). \tag{5–29}$$

Taking the time derivative of ζ_p over $[t_i^p, t_{i+1}^p] \times \{j_i^p\}$ yields

$$\dot{\zeta}_p = \textstyle\sum_{q\in\mathcal{N}_p} \dot{w}_{pq}(x_q - x_p) + \sum_{q\in\mathcal{N}_p} w_{pq}(\eta_q - \eta_p). \tag{5–30}$$

From (5–5), it follows that $\dot{w}_{pq}(s) = 0$ for $s \in [0, \widetilde{R}]$, and $\dot{w}_{pq}(s) = 2\mu\omega s\dot{s}$ for $s \in [\widetilde{R}, R]$. Therefore, $\|\dot{w}_{pq}\| \leq 2\mu\omega R$ because $\dot{s}$ is a unit vector. Combining these bounds with (5–30),

$$\|\dot{\zeta}_p\| \leq 2\mu\omega d_p R^2 + d_p r(R) \cdot 2\Delta(\mathcal{G})Rr(R) \leq Z, \tag{5–31}$$

where Δ_p is the degree of p in $\mathcal{G}$ and $\Delta(\mathcal{G})$ is the maximal degree in $\mathcal{G}$. Over the interval $[t_i^p, t_{i+1}^p] \times \{j_i^p\}$, ζ_p is continuous as a function of t, and differentiable everywhere except

$t = t_j$, $j_i^p \leq j \leq j_{i+1}^p$. Therefore, using $\|\zeta_p(\phi(t_i^p, j_i^p))\| = 0$ one may write:

$$\|\zeta_p(t)\| \leq \int_{t_i^p}^{t} \|\dot{\zeta}_p(s)\| \mathtt{d}s \leq Z\,(t - t_i^p)\,. \tag{5–32}$$

Since $\tau_p = t - t_i^p$ over $[t_i^p, t_{i+1}^p] \times \{j_i^p\}$, $\|\zeta_p(t, j_i^p)\| \leq Z\tau_p$. ■

Corollary 5.1. *The trigger $\mathbf{T}_p = f_p$ is admissible.*

Proof. Clearly, $f_p(\boldsymbol{\xi}^+) \geq \sigma K \widetilde{R}^2$. Also, by Cauchy-Schwartz,

$$\tfrac{\mathtt{d}}{\mathtt{d}t} f_p = -2\zeta_p^\top \dot{\zeta}_p \geq -4\Delta(\mathcal{G}) R r(R) Z,$$

where $\|\zeta_p\| \leq 2\Delta(\mathcal{G}) R r(R)$ and $\|\dot{\zeta}_p\| \leq Z$. ■

Let $0 < \beta \leq \sigma K \widetilde{R}^2$ and $\gamma > 0$. Consider the triggers:

$$\begin{aligned} \mathbf{T}_{p,1}(\boldsymbol{\xi}) &= \|\eta_p\|^2 - \|\zeta_p\|^2 + \alpha(\|\eta_p\|), \\ \mathbf{T}_{p,2}(\boldsymbol{\xi}) &= \|\eta_p\|^2 - Z^2\tau_p^2 + \alpha(\|\eta_p\|), \end{aligned} \tag{5–33}$$

where $\alpha(s) \triangleq \beta - \frac{\beta}{\gamma} s$ for $s \in [0, \gamma]$ and $\alpha(s) = 0$ otherwise.

Remark 5.1. $\mathbf{T}_{p,1}$ is state-based, while $\mathbf{T}_{p,2}$ is a self-trigger.

Corollary 5.2. $\mathbf{T}_{p,1}$ *and* $\mathbf{T}_{p,2}$ *are admissible and satisfy* (5–22)*.*

Proof. $\mathbf{T}_{p,1}$ and $\mathbf{T}_{p,2}$ share the same $\mathfrak{h} \triangleq \min_{s \geq 0}(s^2 + \alpha(s))$. Indeed, $s^2 + \alpha(s)$ coincides with s^2 for $s \geq \gamma$, so, being positive, it has a minimum. By Corollary 5.1, $\mathbf{T}_{p,1}$ is admissible because $\frac{\mathtt{d}}{\mathtt{d}t}\mathbf{T}_{p,1} = \frac{\mathtt{d}}{\mathtt{d}t} f_p$. It also trivially satisfies (5–22). Finally, $\frac{\mathtt{d}}{\mathtt{d}t}\mathbf{T}_{p,2} = -2Z^2\tau_p$, where $Z^2\tau_p^2 \leq \|\eta_p\|^2 + \alpha(\|\eta_p\|)$ with $\|\eta_p\|$ bounded by (5–29). Equation (5–29) holds for $\mathbf{T}_{p,2}$ because $\mathbf{T}_{p,2} \leq \mathbf{T}_{p,1}$ by Lemma 5.2. ■

On first glance, the event trigger $\mathbf{T}_{p,1}$ requires agent p to continuously measure $x_q - x_p$ for each $q \in \mathcal{N}_p$. This could be useful in settings where intermittent actuation is desired and continuous measurements are inexpensive, such as with satellite constellations where power is limited and visual measurements can be made over large distances. For other scenarios, an alternative communication protocol can remove

the need for continuously monitoring the neighbors' states. Recalling that $\dot{x}_p = \eta_p$ is constant over $[t_i^p, t_{i+1}^p)$, observe that $x_p(t) = \eta_p \tau_p + x_p(t_i^p)$ for all $t \in [t_i^p, t_{i+1}^p)$. Under the assumption of instantaneous communication, it suffices for each agent $q \in \mathcal{N}_p$ to broadcast η_q and x_q at each jump time of agent q. Consequently, p can compute ζ_p by using the solution for $x_q(t)$ over the appropriate time interval for each $q \in \mathcal{N}_p$.

5.7 Simulation Example

Putting together the theoretical results, suppose N agents with $\mathbf{x}(0)$ satisfying Assumption 5.1 are given, and $\nu > 0$. At the initial time, $\mathcal{G} = \mathcal{G}_R(\mathbf{x}(0))$, $\lambda_2(\mathcal{G})$, and $|\mathcal{E}|$ are computed. The parameter ε is selected so that $\widetilde{R} > \|\Delta\mathbf{x}(0)\|_\infty$, and ω is selected to satisfy (5–6). For any choice of $\mu, \gamma > 0$, σ is selected according to Theorem 5.2, guaranteeing that *any* collection $\{\mathbf{T}_p\}_{p\in\mathcal{V}}$ of admissible triggers generates a controller driving the MAS to ν'-approximate rendezvous at an exponential rate, uniformly over initial conditions $\phi(0,0) \in \mathcal{C}_{\widetilde{R}}(\mathcal{G})$ satisfying (5–12). Theorem 5.1 guarantees that no edges of $\mathcal{G}$ are broken at any time for any of the above initial conditions.

Figure 5-1 shows the trajectories of a MAS with $N = 9$ agents in the Euclidean plane $\mathbb{R}^2$, randomized initial positions denoted by $\times$'s, and event trigger function $\mathbf{T}_{p,1}$ with the default choice of $\beta = \sigma K \widetilde{R}^2$ for each agent. The communication radius of each agent is $R = 1$. The nodes and edges of the initial graph $\mathcal{G}$ are represented by the $\times$'s and the black-dashed lines, respectively. The graph $\mathcal{G}$ has $|\mathcal{E}| = 20$ and $\lambda_2(\mathcal{G}) = 1.578$. The final configuration (denoted by the $\bullet$'s) is required to be in ν-approximate rendezvous with $\nu = 0.1$. The parameter $\widetilde{R}$ is selected as the length of the longest edge of $\mathcal{G}$ plus the machine epsilon of our computer (10^{-16}), which yields $\widetilde{R} = 0.9392$, corresponding to $\varepsilon = 0.0608$. Then, $\omega = 2541.5$ and $\sigma = 1.8863 \times 10^{-6}$. With the gain $\mu = 1$, approximate rendezvous was achieved within 4 time units. The triggers $\mathbf{T}_{p,1}$ were used with $\beta = 3.8298 \times 10^{-13}$ and γ set to $\gamma = 0.1$. Note how each cusp along an agent's trajectory coincides with a jump time for that agent. Figure 5-2 depicts the consensus error of each agent in the MAS, where the consensus error of agent p is

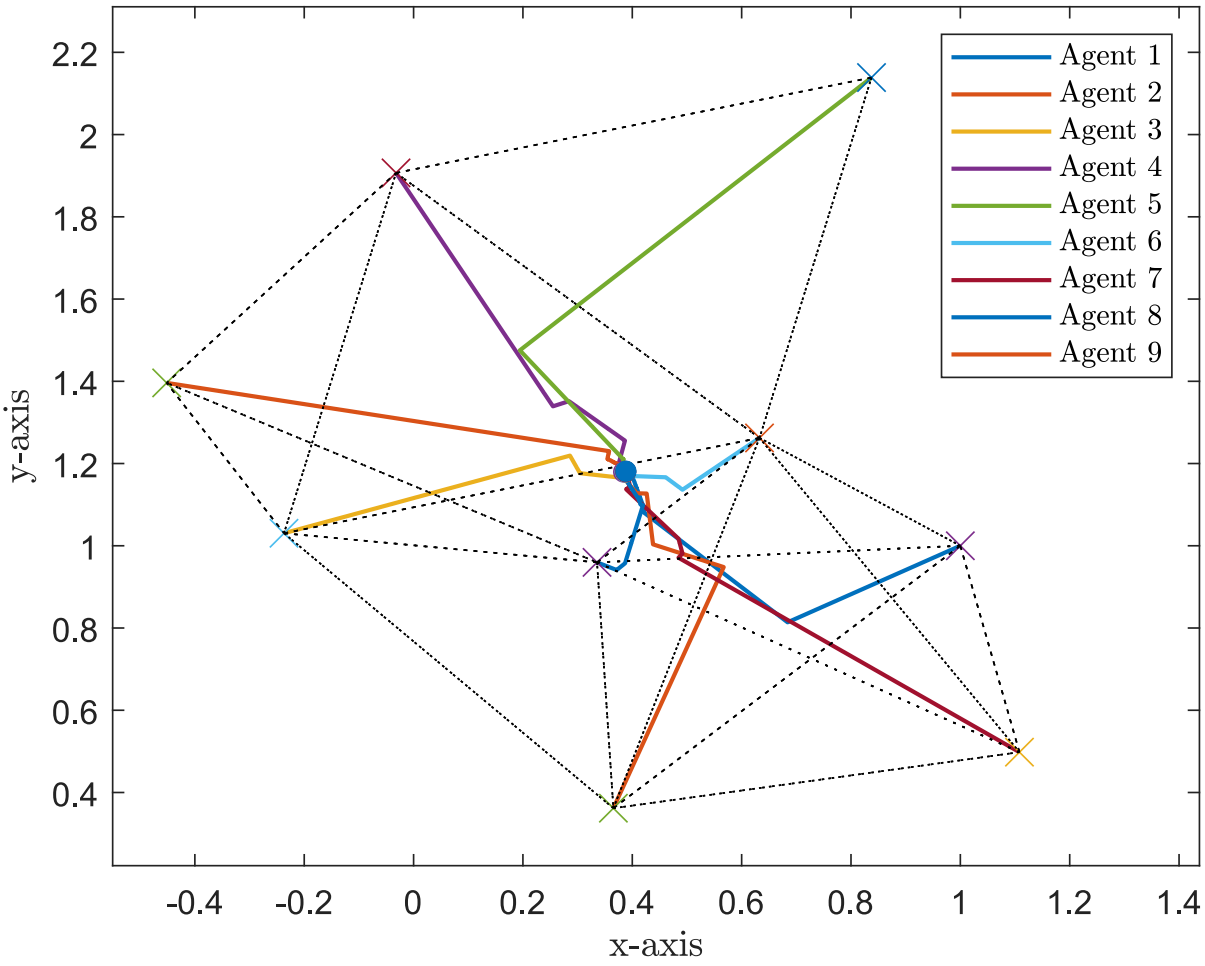

Figure 5-1. Planar trajectories of the simulated MAS and the initial R-threshold communication topology.

given by $e_p = x_p - \frac{1}{N}\sum_{\ell\in\mathcal{V}} x_\ell$. All consensus errors tend to a neighborhood of the origin with a radius of approximately 2×10^{-7}. The event-times, i.e., broadcast times, of each agent are illustrated in Figure 5-3. A blue spike represents a communication event, and a white space represents a period of no communication. The simulation was executed in MATLAB, using [85].

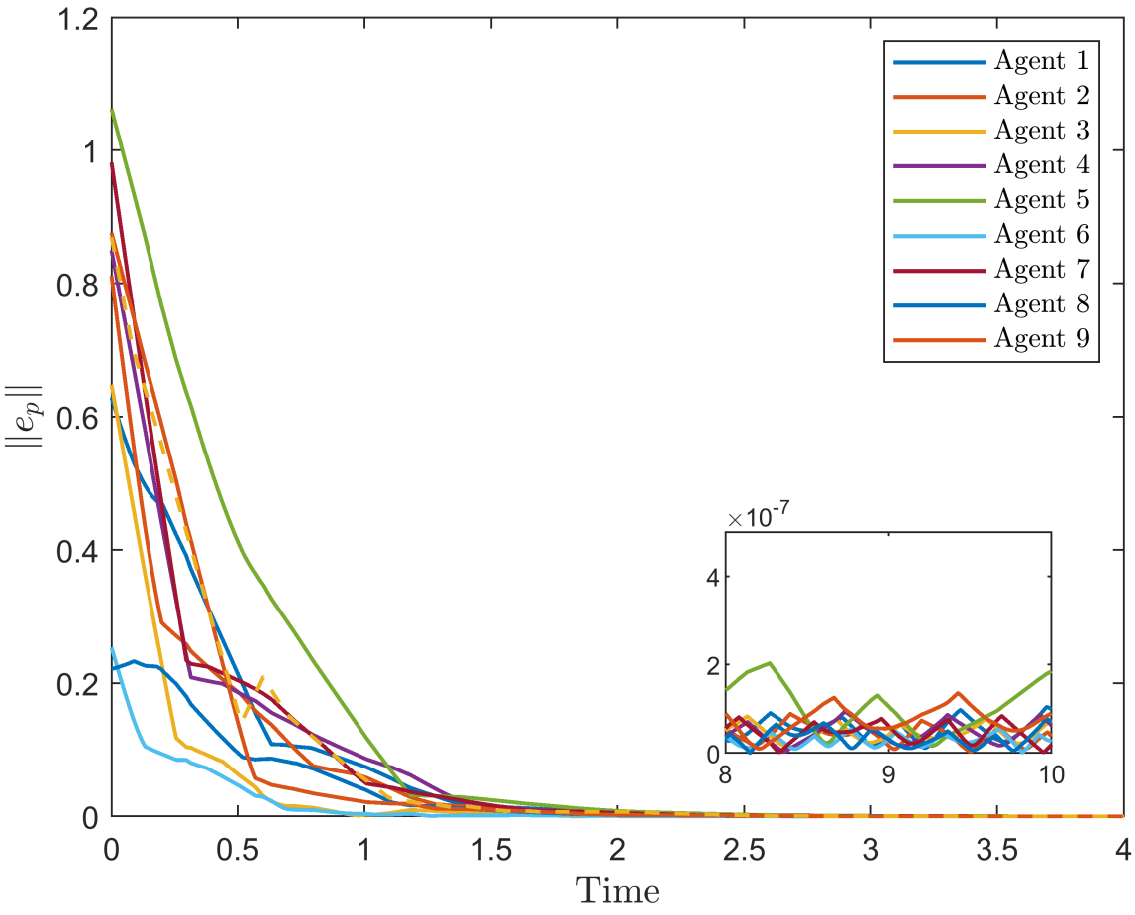

Figure 5-2. Consensus errors of the MAS showing ν-approximate rendezvous.

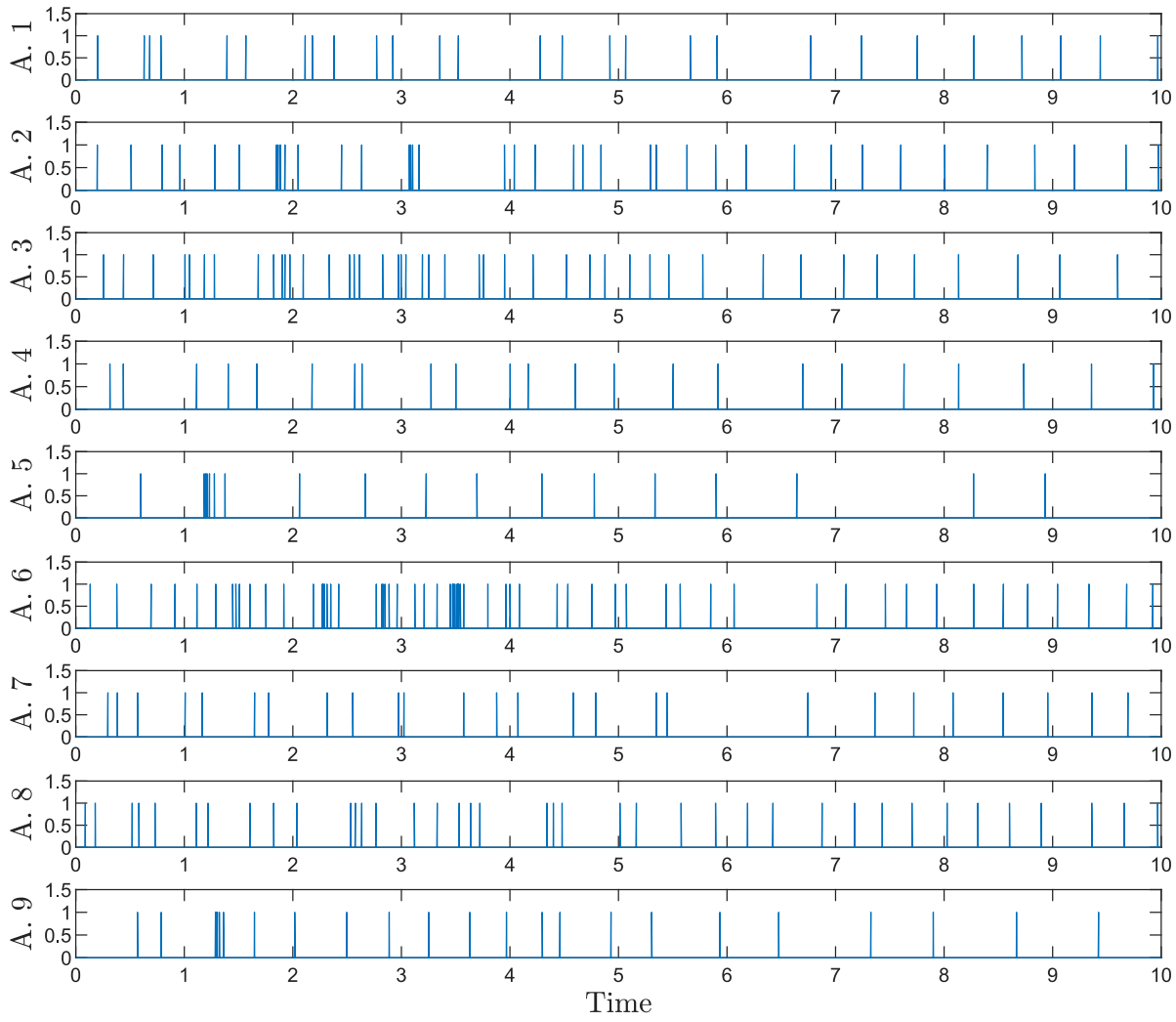

Figure 5-3. Plot of event-times for each agent in the MAS.

CHAPTER 6
CONCLUSIONS

The distributed control of a MAS under intermittent state feedback generates several benefits when compared to alternative control strategies. For example, distributed control can enable a group of cost effective and simple agents to perform complex global behaviors by executing controllers that utilize local information. These desired global behaviors can be readily scaled through the addition of auxiliary agents without incurring unmanageable computational cost. Furthermore, MASs can be partitioned and made to perform a variety of tasks simultaneously, which exemplifies their versatility. Distributed MASs can also be made robust to multiple points of failure (e.g., lost agents and broke communication links) provided the communication network is sufficiently connected. The use of information only when necessary (e.g., intermittently rather than continuously) not only benefits the scalability properties of MASs by reducing the demands on the communication network, but using intermittent information also helps to reduce the energy costs associated with communication. However, distributed MASs operating under intermittent state feedback are especially vulnerable to cyber-attacks, where the injection of inaccurate information can lead to unintended behavior. In addition, several MAS control objectives rely on a communication topology that posses some minimal degree of connectivity for all time. Therefore, the development of control strategies utilizing intermittent state feedback that are robust to cyber-attacks and that can ensure the connectivity of an initially connected distance-based communication network are well motivated.

In Chapter 1, a survey of the literature on the event-triggered control of MASs, Byzantine-resilient network control strategies, the control of clustered MASs, and graph maintenance control methods is presented. Chapter 1 also introduces pertinent notation, elements from graph theory, and the hybrid systems framework of [63]. Event-triggered control, i.e., a state-based trigger strategy, serves as the primary mechanism

by which intermittent state feedback is created in this dissertation (see Chapters 2, 3, and 5). Intermittent state feedback can also be generated through the use of timers, which is shown in Chapter 4.

In Chapter 2, the approximate leader-follower consensus problem in the presence of Byzantine adversaries for a homogeneous MAS is examined. Approximate leader-follower consensus (also known as practical consensus) occurs when the states of a group of followers is driven within a desired distance of the leader's state and remain within such a distance for all future time. Additionally, the homogeneous qualifier refers to a MAS whose agents have identical dynamics. Distributed event- and self-triggered controllers are developed along with a Lyapunov-based detection method that enables followers to discern between cooperative and Byzantine neighbors. Since the agent dynamics are assumed to be known within this chapter, model knowledge is utilized within the Byzantine agent detector. The control strategy can remove the influence from Byzantine agents by altering the interaction topology and enabling consensus for all cooperative followers. Moreover, a time-based estimate for each follower's trigger condition is developed, which allows each follower to estimate the future time when state information from its neighbors will be required. The STC approach alleviates the continuous monitoring requirement of ETC and enables intermittent communication and monitoring. Simulation results demonstrate that both ETC and STC methods enable approximate leader-follower consensus while identifying and mitigating against Byzantine adversaries. Results also show that increased communication leads to better tracking of the leader for both ETC and STC. Moreover, both methods can provide identical tracking performance, but depending on the choice of parameters, one method can provide communication energy savings over the other. Future efforts could focus on generalizing the result to more abstract network topologies, developing more capable and sensitive Byzantine detection and trigger condition estimation methods, and relaxing the network connectivity assumption for the cooperative sub-graph.

Uncertain agent dynamics can be considered, the impact of which could lead to faster divergence rates between the estimated and true follower position and more frequent communication. This strategy only functions for sufficiently connected communication networks. The assumption that the cooperative component of the communication graph remains connected for all time implies that the communication network has a surplus of edges that can be sacrificed without disconnecting the cooperative sub-graph. However, it may not be possible to achieve enough redundancy to ensure the connectivity of the cooperative component given a large number of Byzantine agents. This practical problem motivates the development of control algorithms that can reactively create and delete communication edges to ensure the connectivity of the cooperative sub-graph. Furthermore, if the cooperative agents become divided into multiple isolated but connected components due to the introduction of Byzantine agents or other cyber-attacks, then motivation also exists to develop a control algorithm that can unite the cooperative components.

Chapter 3 examines the formation control while leader tracking problem for a heterogeneous MAS consisting of agents with uncertain nonlinear control-affine dynamics. The heterogeneous qualifier refers to distinct control-affine dynamics between agents. A distributed event-triggered controller is developed along with a reputation-based detection method that enables the cooperative followers to discern between cooperative and Byzantine neighbors, alter the interaction among neighbors to isolate cooperative agents from Byzantine adversaries, and achieve the formation control and leader tracking objective. Once an agent partitions their neighbor set into cooperative and Byzantine subsets through the use of the reputation strategy, the edge weights of Byzantine neighbors are set to zero, which allows the controller to make updates solely based on information from cooperative neighbors. The benefit of the reputation strategy, when compared to the detector in Chapter 2, is that the use of redundant state information enables the

construction of a model-free Byzantine agent detector. Moreover, the decoupling between communication and interaction allows for the admittance of rehabilitated agents into the cooperative component. Like the result in Chapter 2, the proposed strategy is valid under the assumption of a sufficiently connected interaction graph, i.e., edges can be severed to both isolate Byzantine agents and keep the cooperative component connected. Simulation results are presented and show that the strategy can enable a group of cooperative agents to achieve the objective under the use of intermittent state feedback. Future efforts can focus on developing controllers capable of preserving the connectivity of distance-based graphs and constructing adaptive formations. Recall that the relative position vectors used in Chapter 3 to construct the desired formation are fixed, which may be inappropriate in scenarios requiring variable formations, e.g., maneuvering within cities or other environments with obstacles. Furthermore, more sophisticated Byzantine agent detectors that utilize asynchronous sensed and communicated state or output information are motivated. In practice, communicated and sensed information may be obtained at different times, which may prohibit a direct comparison for use in the proposed trust model. However, direct comparisons can be made through synchronous state estimates provided by state observes. While this chapter studies the fundamental case of multiple Byzantine adversaries that act independently, future efforts could examine the case where multiple Byzantine adversaries collaborate between each other to thwart the objective. Several open questions still remain. For example, how can accurate state information be determined in the absence of a ground-truth? Moreover, for agents with multiple common neighbors and no available ground-truth information, how can an agent determine its cooperative neighbor set if both the true cooperative neighbor set and the true Byzantine neighbor set seem cooperative?

Chapter 4 studies the consensus problem for clustered MASs through the lens of the hybrid systems framework of [63], where the objective is to drive all agent states to a common value. In the C-MAS, each agent computes a homogeneous process with a

distributed controller that only uses locally available state information, where each agent can measure their state. The controller is continuously updated with state information from neighbors in the same cluster and intermittently updated with state information from neighbors in different clusters. The controller also renders the consensus set exponentially stable despite the clustered graph structure, which may result in disconnected distanced-based communication graphs as modeled through the timer dynamics. Moreover, the proposed hybrid system is robust to vanishing perturbations given its satisfaction of the hybrid basic conditions. The proposed result can also accommodate any desired partition of the vertex set given a connected interaction graph. Simulation results for a 16-agent MAS are provided for both the unperturbed and perturbed cases. While exponential stability is achieved in the unperturbed case, perturbations in the state lead to a uniformly ultimately bounded result. Future works may consider linear, nonlinear, heterogeneous, and/or uncertain process models that are subject to disturbances. The result employs a zero-order hold when sampling the state of neighbors within inter-clusters, which limits the selection of the T_1^r and T_2^r parameters to small values. Future efforts could leverage model knowledge or state observers to enable the selection of larger T_1^r and T_2^r parameters, which may allow inter-clusters to go without communication for longer time periods. State-based triggers or timers with variable rates can be explored as an alternative to the fixed-rate timers used to determine the instances of inter-cluster communication. Another line of research could be an analysis of the proposed controller to perturbations in the timer and how to robustify the controller if necessary. The result also relies on the ability of each agent to measure their state, which is not possible in many cases. Hence, the development of an output feedback extension is also motivated.

In Chapter 5, distributed controllers with intermittent distance-limited communication were developed for the rendezvous problem. Applying the hybrid differential inclusions framework of [63] enables an especially simple and systematic approach to the analysis

of the closed-loop system, tying together personal clocks, triggering conditions, stability, and topological properties of solutions. This results in a family of controllers which yield complete, Zeno-free solutions while maintaining the initial graph structure and keeping the prescribed approximate rendezvous set exponentially stable with respect to continuous time. In contrast with [54], where the growth of the edge potentials is insufficient for providing a graph maintenance guarantee for all initial configurations with a connected communication graph, and where this guarantee shrinks as the number of agents grows, the proposed design fits any such configuration with a controller capable of maintaining the initial graph. Another contribution of this result is that it provides a framework for the design of event- and self-triggered controllers capable of achieving approximate rendezvous while ensuring the maintenance of an initially connected graph. Rather than provide specific trigger functions with adjustable parameters like in several other works, this result identifies properties the trigger function must satisfy to ensure graph maintenance and stability. A simulation for a 9-agent MAS is provided and shows that approximate rendezvous is achieved while preserving the connectivity of the initially connected distance-based graph. Future research may address less conservative triggers, more complex agent dynamics, heterogeneous networks, and exogenous disturbances. Accounting for perturbations—not only in the state, but in the triggers as well—is especially important in the context of the current construction, since it does not satisfy the hybrid basic conditions. Other control objectives that rely on a connected distance-based communication graph can be explored, such as the synchronization of a MAS to a time-varying trajectory, formation control, containment control, and their appropriate combinations. Another line of work would be the study of potential functions that can be either repulsive or attractive depending on the argument, and how to employ these potentials in a distributed event-triggered controller to facilitate edge maintenance with collision avoidance for MASs. Interestingly, an event trigger mechanism can be combined with model knowledge to obtain a self-trigger, which can be thought of as a

timer. Hence, the use of state-based trigger mechanisms to design timers or vice versa can also be examined.

Clearly, each chapter has several lines of expansion. Nevertheless, there are open problems that can benefit from the combination or advancement of the proposed results. One open problem is how to combine distributed cyber-attack detectors with the potential functions used for edge maintenance. As shown in Chapters 2, 3, and 5, cooperative agents can achieve a control objective with adversarial agents in the network and preserve the edges of a distance-limited graph by manipulating the edge weights. Currently, it is unclear if the two strategies can be directly stitched together, e.g., taking the Hadamard product between the weight matrices of the trust/reputation values and the edge tension values, without encountering challenges. Nonetheless, the ability to maintain a distance-limited graph while isolating adversarial neighbors has profound practical applications, especially in mobile MASs operating in contested environments.

Another open problem is the coordination of MASs in feedback denied environments. All of the results in this dissertation rely on each agent being able to measure their state, and this may not be possible everywhere, e.g., underwater domains. One way to facilitate MAS objectives in these challenging spaces would be to leverage clustered MASs, where one cluster can continuously operate in the feedback denied space while another cluster ferries state information between feedback-available and feedback-unavailable regions. Another strategy would be to have a cluster of agents form a fixed grid that extends from a feedback-available region to the feedback-unavailable region. The agents in the grid can then compute their location relative to a desired origin in a distributed way to build a local positioning system. A second cluster can then operate under the MAS grid, where state feedback can be obtained through radio communication with the grid agents (essentially combing solutions from the coverage and exploration problems).

APPENDIX A
PROOFS OF SUPPORTING LEMMAS IN CHAPTER 2

A.1 Proof of Lemma 2.1

Proof. Assume the hypothesis of Lemma 2.1, and fix $t_1 \geq 0$. By Assumptions 2.5 and 2.6, $H(t_1)$ is a diagonally dominant matrix, where each row of $H(t_1)$ is non-zero. By Assumptions 2.4 and 2.5, $H(t_1)$ contains a strictly diagonally dominant row, i.e., $|H_{ii}(t_1)| > \sum_{j \in \mathcal{V}, j \neq i} |H_{ij}(t_1)|$ for some $i \in \mathcal{V}$. Claim: if $H(t_1)$ is a diagonally dominant matrix with a strictly diagonally dominant row, then $H_{\text{sym}}(t_1)$ is a symmetric, diagonally dominant matrix with a strictly diagonally dominant row. Suppose the claim is true. Therefore, $H_{\text{sym}}(t_1)$ is a symmetric, diagonally dominant matrix with a strictly diagonally dominant row. Since $I_N + |H_{\text{sym}}(t_1)|$ is a symmetric, strictly diagonally dominant matrix, $I_N + |H_{\text{sym}}(t_1)|$ is positive definite by the Gershgorin Disk Theorem in [53, Theorem 3.9.]. Let $\{\lambda_i\}_{i=1}^N \subset \mathbb{R}_{>0}$ denote the eigenvalues of $I_N + |H_{\text{sym}}(t_1)|$. Since $\lambda_i \in \mathbb{R}_{>0}$ for all $i \in \mathcal{V}$, and the eigenvalues of $(I_N + |H_{\text{sym}}(t_1)|)^{N-1}$ are $\left\{\lambda_i^{N-1}\right\}_{i=1}^N$, $\lambda_i^{N-1} \in \mathbb{R}_{>0}$ for each $i \in \mathcal{V}$. Since $(I_N + |H_{\text{sym}}(t_1)|)^{N-1}$ is a symmetric matrix with positive eigenvalues, $(I_N + |H_{\text{sym}}(t_1)|)^{N-1}$ is positive definite. Hence, $H_{\text{sym}}(t_1)$ is irreducible by [86, Theorem 6.2.24.]. Since $H_{\text{sym}}(t_1)$ is an irreducible, diagonally dominant matrix with a strictly diagonally dominant row, $H_{\text{sym}}(t_1)$ is irreducibly diagonally dominant by [86, Definition 6.2.25.]. Since $H_{\text{sym}}(t_1)$ is irreducibly diagonally dominant, $H_{\text{sym}}(t_1)$ is non-singular [86, Corollary 6.2.27.], i.e., $\lambda_{\min}(H_{\text{sym}}(t_1)) > 0$. Since t_1 is arbitrary, $\lambda_{\min}(H_{\text{sym}}(t)) > 0$ for all $t \geq 0$. Since $\{\lambda_{\min}(H_{\text{sym}}(t)) : \forall t \geq 0\}$ is a finite set, $\lambda_{\min}(H_{\min}) \triangleq \min\{\lambda_{\min}(H_{\text{sym}}(t))\} \in \mathbb{R}_{>0}$ is well defined.

Proof of Claim: Let $H(t_1)$ be a diagonally dominant matrix, i.e., row diagonally dominant, where $|H_{ii}(t_1)| \geq \sum_{j \neq i} |H_{ij}(t_1)|$ for all $i \in \mathcal{V}$. Then, $H(t_1)^T$ is a column diagonally dominant matrix, where $|H_{ii}(t_1)| \geq \sum_{j \neq i} |H_{ji}(t_1)|$ for all $i \in \mathcal{V}$. Recall that

$H_{\text{sym}}(t_1) = \frac{1}{2}\left(H(t_1) + H(t_1)^T\right)$. Then, for fixed $i \in \mathcal{V}$, it follows that

$$\begin{aligned}
\sum_{j\neq i} |H_{\text{sym},ij}| &= \sum_{j\neq i} \left|\frac{1}{2}\left(H_{ij}(t_1) + H_{ji}(t_1)\right)\right| \\
&= \frac{1}{2}\sum_{j\neq i} |H_{ij}(t_1) + H_{ji}(t_1)| \\
&\leq \frac{1}{2}\sum_{j\neq i} \left(|H_{ij}(t_1)| + |H_{ji}(t_1)|\right) \\
&\leq |H_{ii}(t_1)| \\
&= |H_{\text{sym},ii}(t)|.
\end{aligned}$$

Since $\sum_{j\neq i} |H_{\text{sym},ij}| \leq |H_{\text{sym},ii}(t)|$ for each $i \in \mathcal{V}$, $H_{\text{sym}}(t_1)$ is diagonally dominant. The existence of a strictly diagonally dominant row/column follows by a similar argument. ■

A.2 Proof of Lemma 2.2

Proof. Let $t \geq 0$. Given (2–12) and $K = B^T P$, it follows that

$$\|u_i(t)\| \leq S_{\max}\left(B^T P\right)\|z_i(t)\| + S_{\max}\left(B^T P\right)\|e_{2,i}(t)\|. \tag{A–1}$$

Provided the self-trigger in (2–44) is satisfied for all $t \geq 0$, $\phi_2\|e_{2,i}(t)\|^2 - \frac{\theta}{N} \leq 0$ for all $t \geq 0$ by Theorem 2.3, where

$$\|e_{2,i}(t)\| \leq \sqrt{\frac{\theta}{N\phi_2}}. \tag{A–2}$$

By (2–22), it follows that

$$\|z(t)\| \leq \max\{\|H(t) \otimes I_m\|\}\left(\|e_2(t)\| + \|e_1(t)\|\right). \tag{A–3}$$

Since $\|e_1(t)\| \leq \beta_1 + \beta_2 e^{-\beta_3 t}$ for all $t \geq 0$ by Theorem 2.1,

$$\|e_1(t)\| \leq \beta_1 + \beta_2. \tag{A–4}$$

Substituting (A–2) into $\|e_2(t)\|^2 = \sum_{i\in\mathcal{V}} \|e_{2,i}(t)\|^2$ implies

$$\|e_2(t)\| \leq \sqrt{\frac{\theta}{\phi_2}}. \tag{A–5}$$

Since $\|z_i(t)\| \leq \|z(t)\|$, (A–3) implies

$$\|z_i(t)\| \leq \max\{\|H(t) \otimes I_m\|\}(\|e_2(t)\| + \|e_1(t)\|) \tag{A–6}$$

Substituting (A–2), (A–4), (A–5), and (A–6) into (A–1) yields (2–43). ■

A.3 Proof of Lemma 2.3

Proof. Consider the candidate Lyapunov function $V_0 : \mathbb{R}^m \to \mathbb{R}_{\geq 0}$ defined as

$$V_0(e_0(t)) \triangleq \frac{1}{2} e_0^T(t) e_0(t). \tag{A–7}$$

Substituting (2–1) and (2–51) into the time-derivative of (2–50) yields

$$\dot{e}_0(t) = -k_0 e_0(t). \tag{A–8}$$

Substituting (A–8) into the time-derivative of (A–7) yields

$$\dot{V}_0(e_0(t)) = -k_0 e_0^T(t) e_0(t), \tag{A–9}$$

where substituting (A–7) into (A–9) yields

$$\dot{V}_0(e_0(t)) = -2k_0 V_0(e_0(t)). \tag{A–10}$$

Solving (A–10) yields $V_0(e_0(t)) = V_0(e_0(0)) e^{-2k_0 t}$. Since $V_0(e_0(t))$ is radially unbounded with an unrestricted domain, (2–50) is globally exponentially regulated. Since $V_0(e_0(t))$ is positive definite and $\dot{V}_0(e_0(t))$ is negative definite, provided $k_0 > 0$, $V_0(e_0(t)) \in \mathcal{L}_\infty$. Since $V_0(e_0(t)) \in \mathcal{L}_\infty$, $e_0(t) \in \mathcal{L}_\infty$. Since $x_d(t) \in \mathcal{L}_\infty$, $x_0(t) \in \mathcal{L}_\infty$. Since $x_d(t) \in \mathcal{L}_\infty$, $\dot{x}_d(t) \in \mathcal{L}_\infty$, and $x_0(t) \in \mathcal{L}_\infty$, we see that $u_0(t) \in \mathcal{L}_\infty$. ■

APPENDIX B
PROOFS OF SUPPORTING LEMMAS AND THEOREMS IN CHAPTER 3

B.1 Proof of Lemma 3.1

Proof. Let $\mathcal{H} \triangleq \{\|H(t) \otimes I_n\| : t \geq 0\}$. Fix $t_1 \geq 0$, and suppose $\mathcal{C}(t_1) = \mathcal{V}, \mathcal{G}(t_1)$ is complete, and $B(t) = b_{\max} \cdot I_N$. Then, $\|H(t) \otimes I_n\|_F$ is maximum at t_1, where $\Lambda_{\max} \triangleq \sqrt{n\left(N(N-1+b_{\max})^2 + N^2 - N\right)} = \|H(t_1) \otimes I_n\|_F$. Since $\|H(t) \otimes I_n\| \leq \|H(t) \otimes I_n\|_F \leq \Lambda_{\max}$ for all $t \geq 0$, $\mathcal{H}$ is a non-empty set that is bounded above. Therefore, $\Lambda_{\max} \geq \sup\{\mathcal{H}\}$. ■

B.2 Proof of Lemma 3.2

Proof. Fix $t_2 \geq 0$, and suppose that at time t_2 the MAS consists of $N_C(t_2) \in \mathbb{Z}_{\geq 0}$ cooperative followers and $N_B(t_2) \in \mathbb{Z}_{\geq 0}$ Byzantine adversaries, where $N_C(t_2) + N_B(t_2) = N$. Using Assumptions 3.4 and 3.7, the trust model in (3–4), the reputation model in (3–5), and the edge weight policy in (3–6), the connectivity matrix $\overline{H}(t_2)$ can be expressed as the block matrix

$$\overline{H}(t_2) = \begin{bmatrix} H_{CC}(t_2) & H_{CB}(t_2) \\ H_{BC}(t_2) & H_{BB}(t_2) \end{bmatrix},$$

where $H_{CC}(t_2) \in \mathbb{R}^{N_C(t_2) \times N_C(t_2)}$ is a diagonally dominant matrix with positive diagonal entries by construction, $H_{BB}(t_2) \in \mathbb{R}^{N_B(t_2) \times N_B(t_2)}$, $H_{BC}(t_2) \in \mathbb{R}^{N_B(t_2) \times N_C(t_2)}$, and $H_{CB}(t_2) \in \mathbb{R}^{N_C(t_2) \times N_B(t_2)}$. Note that $\overline{H}(t_2) = P(t_2) H(t_2) P^{-1}(t_2)$, where $\overline{H}(t_2)$ is permutation-similar to $H(t_2)$, and $P(t_2)$ is an orthogonal permutation matrix. Since $H_{CC}(t_2)$ is irreducibly diagonally dominant by Assumption 3.8, $H_{CC}(t_2)$ is non-singular, i.e., $H_{CC}(t_2)$ is invertible [86, Corollary 6.2.27].[1]

[1] Every graph Laplacian is diagonally dominant because it has zero row sums. For connected graphs, their Laplacians are irreducible. Adding the Laplacian of a connected graph to a diagonal matrix with at least one positive entry makes at least one row strictly

Next, we show that the eigenvalues of $H_{CC}(t_2)$ have positive real parts. Since $P(t_2)$ is orthogonal, $P(t_2)$ is invertible, where $P^{-1}(t_2) = P^{\top}(t_2)$. Let $\overline{E}_1 \triangleq (P(t_2) \otimes I_n) E_1 \in \mathbb{R}^{nN}$, where $\overline{E}_1 \triangleq [E_{1,C}^{\top}, E_{1,B}^{\top}]^{\top} \in \mathbb{R}^{nN}$ such that $E_{1,C} \triangleq [e_{1,1}^{\top}(t_2), e_{1,2}^{\top}(t_2), ..., e_{1,N_C(t_2)}^{\top}(t_2)]^{\top} \in \mathbb{R}^{nN_C(t_2)}$ and $E_{1,B} \triangleq [e_{1,N_C(t_2)+1}^{\top}(t_2), e_{1,N_C(t_2)+2}^{\top}(t_2), ..., e_{1,N}^{\top}(t_2)]^{\top} = 0_{nN_B(t_2)}$ by convention. Substituting $\overline{H}(t_2)$ and $\overline{E}_1$ into $E_1^{\top}(H(t_2) \otimes I_n) E_1$ yields $E_1^{\top}(H(t_2) \otimes I_n) E_1 = E_{1,C}^{\top}(H_{CC}(t_2) \otimes I_n) E_{1,C}$. Let $H_{\text{sym}}(t_2) \triangleq \frac{1}{2}\left(H_{CC}(t_2) + H_{CC}^{\top}(t_2)\right)$ and $H_{\text{skew}}(t_2) \triangleq \frac{1}{2}\left(H_{CC}(t_2) - H_{CC}^{\top}(t_2)\right)$, where $H_{\text{sym}}(t_2)$ and $H_{\text{skew}}(t_2)$ are symmetric and skew-symmetric matrices, respectively, by construction. Moreover, $H_{CC}(t_2) = H_{\text{sym}}(t_2) + H_{\text{skew}}(t_2)$. Since $H_{\text{skew}} \otimes I_n$ is a skew-symmetric matrix, $E_{1,C}^{\top}(H_{\text{skew}}(t_2) \otimes I_n) E_{1,C} = 0$ and $E_{1,C}^{\top}(H_{CC}(t_2) \otimes I_n) E_{1,C} = E_{1,C}^{\top}(H_{\text{sym}}(t_2) \otimes I_n) E_{1,C}$. Since $H_{CC}(t_2)$ is a diagonally dominant matrix with positive diagonal entries, the real part of the eigenvalues of $H_{CC}(t_2)$ are non-negative by the Gershgorin Disk Theorem in [53, Theorem 3.9.]. Moreover, since the real part of the eigenvalues of $H_{CC}(t_2)$ are non-negative and $H_{CC}(t_2)$ is invertible, the real part of the eigenvalues of $H_{CC}(t_2)$ are positive.

We next show that the symmetric component of $H_{CC}(t_2)$ is positive definite. Since $H_{CC}(t_2)$ is invertible, for all non-zero $w \in \mathbb{R}^{N_C(t_2)}$ $H_{CC}(t_2) w \neq 0_{N_C(t_2)}$ and $H_{CC}^{\top}(t_2) w \neq 0_{N_C(t_2)}$. Moreover, $H_{CC}(t_2) w + H_{CC}^{\top}(t_2) w \neq 0_{N_C(t_2)}$ since $H_{CC}(t_2) + H_{CC}^{\top}(t_2) \neq 0_{N_C(t_2) \times N_C(t_2)}$, i.e., $H_{CC}(t_2)$ is not skew-symmetric. It then follows that $H_{\text{sym}}(t_2) w = \frac{1}{2}\left(H_{CC}(t_2) w + H_{CC}^{\top}(t_2) w\right) \neq 0_{N_C(t_2)}$ for all non-zero $w \in \mathbb{R}^{N_C(t_2)}$. Hence, $H_{\text{sym}}(t_2)$ has the trivial null space and 0 fails to be an eigenvalue of $H_{\text{sym}}(t_2)$. Furthermore, $H_{\text{sym}}(t_2)$ is a diagonally dominant matrix by construction with non-negative eigenvalues by the Gershgorin Disk Theorem. Since $H_{\text{sym}}(t_2)$ is a symmetric matrix with positive real eigenvalues, $H_{\text{sym}}(t_2)$ is positive definite.

---

diagonally dominant. Hence, summing a connected graph Laplacian with the leader pinning matrix yields an irreducibly diagonally dominant matrix.

We next show $E_1^\top (H(t) \otimes I_n) E_1 \geq \Lambda_{\min} \|E_1\|^2$ for all $t \geq 0$, where $\Lambda_{\min} \in \mathbb{R}_{>0}$. By the Rayleigh quotient, it follows that $E_{1,C}^\top (H_{CC}(t_2) \otimes I_n) E_{1,C} \geq \lambda_{\min}(H_{\text{sym}}(t_2) \otimes I_n) E_{1,C}^\top E_{1,C}$. Since $E_{1,B}^\top E_{1,B} = 0$, $E_{1,C}^\top (H_{CC}(t_2) \otimes I_n) E_{1,C} \geq \lambda_{\min}(H_{\text{sym}}(t_2) \otimes I_n) \overline{E}_1^\top \overline{E}_1$. Since $E_1^\top (H(t_2) \otimes I_n) E_1 = E_{1,C}^\top (H_{CC}(t_2) \otimes I_n) E_{1,C}$, $E_{1,C}^\top (H_{CC}(t_2) \otimes I_n) E_{1,C} \geq \lambda_{\min}(H_{\text{sym}}(t_2) \otimes I_n) \overline{E}_1^\top \overline{E}_1$, and $\overline{E}_1^\top \overline{E}_1 = E_1^\top E_1$, $E_1^\top (H(t_2) \otimes I_n) E_1 \geq \lambda_{\min}(H_{\text{sym}}(t_2) \otimes I_n) E_1^\top E_1$. Since t_2 was arbitrary, $E_1^\top (H(t) \otimes I_n) E_1 \geq \lambda_{\min}(H_{\text{sym}}(t) \otimes I_n) \|E_1\|^2$ for all $t \geq 0$. Let $\lambda_{\min}(\mathcal{H}_{\text{sym}}) \triangleq \{\lambda_{\min}(H_{\text{sym}}(t) \otimes I_n) : t \geq 0\} \subset (0, \infty)$. Since $\lambda_{\min}(H_{\text{sym}}(t) \otimes I_n) > 0$ for all $t \geq 0$ and $\lambda_{\min}(\mathcal{H}_{\text{sym}}) \neq \varnothing$, $\lambda_{\min}(\mathcal{H}_{\text{sym}})$ is a non-empty set that is bounded below. Hence, $\Lambda_{\min} \triangleq \inf(\lambda_{\min}(\mathcal{H}_{\text{sym}})) \in \mathbb{R}_{>0}$. ■

B.3 Proof of Theorem 3.2

Proof. Let $t \geq t_k^0 \geq 0$. Substituting (3–1) and (3–7) into the time-derivative of (3–3) yields $\dot{e}_{2,0}(t) \overset{a.e.}{=} -f_0(x_0(t)) - g_0(x_0(t)) u_0(t) - d_0(t)$. By Assumption 3.3, $\|d_0(t)\| \leq d_{0,\max}$. Recall that $\|x_0(t)\| \leq x_{0,\max}$ and $\|u_0(t)\| \leq u_{0,\max}$ by Assumption 3.6. Since $\|x_0(t)\| \leq x_{0,\max}$, Assumptions 3.1 and 3.2 imply that $\|f_0(x_0(t))\| \leq f_{0,\max}$ for some $f_{0,\max} \in \mathbb{R}_{>0}$ and $\|g_0(x_0(t))\| \leq g_{0,\max}$ for some $g_{0,\max} \in \mathbb{R}_{>0}$, respectively. It then follows that $\|\dot{e}_{2,0}(t)\| \leq \theta_{0,\max}$, where $\theta_{0,\max} \geq f_{0,\max} + g_{0,\max} u_{0,\max} + d_{0,\max} \in \mathbb{R}_{>0}$. Observe that $\frac{d}{dt}\|e_{2,0}(t)\| = \frac{e_{2,0}^\top(t)\dot{e}_{2,0}(t)}{\|e_{2,0}(t)\|} \overset{a.e.}{\leq} \|\dot{e}_{2,0}(t)\|$. Since $\frac{d}{dt}\|e_{2,0}(t)\| \overset{a.e.}{\leq} \|\dot{e}_{2,0}(t)\|$ and $\|\dot{e}_{2,0}(t)\| \leq \theta_{0,\max}$, it follows that $\frac{d}{dt}\|e_{2,0}(t)\| \overset{a.e.}{\leq} \theta_{0,\max}$, whose solution over $[t_k^0, \infty)$ is $\|e_{2,0}(t)\| \leq \theta_{0,\max}(t - t_k^0)$ since $\|e_{2,i}(t_k^0)\| = 0$. Hence, (3–19) and $\|e_{2,0}(t)\| \leq \theta_{0,\max}(t - t_k^0)$ imply (3–30). ■

B.4 Proof of Theorem 3.3

Proof. Let $t \geq t_k^i \geq 0$ and $i \in \mathcal{V}$. Substituting (3–1), (3–7), and (3–8) into the time-derivative of (3–3) yields $\dot{e}_{2,i}(t) \overset{a.e.}{=} -f_i(x_i(t)) - k_1 z_i(t) - k_2 e_{2,i}(t) - d_i(t)$. By Assumption 3.3, $\|d_i(t)\| \leq d_{i,\max}$. Recall that $x_i(t) \in \mathcal{L}_\infty$ and $z_i(t) \in \mathcal{L}_\infty$ from the proof of Theorem 3.1. Therefore, there exists $x_{i,\max} \in \mathbb{R}_{>0}$ and $z_{i,\max} \in \mathbb{R}_{>0}$ such that $\|x_i(t)\| \leq x_{i,\max}$ and $\|z_i(t)\| \leq z_{i,\max}$, respectively. Since $\|x_i(t)\| \leq x_{i,\max}$, Assumption 3.1 implies that

$\|f_i(x_i(t))\| \leq f_{i,\max}$ for some $f_{i,\max} \in \mathbb{R}_{>0}$. It then follows that $\|\dot{e}_{2,i}(t)\| \leq k_2 \|e_{2,i}(t)\| + \theta_{i,\max}$, where $\theta_{i,\max} \geq f_{i,\max} + k_1 z_{i,\max} + d_{i,\max} \in \mathbb{R}_{>0}$. Let $\upsilon_i : [t_k^i, \infty) \to \mathbb{R}_{\geq 0}$ satisfy $\dot{\upsilon}_i(t) = k_2 \upsilon_i(t) + \theta_{i,\max}$ with initial condition $\upsilon_i(t_k^i) = \|e_{2,i}(t_k^i)\|$. Then, $\upsilon_i(t_k^i) = 0$ and $\upsilon_i(t) = \frac{\theta_{i,\max}}{k_2}\left(e^{k_2(t-t_k^i)} - 1\right)$. Observe that $\frac{d}{dt}\|e_{2,i}(t)\| = \frac{e_{2,i}^\top(t)\dot{e}_{2,i}(t)}{\|e_{2,i}(t)\|} \overset{a.e.}{\leq} \|\dot{e}_{2,i}(t)\|$. Since $\frac{d}{dt}\|e_{2,i}(t)\| \overset{a.e.}{\leq} \|\dot{e}_{2,i}(t)\|$ and $\|\dot{e}_{2,i}(t)\| \leq k_2 \|e_{2,i}(t)\| + \theta_{i,\max}$, it follows that $\frac{d}{dt}\|e_{2,i}(t)\| \overset{a.e.}{\leq} k_2 \|e_{2,i}(t)\| + \theta_{i,\max}$. Using the solution of $\frac{d}{dt}\|e_{2,i}(t)\| \overset{a.e.}{\leq} k_2 \|e_{2,i}(t)\| + \theta_{i,\max}$ and $\upsilon_i(t) = \frac{\theta_{i,\max}}{k_2}\left(e^{k_2(t-t_k^i)} - 1\right)$, we see that $\|e_{2,i}(t)\| \leq \upsilon_i(t)$ for all $t \in [t_k^i, \infty)$. Since $\|e_{2,i}(t)\| \leq \upsilon_i(t)$ and $\upsilon_i(t) = \frac{\theta_{i,\max}}{k_2}\left(e^{k_2(t-t_k^i)} - 1\right)$, (3–20) yields (3–31). ■

APPENDIX C
CONTROL ALGORITHM FOR CHAPTER 3

C.1 Algorithm that Summarizes the Control Strategy of Chapter 3: Part I

Algorithm C.1 Control Algorithm for Follower *i*: Part I

Select $\Lambda_{\max} > 0$ and $\Lambda_{\min} > 0$ according to Lemmas 1 and 2, respectively.
Select $x_0(0)$, $x_i(0)$, $\hat{x}_i(0)$, and v_i for all $i \in \mathcal{V}$.
Set $N = |\mathcal{V}|$. Select $b_{\max} > 0$.
Select κ, c_0, ε, $k_{1,3}$, $k_{2,1}$, ρ_1, ρ_2, δ_1, δ_2, and $k_{1,2}$ according to (3-21) and $E(0) \in \mathcal{S}_{\mathcal{D}}$.
Compute $k_1 = \frac{1}{\Lambda_{\min}}\left(k_{1,1} + \frac{\rho_1^2}{\delta_1}\right)$, $k_2 = k_{2,1} + \frac{\rho_2^2}{\delta_2}$, and $k_{1,1} = k_{1,2} + k_{1,3}$.
Compute ϕ_1 through ϕ_6 according to (3-17).
Set $\tau_{ij}(0) = 1$ and $\zeta_{ij}(0) = 1$ for all $i, j \in \mathcal{V}$.
Select $s_1 > 0$, $\zeta_{\min} \in [0, 1]$, $t_{\text{reset}} > 0$, $\eta_\tau > 0$, and $\eta_\zeta \geq 0$.
Select $\vartheta > 0$, $r \in (0, R)$, and $\Delta_i > 0$ for all $i \in \mathcal{V}$.
Set $k(i) = 0$ and $t_0^i = 0$ for all $i \in \mathcal{V} \cup \{0\}$.
Set $a_{ij}(t) = 1$ for all $j \in \mathcal{N}_i(0)$.
Set $\hat{x}_j(t) = x_j\left(t_{k(j)}^j\right)$ for all $j \in \mathcal{N}_i(0) \cup \{i\}$.
if $0 \in \mathcal{N}_i(0)$ **then**
    Set $\hat{x}_0(t) = x_0\left(t_{k(0)}^0\right)$. Set $b_i(t) = b_{\max}$.
end if
while true **do**
    Compute $\zeta_{ij}(t)$ according to (3-5) for each $j \in \mathcal{N}_i(t)$.
    Compute $a_{ij}(t)$ according to (3-6) for each $j \in \mathcal{N}_i(t)$.
    Compute $z_i(t)$ according to (3-9).
    Compute $e_{2,i}(t) = \hat{x}_i(t) - x_i(t)$.
    Compute $u_i(t) = g_i^+(x_i(t))(k_1 z_i(t) + k_2 e_{2,i}(t))$.
    if $\phi_4 \|e_{2,i}(t)\|^2 \geq \phi_5 \|z_i(t)\|^2 + \frac{\varepsilon}{N}$ **then**
        Set $k(i) = k(i) + 1$. Set $t_{k(i)}^i = t$.
        Set $\hat{x}_i(t) = x_i\left(t_{k(i)}^i\right)$.
        Broadcast $x_i\left(t_{k(i)}^i\right)$ to all $j \in \mathcal{N}_i(t)$.
        Broadcast $\zeta_{ij}\left(t_{k(i)}^i\right)$ to all $j \in \mathcal{N}_i(t)$.
    end if

C.2 Algorithm that Summarizes the Control Strategy of Chapter 3: Part II

Algorithm C.2 Control Algorithm for Follower *i*: Part II

if agent $j \in \mathcal{N}_i(t) \cup \{0\}$ broadcasts **then**
  Set $k(j) = k(j) + 1$. Set $t^j_{k(j)} = t$.
  Receive $x_{j,1}\left(t^j_{k(j)}\right)$. Set $\hat{x}_j(t) = x_{j,1}\left(t^j_{k(j)}\right)$.
  Measure $x_{j,2}\left(t^j_{k(j)}\right)$.
  Receive $\zeta_{jp}\left(t^j_{k(j)}\right)$ for each $p \in \mathcal{N}_j(t)$.
  if $\omega_{ij}\left(t^j_{k(j)}\right) \leq r$ and $\Delta t^j_{k(j)} \leq \Delta_j$ **then**
    Compute $\Psi_{ij}\left(t^j_{k(j)}\right)$ according to (3-4) for each
    $t^j_{k(j)} \in S_j$.
  else
    Set $\Psi_{ij}\left(t^j_{k(j)}\right) = \vartheta$.
  end if
  Set $S_j = \left\{t^j_{k(j)} : t - t_{\text{reset}} \leq t^j_{k(j)} < t\right\}$.
  Store $\left\{\Psi_{ij}\left(t^j_{k(j)}\right) : t^j_{k(j)} \in S_j\right\}$.
  Compute $\tau_{ij}(t) = \frac{1}{|S_j|} \sum_{t^j_{k(j)} \in S_j} e^{-s_1 \Psi_{ij}\left(t^j_{k(j)}\right)}$.
end if
end while

REFERENCES

[1] W. Yu, W. X. Zheng, G. Chen, W. Ren, and J. Cao, "Second-order consensus in multi-agent dynamical systems with sampled position data," *Automatica*, vol. 47, no. 7, pp. 1496–1503, 2011.

[2] W. Ren, R. Beard, and E. Atkins, "A survey of consensus problems in multi-agent coordination," in *Proc. Am. Control Conf.* IEEE, 2005, pp. 1859–1864.

[3] J. Cortés, "Distributed algorithms for reaching consensus on general functions," *Automatica*, vol. 44, no. 3, pp. 726–737, 2008.

[4] R. Olfati-Saber, J. A. Fax, and R. M. Murray, "Consensus and cooperation in networked multi-agent systems," *Proc. IEEE*, vol. 95, no. 1, pp. 215–233, Jan. 2007.

[5] L. Ding, Q.-L. Han, and G. Guo, "Network-based leader-following consensus for distributed multi-agent systems," *Automatica*, vol. 49, no. 7, pp. 2281–2286, 2013.

[6] T. Gustavi, D. Dimarogonas, M. Egerstedt, and X. Hu, "Sufficient conditions for connectivity maintenance and rendezvous in leader–follower networks," *Automatica*, vol. 46, no. 1, pp. 133–139, 2010.

[7] M. Ji and M. Egerstedt, "Distributed coordination control of multiagent systems while preserving connectedness," *IEEE Trans. Robot.*, vol. 23, no. 4, pp. 693–703, Aug. 2007.

[8] X. Wang, J. Wu, and X. Wang, "Distributed attitude consensus of spacecraft formation flying," *J. Syst. Eng. Elec.*, vol. 24, no. 2, pp. 296–302, 2013.

[9] J. Li and K. D. Kumar, "Decentralized fault-tolerant control for satellite attitude synchronization," *IEEE Trans. Fuzzy Syst.*, vol. 20, no. 3, pp. 572–586, 2012.

[10] L. S. Sankar, M. Sindhu, and M. Sethumadhavan, "Survey of consensus protocols on blockchain applications," in *In Proc. 2017 Int. Conf. Adv. Comp. Comms. Syst.*, 2017, pp. 1–5.

[11] A. Adaldo, F. Alderisio, D. Liuzza, G. Shi, D. V. Dimarogonas, M. di Bernardo, and K. H. Johansson, "Event-triggered pinning control of switching networks," *IEEE Trans. Control Netw. Syst.*, vol. 2, no. 2, pp. 204–213, Jun. 2015.

[12] D. V. Dimarogonas, E. Frazzoli, and K. H. Johansson, "Distributed event-triggered control for multi-agent systems," *IEEE Trans. Autom. Control*, vol. 57, no. 5, pp. 1291–1297, May 2012.

[13] T. H. Cheng, Z. Kan, J. R. Klotz, J. M. Shea, and W. E. Dixon, "Event-triggered control of multi-agent systems for fixed and time-varying network topologies," *IEEE Trans. Autom. Control*, vol. 62, no. 10, pp. 5365–5371, 2017.

[14] A. Adaldo, D. Liuzza, D. V. Dimarogonas, and K. H. Johansson, “Control of multi-agent systems with event-triggered cloud access,” in *Proc. Euro. Control Conf.*, 2015, pp. 954–961.

[15] X. Dong and G. Hu, “Time-varying formation control for general linear multi-agent systems with switching directed topologies,” *Automatica*, vol. 73, pp. 47–55, 2016.

[16] G. Wen, W. Yu, G. Hu, J. Cao, and X. Yu, “Pinning synchronization of directed networks with switching topologies: A multiple lyapunov functions approach,” *IEEE Trans. Neural Netw. Learn. Syst.*, vol. 26, no. 12, pp. 3239–3250, 2015.

[17] C. Nowzari and J. Cortés, “Distributed event-triggered coordination for average consensus on weight-balanced digraphs,” *Automatica*, vol. 68, pp. 237–244, 2016.

[18] P. Tabuada, “Event-triggered real-time scheduling of stabilizing control tasks,” *IEEE Trans. Autom. Control*, vol. 52, no. 9, pp. 1680–1685, Sep. 2007.

[19] A. Adaldo, D. Liuzza, D. V. Dimarogonas, and K. H. Johansson, “Cloud-supported formation control of second-order multi-agent systems,” *IEEE Trans. Control Netw. Syst.*, 2017.

[20] W. Heemels, K. Johansson, and P. Tabuada, “An introduction to event-triggered and self-triggered control,” in *Proc. IEEE Conf. Decis. Control*, Dec. 2012, pp. 3270–3285.

[21] X. Yi, K. Liu, D. V. Dimarogonas, and K. H. Johansson, “Dynamic event-triggered and self-triggered control for multi-agent systems,” *IEEE Trans. Autom. Control*, 2018.

[22] Y. Fan, L. Liu, G. Feng, and Y. Wang, “Self-triggered consensus for multi-agent systems with zeno-free triggers,” *IEEE Trans. Autom. Control*, vol. 60, no. 10, pp. 2779–2784, 2015.

[23] Z. Feng and G. Hu, “Secure cooperative event-triggered control of linear multiagent systems under dos attacks,” *IEEE Trans. Control Syst. Tech.*, 2019.

[24] N. H. Vaidya, L. Tseng, and G. Liang, “Iterative approximate byzantine consensus in arbitrary directed graphs,” *Proc. ACM Symp. Prin. Distrib. Comput.*, pp. 365–374, 2012.

[25] J. Hromkovič, R. Klasing, A. Pelc, P. Ruzicka, and W. Unger, *Dissemination of information in communication networks: broadcasting, gossiping, leader election, and fault-tolerance*. Springer Science & Business Media, 2005.

[26] H. J. LeBlanc, H. Zhang, X. Koutsoukos, and S. Sundaram, “Resilient asymptotic consensus in robust networks,” *IEEE J. Sel. Areas Commun.*, vol. 31, no. 4, pp. 766–781, 2013.

[27] S. M. Dibaji and H. Ishii, “Resilient consensus of second-order agent networks: Asynchronous update rules with delays,” *Automatica*, vol. 81, pp. 123–132, 2017.

[28] D. Senejohnny, S. Sundaram, C. De Persis, and P. Tesi, “Resilience against misbehaving nodes in self-triggered coordination networks,” *Proc. IEEE Conf. Decis. Control*, pp. 2848–2853, 2018.

[29] J. Usevitch and D. Panagou, “Resilient leader-follower consensus to arbitrary reference values,” *Proc. Am. Control Conf.*, pp. 1292–1298, 2018.

[30] Y. Hou, J. Li, and Y. Pan, “On the laplacian eigenvalues of signed graphs,” *Linear and Multilinear Algebra*, vol. 51, no. 1, pp. 21–30, 2003.

[31] T. Zaslavsky, “Signed graphs,” *Discrete Appl. Math.*, vol. 4, no. 1, pp. 47–74, 1982.

[32] C. Altafini, “Consensus problems on networks with antagonistic interactions,” *IEEE Trans. Autom. Control*, vol. 58, no. 4, pp. 935–946, 2013.

[33] M. E. Valcher and P. Misra, “On the consensus and bipartite consensus in high-order multi-agent dynamical systems with antagonistic interactions,” *Syst. Control Lett.*, vol. 66, pp. 94–103, 2014.

[34] J. Qin, W. Fu, W. X. Zheng, and H. Gao, “On the bipartite consensus for generic linear multiagent systems with input saturation,” *IEEE Trans. Cybern.*, vol. 47, no. 8, pp. 1948–1958, 2017.

[35] A. Sargolzaei, K. K. Yen, and M. N. Abdelghani, “Preventing time-delay switch attack on load frequency control in distributed power systems,” *IEEE Trans. Smart Grid*, vol. 7, no. 2, pp. 1176–1185, 2015.

[36] F. M. Zegers, P. Deptula, J. M. Shea, and W. E. Dixon, “Event-triggered approximate leader-follower consensus with resilience to byzantine adversaries,” in *Proc. IEEE Conf. Decis. Control*, Nice, Fr, Dec. 2019, pp. 6412–6417.

[37] J. R. Klotz, A. Parikh, T.-H. Cheng, and W. E. Dixon, “Decentralized synchronization of uncertain nonlinear systems with a reputation algorithm,” *IEEE Trans. Control Netw. Syst.*, vol. 5, no. 1, pp. 434–445, 2018.

[38] D. Spanos, R. Olfati-Saber, and R. Murray, “Dynamic consensus on mobile networks,” in *Proc. IFAC World Congress*, 2005.

[39] S. S. Kia, J. Cortés, and S. Martínez, “Dynamic average consensus under limited control authority and privacy requirements,” *Int. J. Robust Nonlin. Control*, vol. 25, no. 13, pp. 1941–1966, 2015.

[40] D. Mateos-Núñez and J. Cortés, “Distributed online convex optimization over jointly connected digraphs,” *IEEE Trans. Netw. Sci. Eng.*, vol. 1, no. 1, pp. 23–37, 2014.

[41] H. Yu and X. Xia, “Adaptive consensus of multi-agents in networks with jointly connected topologies,” *Automatica*, vol. 48, no. 8, pp. 1783–1790, 2012.

[42] P. Lin and Y. Jia, “Consensus of a class of second-order multi-agent systems with time-delay and jointly-connected topologies,” *IEEE Trans. Autom. Control*, vol. 55, no. 3, pp. 778–784, 2010.

[43] J. Qin and C. Yu, “Cluster consensus control of generic linear multi-agent systems under directed topology with acyclic partition,” *Automatica*, vol. 49, no. 9, pp. 2898–2905, 2013.

[44] X. Ge, Q.-L. Han, and X.-M. Zhang, “Achieving cluster formation of multi-agent systems under aperiodic sampling and communication delays,” *IEEE Trans. Ind. Elec.*, vol. 65, no. 4, pp. 3417–3426, 2018.

[45] V. T. Pham, N. Messai, and N. Manamanni, “Impulsive observer-based control in clustered networks of linear multi-agent systems,” *IEEE Trans. Netw. Sci. Eng.*, vol. 7, no. 3, pp. 1840–1851, 2020.

[46] F. Zegers, M. Hale, J. M. Shea, and W. E. Dixon, “Reputation-based event-triggered formation control and leader tracking with resilience to byzantine adversaries,” in *Proc. Am. Control Conf.*, 2020, pp. 761–766.

[47] W. Ren, “Consensus based formation control strategies for multi-vehicle systems,” in *Proceedings of the American Control Conference*, Minneapolis, Minnesota, Jun. 2006, pp. 4237–4242.

[48] J. Cortes, S. Martinez, T. Karatas, and F. Bullo, “Coverage control for mobile sensing networks,” *IEEE Trans. Robot. Autom.*, vol. 20, no. 2, pp. 243–255, 2004.

[49] M. Zavlanos and G. Pappas, “Potential fields for maintaining connectivity of mobile networks,” *IEEE Trans. Robot.*, vol. 23, no. 4, pp. 812–816, Aug. 2007.

[50] D. Spanos and R. Murray, “Robust connectivity of networked vehicles,” in *Proc. IEEE Conf. Decis. Control*, vol. 3, Dec. 2004, pp. 2893–2898.

[51] Z. Kan, A. Dani, J. M. Shea, and W. E. Dixon, “Network connectivity preserving formation stabilization and obstacle avoidance via a decentralized controller,” *IEEE Trans. Autom. Control*, vol. 57, no. 7, pp. 1827–1832, 2012.

[52] Z. Kan, E. Doucette, and W. E. Dixon, “Distributed connectivity preserving target tracking with random sensing,” *IEEE Trans. Autom. Control*, vol. 64, no. 5, pp. 2166–2173, 2019.

[53] M. Mesbahi and M. Egerstedt, *Graph theoretic methods in multiagent networks*. Princeton University Press, 2010.

[54] D. Boskos and D. V. Dimarogonas, “Robustness and invariance of connectivity maintenance control for multiagent systems,” *SIAM J. Control Opt.*, vol. 55, no. 3, pp. 1887–1914, 2017.

[55] M. Fiacchini and I.-C. Morarescu, “Convex conditions on decentralized control for graph topology preservation,” *IEEE Trans. Autom. Control*, vol. 59, no. 6, pp. 1640–1645, 2014.

[56] Y. Fan and G. Hu, “Connectivity-preserving rendezvous of multi-agent systems with event-triggered controllers,” in *Proc. IEEE Conf. Decis. Control*, 2015, pp. 234–239.

[57] X. Yi, J. Wei, D. V. Dimarogonas, and K. H. Johansson, “Formation control for multi-agent systems with connectivity preservation and event-triggered controllers**this work was supported by the knut and alice wallenberg foundation, the swedish foundation for strategic research, and the swedish research council.” *IFAC-PapersOnLine*, vol. 50, no. 1, pp. 9367–9373, 2017, 20th IFAC World Congress.

[58] Y. Dong and S. Xu, “Rendezvous with connectivity preservation problem of linear multiagent systems via parallel event-triggered control strategies,” *IEEE Trans. Cybern.*, pp. 1–10, 2020.

[59] F. Zegers, P. Deptula, J. Shea, and W. E. Dixon, “Event/self-triggered approximate leader-follower consensus with resilience to byzantine adversaries,” *IEEE Trans. Autom. Control*, to appear.

[60] F. Zegers, M. Hale, J. Shea, and W. E. Dixon, “Event-triggered formation control and leader tracking with resilience to byzantine adversaries: A reputation-based approach,” *IEEE Trans. Netw. Syst.*, to appear.

[61] S. Phillips and R. G. Sanfelice, “Robust distributed synchronization of networked linear systems with intermittent information,” *Automatica*, vol. 105, pp. 323–333, 2019.

[62] F. Zegers, S. Phillips, and W. E. Dixon, “Consensus over clustered networks with asynchronous inter-cluster communication,” in *Proc. Am. Control Conf.*, 2021.

[63] R. G. Goebel, R. Sanfelice, and A. R. Teel, *Hybrid Dynamical Systems*. Princeton University Press, 2012.

[64] F. M. Zegers, D. P. Guralnik, and W. E. Dixon, “Event/self-triggered multi-agent system rendezvous with graph maintenance,” in *Proc. IEEE Conf. Decis. Control*, submitted.

[65] H. K. Khalil, *Nonlinear Systems*, 3rd ed. Upper Saddle River, NJ: Prentice Hall, 2002.

[66] A. R. Teel, F. Forni, and L. Zaccarian, “Lyapunov-based sufficient conditions for exponential stability in hybrid systems,” *IEEE Trans. Autom. Control*, vol. 58, no. 6, pp. 1591–1596, 2012.

[67] A. Rahnama and P. J. Antsaklis, “Learning-based event-triggered control for synchronization of passive multiagent systems under attack,” *IEEE Trans. Autom. Control*, vol. 65, no. 10, pp. 4170–4185, 2020.

[68] F. Pasqualetti, A. Bicchi, and F. Bullo, “Consensus computation in unreliable networks: A system theoretic approach,” *IEEE Trans. Autom. Control*, vol. 57, no. 1, pp. 90–104, 2012.

[69] F. Pasqualetti, F. Dörfler, and F. Bullo, “Attack detection and identification in cyber-physical systems,” *IEEE Trans. Autom. Control*, vol. 58, no. 11, pp. 2715–2729, 2013.

[70] A. Barboni, H. Rezaee, F. Boem, and T. Parisini, “Detection of covert cyber-attacks in interconnected systems: A distributed model-based approach,” *IEEE Trans. Autom. Control*, vol. 65, no. 9, pp. 3728–3741, 2020.

[71] H. Liu, M. Xu, Y. Wu, N. Zheng, Y. Chen, and M. Z. A. Bhuiyan, “Resilient bipartite consensus for multi-agent networks with antagonistic interactions,” *Proc. Int. Conf. Trust Secu. Priv. Comp. Commun.*, pp. 1262–1269, 2018.

[72] E. Garoudja, F. Harrou, Y. Sun, K. Kara, A. Chouder, and S. Silvestre, “Statistical fault detection in photovoltaic systems,” *Solar Energy*, vol. 150, pp. 485–499, 2017.

[73] L. Li, H. Luo, S. X. Ding, Y. Yang, and K. Peng, “Performance-based fault detection and fault-tolerant control for automatic control systems,” *Automatica*, vol. 99, pp. 308–316, 2019.

[74] E. Garcia, Y. Cao, and D. W. Casbeer, “Decentralized event-triggered consensus with general linear dynamics,” *Automatica*, vol. 50, no. 10, pp. 2633–2640, 2014.

[75] B. E. Paden and S. S. Sastry, “A calculus for computing Filippov’s differential inclusion with application to the variable structure control of robot manipulators,” *IEEE Trans. Circuits Syst.*, vol. 34, no. 1, pp. 73–82, Jan. 1987.

[76] D. Shevitz and B. Paden, “Lyapunov stability theory of nonsmooth systems,” *IEEE Trans. Autom. Control*, vol. 39 no. 9, pp. 1910–1914, 1994.

[77] V. I. Bogachev, *Measure Theory*. Berlin: Springer, 2007, vol. One.

[78] M. Mazo and P. Tabuada, “On event-triggered and self-triggered control over sensor/actuator networks,” in *Proc. IEEE Conf. Decis. Control*, 2008, pp. 435–440.

[79] A. V. Proskurnikov, A. S. Matveev, and M. Cao, “Opinion dynamics in social networks with hostile camps: Consensus vs. polarization,” *IEEE Trans. Autom. Control*, vol. 61, no. 6, pp. 1524–1536, 2016.

[80] W. Xia, M. Cao, and K. H. Johansson, “Structural balance and opinion separation in trust mistrust social networks,” *IEEE Trans. Control Netw. Syst.*, vol. 3, no. 1, pp. 46–56, 2016.

[81] Z. Cai, M. S. de Queiroz, and D. M. Dawson, “A sufficiently smooth projection operator,” *IEEE Trans. Autom. Control*, vol. 51, no. 1, pp. 135–139, Jan. 2006.

[82] R. Kamalapurkar, J. A. Rosenfeld, J. Klotz, R. J. Downey, and W. E. Dixon. (2014) Supporting lemmas for RISE-based control methods. arXiv:1306.3432.

[83] Y. Li, S. Phillips, and R. G. Sanfelice, “Robust distributed estimation for linear systems under intermittent information,” *IEEE Trans. Autom. Control*, vol. 63, no. 4, pp. 973–988, 2018.

[84] T. Liu, D. J. Hill, and B. Liu, “Synchronization of dynamical networks with distributed event-based communication,” in *Proc. IEEE Conf. Decis. Control*, 2012, pp. 7199–7204.

[85] R. Sanfelice, D. Copp, and P. Nanez, “A toolbox for simulation of hybrid systems in matlab/simulink: Hybrid equations (hyeq) toolbox,” in *Proc. Int. Conf. Hybrid Syst.: Comp. Control*, ser. HSCC ’13. New York, NY, USA: Association for Computing Machinery, 2013.

[86] R. A. Horn and C. R. Johnson, *Matrix Analysis*. Cambridge: Cambridge Uni. Press, 1990.

BIOGRAPHICAL SKETCH

Federico Maximiliano Zegers Urrutia was born in Santiago, Chile in 1991. He received B.S. degrees in mechanical engineering and mathematics in May 2016 from the University of Florida. In June 2017, Federico joined the Nonlinear Controls and Robotics group under the guidance of Dr. Warren Dixon to pursue doctoral studies, where he received the M.S. degree in mechanical engineering from University of Florida in May 2019. In the summer of 2020, Federico was an Air Force Research Laboratory Scholar and conducted research on the control of clustered multi-agent systems. Federico was given the 2020 Graduate Student Research Award in Dynamics, Systems, and Control by the Department of Mechanical and Aerospace Engineering at the University of Florida. He subsequently received the Ph.D. degree in mechanical engineering from the University of Florida in August 2021. His research focuses on robotics, nonlinear and adaptive control, switched and hybrid systems, multi-agent systems, resilience and autonomy, and intermittent/asynchronous sensing and communication.